Dissertation

Study toward Signal Processing and Channel Model for 5G Massive MIMO Systems

Niigata University
Graduate School of Science and Technology
Department of Electrical and Information Engineering
Information Engineering Course

February 5, 2021

Contents

Chapter 1

Introduction

1.1 Widespread use of wireless terminals and speeding up of wireless communication technology

In recent years, the 5th generation wireless communication system for mobile communication [24], the IEEE802.11 standard for fixed wireless local area networks (LANs) [2], and the IEEE802.16 standard for mobile wireless LAN Broadband wireless systems, such as [3], have been implemented in many devices such as notebook PCs, smartphones, tablet PCs, and game machines. Here, Figure 1.1 shows the variation in the number of communication service subscribers, and Figure 1.2 shows the variation in the total monthly average traffic of mobile communication upstream ·. Shown based on the data released by the Ministry [4]. From Figures 1.1 and 1.2, it can be seen that there is significant growth in the application of mobile communication using smartphones and tablet PCs, and the amount of data traffic over these networks is rapidly increasing [5]. In addition, cloud computing and the Internet of Things (IoT) are topics that have attracted much attention worldwide, and the development of communication methods with high efficiency is important for the continued development of cloud computing in the future.

As the amount of data handled in communication networks increases, the transmission speed of commercial services also increases. Figure 1.3 shows the variation in the transmission speed in a commercial system. In the IEEE 802.11 standardization standard for fixed wireless LANs, 11a, which achieves a maximum of 54 Mbps in the 5 GHz band, and 11b, which achieves a maximum of 11 Mbps in the 2.4 GHz band, were both formulated in 1999. After that, 11g was developed in 2003 to achieve a maximum of 54 Mbps in the 2.4 GHz band; in 2009, it achieved a maximum of 600 Mbps in the $2.4 \cdot 5$ GHz bands, and in 2014, 11ac was developed to achieve a maximum of 6.93 Gbps in the 5 GHz band. Further, in 2018, 11ax was developed to realize 9.6 Gbps [6]-[13].

As the amount of data handled in communication increases, the transmission speed of commercial services also increases. Figure 1.3 shows the variation in the transmission speed for a commercial system. In the IEEE 802.11 standard for fixed wireless LAN, 11a, which achieves a maximum of 54 Mbps in the 5 GHz band, and 11b, which achieves a maximum of 11 Mbps in the 2.4 GHz band, were both developed in 1999. After that, 11g was formulated in 2003 to achieve a maximum of 54 Mbps in the 2.4 GHz band, 11g was formulated in 2009 to achieve a maximum of 600 Mbps in the $2.4 \cdot 5$ GHz band, and in 2014 a maximum of 6.93 Gbps was achieved in the 5 GHz band. 11ac was formulated, and 11ax to realize 9.6 Gbps was formulated in 2018 [6]-[13].

However, for mobile communications, in 2G (2nd generation), which has shifted from analog to digital, 9.6kbps was used in 1997 by PDC-P (Personal Digital Cellular-Packet) and GPRS (General Packet Radio Service). Data communication of about 100 kbps then became possible. After that, 3G attained 384 kbps by W-CDMA (Wideband –Code Division Multiple Access) in 2001, 2.4 Mbps was attained by 1xEV-DO (Evolution Data Optimized) in 2003 using 3.5G, and HSDPA (High Speed Downlink Packet Access) was developed in 2006. In 2009, the 3GPP (3rd Generation Partnership Project) developed a specification with 100 Mbps as the minimum requirement for LTE (3.9G). In 2012, the ITU-R (International Telecommunication Union Radiocommunication Sector) recommended that LTE-Advanced (4G) achieve a downlink speed of 1 Gbps or higher. Furthermore, using 5G, a downlink of 3.4 Gbps was achieved by eMBB (enhanced Mobile Broadband) in 2020 [13]-[15]. From the figure 1.3, it can be seen that the transmission speed of commercial services is increasing annually, and the need for high-speed and stable wireless communication technology is increasing.

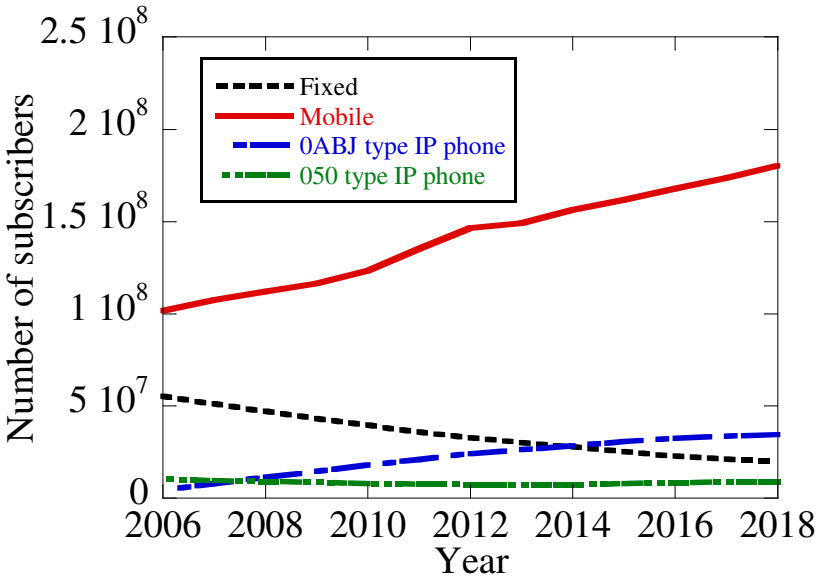

Figure 1.1: Variation in the number of communication service subscribers.

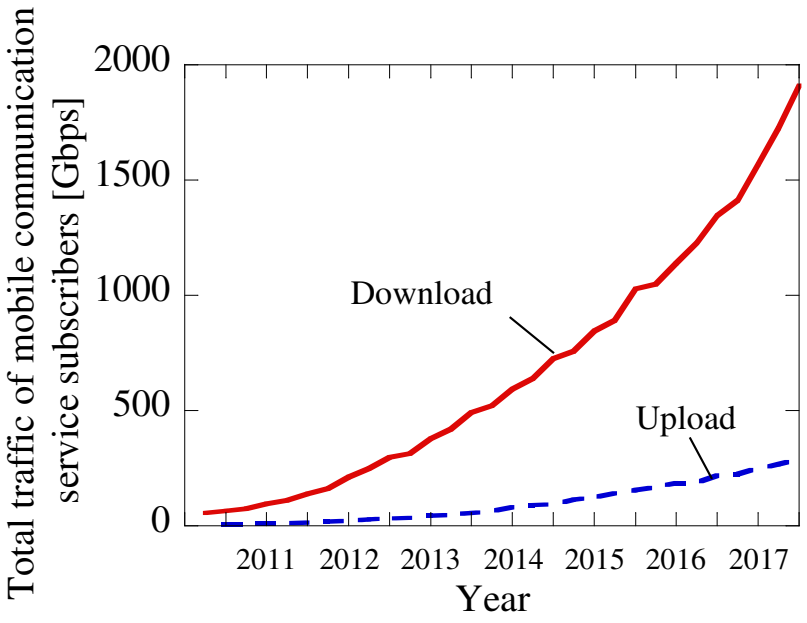

Figure 1.2: Variation in monthly average traffic for mobile communications.

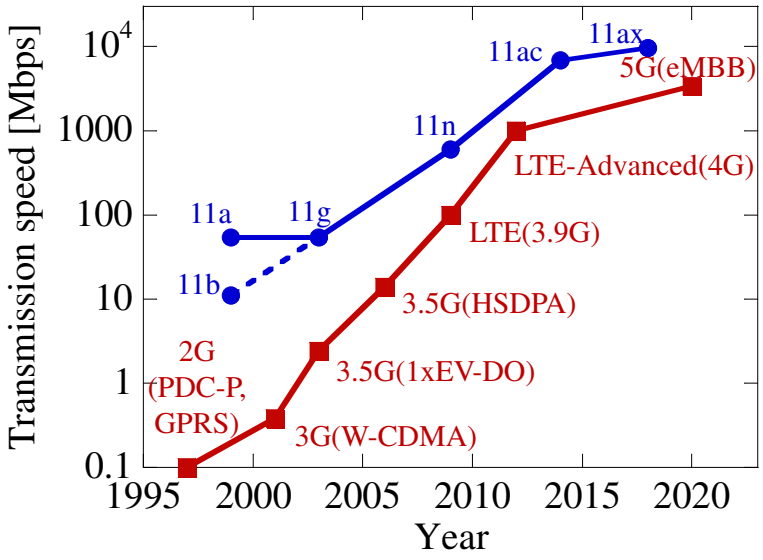

Figure 1.3: Variations of transmission speed in commercial systems.

Therefore, as a communication approach that enables high-speed transmission in a limited frequency band, multiple antennas are used for transmission and reception, and multiple data that enables transmission and reception of multiple data at the same time and · frequency between them is possible. Multiple Input Multiple Output (MIMO) Transmission has attracted much attention [16]. MIMO transmission has already been adopted in LTE-Advanced / 5G, IEEE802.11ac / ax, etc., which are the latest standardization standards for mobile phones and wireless LANs, and these are transmissions of commercial services shown in Fig. 1.3. In terms of speed, all have achieved transmission speeds exceeding 100 Mbps. In the future, 5G will require a transmission speed of 20 Gbps, and a further speedup of MIMO transmission · and higher efficiency will be required [17]-[20].

1.2 Speeding up of MIMO transmission and its challenges

The following are the two main guidelines for further speeding up MIMO transmission.

- Increase in the number of transmitting and receiving elements
- Use of high frequency band

1.2.1 Increase in the number of transmitting and receiving elements

In MIMO transmission, by increasing the number of elements on the transmitting · receiving sides, it is theoretically possible to obtain a channel capacity that is several times that of the transmitting and receiving antenna elements. However, when high-performance signal processing, such as the zero

forcing (ZF) method or natural mode-beamforming (EM-BF) is applied, there is a problem in that the amount of signal processing increases. This is because the calculation of the inverse matrix and eigenvalue decomposition becomes complicated as the number of elements increases.

In addition, a multiuser MIMO (MU-MIMO) technology has been proposed that spatially separates multiple users and performs MIMO transmission individually with the base station (BS: Base Station) [22] [23]. In MU-MIMO, only users with less than the number of BS elements can communicate at the same time, and it is necessary to increase the number of elements on the BS side to cope with the increase in the number of users. In addition, MU-MIMO requires advanced signal processing such as the Block Diagonalization (BD) method to spatially divide users. In this case, there is also a problem in that signal processing becomes complicated as the number of elements increases.

Problems associated with the increase in the number of elements include not only the complication of signal processing but also the increase in power consumption. This is because the D/A (Digital · Analog) · A/D (Analog · Digital) converter, etc., increases as the number of elements increases, thus the power consumption of the entire system increases. This is because it increases.

1.2.2 Use of high frequency band

The higher the frequency used, the greater the amount of information that can be transmitted. In addition, by using a high frequency band, the bandwidth that can be used for communication can be expected to increase. This is because the bandwidth at 800 MHz in the UHF band is 1%, which is 8 MHz, whereas it increases to 15 MHz at 1.5GHz in the UHF band and up to 30 MHz at 30 GHz in the SHF band. In reality, the available frequency allocation is limited; thus it does not increase ideally, but basically, the higher the frequency band, the greater is the amount by which the available bandwidth can be expected to increase [21]. As described above, the higher the frequency band ·, the greater the amount of information that can be transmitted.

1.2.3 Acceleration with Massive MIMO

MIMO with an extremely large number of transmitting and receiving elements is called Massive MIMO. Massive MIMO uses high frequency bands not only to increase the communication speed but also to reduce the scale of the system. Based on the guidelines for speeding up MIMO transmission shown above, in order to realize a system for Massive MIMO transmission that uses multiple base stations, especially for a multibeam Massive MIMO system that uses an analog multibeam, this paper proposes · a signal control method, propagation analysis, and model design in the high SHF band.

1.3 Structure and outline of this paper

Figure 1.4 displays the outline of the paper, composed of six chapters. After discussing the background of the research, issues and objectives are presented in Chapters 1 and 2, whereas signal processing is explained in Chapters 3 and 4. Chapter 5 presents the content of studies on propagation in the high SHF band, and it then summarizes it at the end.

The outline of this paper is shown below. Chapter 1 is an introduction and explains the spread of wireless terminals and the speeding up of wireless communication technology, which form the background of the study. After that, the author describes the issues related to speeding up MIMO transmission, and shows the purpose of this research and the structure of the paper. Chapter 2 summarizes the high-speed transmission technology related to Massive MIMO transmission, and presents the research issues and the contents of the study. Chapter 3 describes the basic characteristics of Massive MIMO based on actually measured propagation channels. Chapter 4 describes the performance evaluation of analog–digital hybrid Massive MIMO as a digital-analog fusion control method. Chapter 5 describes performance evaluation using multivalue modulation, modulation method estimation using deep learning, and performance evaluation for wideband signals as methods for eliminating interference and reducing the number of control signals. Chapter 6 describes the channel capacity comparison between the low-SHF band and the high SHF band, the number of clusters in the high-SHF band, and the new cluster model in the high-SHF band as propagation analysis and model design. Chapter 7 concludes the paper with a summary of the overall paper and of multibeam Massive MIMO.

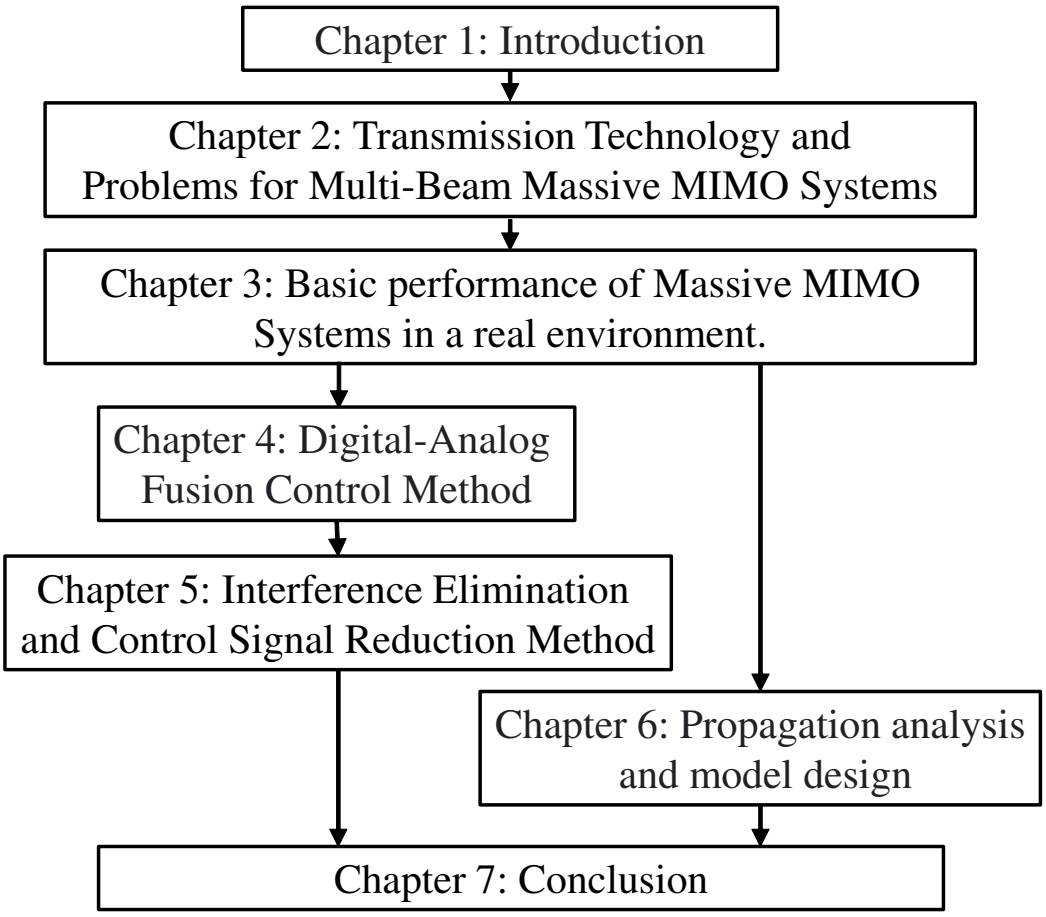

Figure 1.4: Outline of the paper structure.

Chapter 2

Features of Massive MIMO and its issues

This chapter discusses the characteristics of the proposed Massive MIMO based on the guidelines for speeding up MIMO transmission described in Chapter 1, and the issues to be examined in Massive MIMO and this paper are clarified.

2.1 What is Massive MIMO?

As a technology for spatially separating multiple users, SDMA (space division multiple access), which is a signal processing technology using an array antenna, has been studied. Figure 2.1 shows a conceptual diagram of SDMA. In SDMA, the adaptive array antenna is used on the base station (BS) side to enable a different directivity for each user, thereby improving the frequency utilization efficiency of the entire system [23]. At this time, the directivity formed from BS to each user is orthogonal, and a directivity null is formed in the direction of other users.

SDMA is a technology that uses adaptive array antennas, and there is usually one antenna on the user side. Here, the propagation channel between the BS and multiple user terminals (UE: User Equipment) can be regarded as one MIMO propagation channel, and MIMO transmission can be performed individually with multiple users by increasing the number of antennas of each UE. This technology is generally called multiuser MIMO (MU-MIMO: multi-user MIMO).

In MIMO transmission, by increasing the number of elements on the transmitting · receiving sides, it is theoretically possible to obtain a channel capacity that is several times that of the transmitting and receiving antenna elements. However, in an actual system, it is not realistic to mount a large number of antennas on a terminal. Therefore, MU-MIMO, which installs many antennas in the base station and performs MIMO communication with many users, has been proposed [22] [23]. MU-MIMO

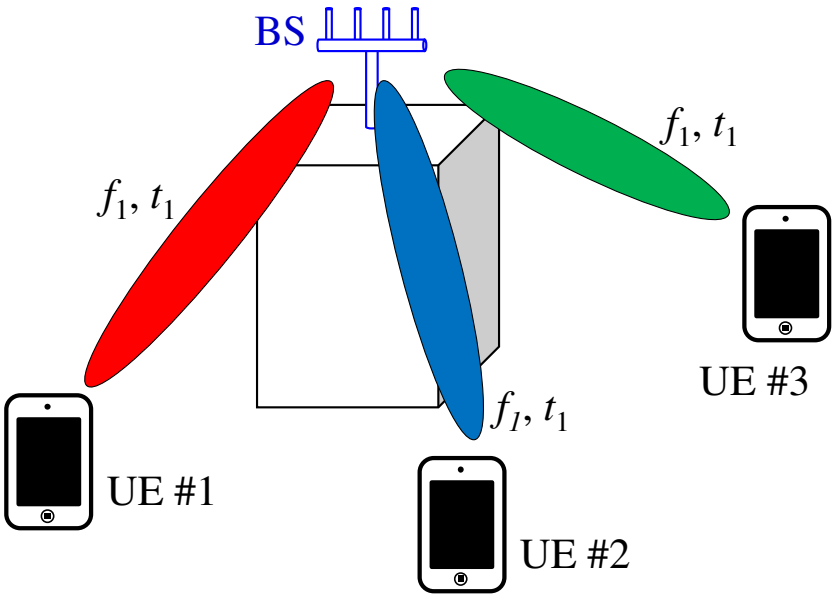

Figure 2.1: Conceptual diagram of SDMA.

has been introduced in the latest wireless LAN standard, IEEE802.11ax and the 5th generation mobile communication system (5G) [10] [24]

Figure 2.1 is exactly multi-user MIMO. By increasing the number of base station antennas in MU-MIMO, it is possible to communicate with multiple small terminals simultaneously. However, in MU-MIMO, because it is necessary to spatially separate multiple users by control through the transmitting side using an approach such as the BD method, there is a problem in that signal processing becomes extremely complicated as the number of terminals increases.

It is known that the directivity of linear and planar array antennas increases as the number of antenna elements increases. Therefore, in Massive MIMO, users are separated by installing a large number of antennas in the base station, thus resulting in increased directivity [34]-[36].

Figure **??** shows a conceptual diagram of Massive MIMO. Massive MIMO communicates simultaneously with a considerably smaller number of users (the number of UE antennas) than the number of base station antennas, and improves the communication speed while reducing the signal processing load. Specifically, the effect has been clarified for a situation where there are 100 BS antenna elements (N_{BS}) and one UE antenna element (N_{UE}) [34]. Massive MIMO takes advantage of the narrowing of directivity that accompanies the increase in the number of elements in the base station, and it uses relatively simple directivity control, such as maximum ratio combining (MRC), to address problems with MU-MIMO. It is expected to improve the characteristics while suppressing the amount of signal

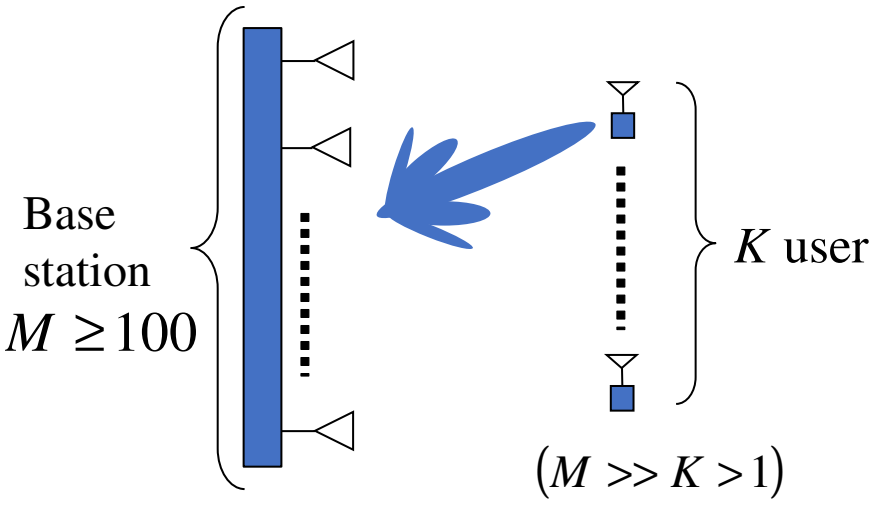

Figure 2.2: Conceptual diagram of Massive MIMO.

processing required [**?**].

2.2 Features of Massive MIMO

There are various characteristics of Massive MIMO. Here, the author focuses on the following four points.

- Very large number of antenna elements
- Frequency is higher than conventional system
- Communication is possible at the same time using multiple terminals with a small number of calculations
- Increased power consumption of base stations

2.2.1 Very large number of antenna elements

MIMO transmission technology makes it possible to improve transmission speed and/or reliability by using array antennas on both the transmitting side and the receiving side. As the most basic method of improving the transmission speed in MIMO transmission, Massive MIMO increases the number of antennas on the transmitting side · receiving side. Figure 2.3 shows the relationship between the number of transmitting and receiving elements and the channel capacity [bits/s/Hz]. From the figure, it is theoretically possible to obtain a channel capacitance that is several times the number of antenna elements by simultaneously increasing the number of transmitting and receiving elements.

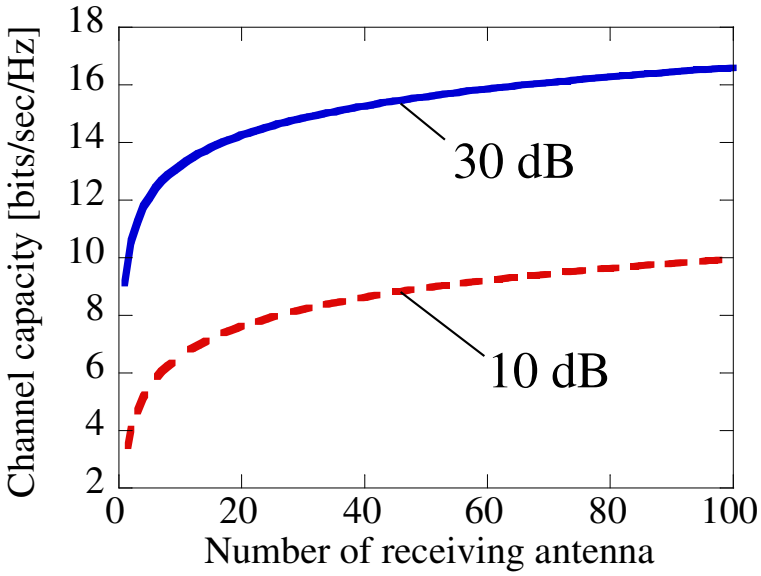

Figure 2.3: Relationship between the number of transmitting and receiving elements and the channel capacity.

MIMO transmission plays an important role in commercial services. LTE-Advanced and 5G, which are the current standards for mobile communications, have specifications of up to 8 × 8 MIMO. Similarly, fixed wireless LAN IEEE802.11n has a maximum of 4 × 4 MIMO, IEEE802.11ac and IEEE802.11ax have a maximum of 8 × 8 MIMO, mobile wireless LAN IEEE802.16e (WiMAX) has a maximum of 2 × 2 MIMO, and IEEE802.16m (WiMAX2) has a maximum of 4 × 4MIMO.

For both mobile communication and wireless LAN, it is expected that a system exceeding 100 Gbps will be developed in the future, and further multielement MIMO transmission is expected. In addition, the MU-MIMO described above can only achieve simultaneous communication when the number of users is less than the number of elements in the base station, and it is important to increase the number of elements to cope with the increasing number of future users.

As described above, increasing the number of elements in MIMO transmission is the most basic guideline for improving the transmission speed, and it is an important element common to short-distance MIMO transmission · MU-MIMO transmission.

When mounting an antenna of about 100 elements in a base station, a problem is that the physical antenna size becomes large. Figure 2.4 shows the variations of the array size in a linear array consisting of 100 sleeve antenna elements. The sleeve antennas were arranged at intervals of 0.5 λ. From Figure 2.4, when Massive MIMO is configured in the 800 MHz band, the antenna size is 18.75 m, which

is impractical. Even in the 3 GHz band, the antenna size becomes 3 m, and it is conceivable that a frequency band higher than the frequency band used in conventional mobile communications will be used in practice.

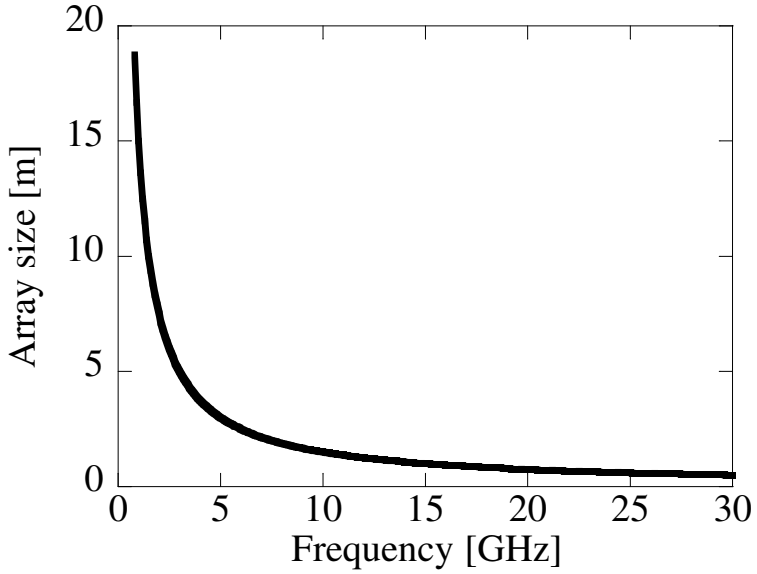

Figure 2.4: Relationship between frequency and array size.

2.2.2 Case when frequency is higher than in conventional system

Because there are several dozen to hundreds of antennas in Massive MIMO, the scale of the base station of the system increases with the increasing antenna size and wavelength interval of the UHF band (0.3 $\sim$ 3 GHz) used in mobile communication so far. For example, in a Massive MIMO system with a center frequency of 2 GHz, if 100 antennas are installed at half wavelength intervals, the diameter will be about 7.5 m, and the scale of the antenna alone will be large. In general, the device sizes such as A/D $\cdot$ D/A converters and signal amplifiers increase as the frequency decreases, thus the scale of the entire system becomes larger and more difficult to realize. However, if for example a system with a half-length straight array is formed with a 30 GHz system, the diameter will be 0.5 m, which is a realistic size. From the above, it is essential to use frequencies above the SHF band (3 $\sim$ 30 GHz) to realize Massive MIMO.

As the frequency increases, not only can the system be realized with a smaller overall size, but faster communication can also be expected. Figure 2.5 shows the relationship between the frequency band used for communication and the bandwidth. As shown in Figure 2.5, even if the bandwidth remains at

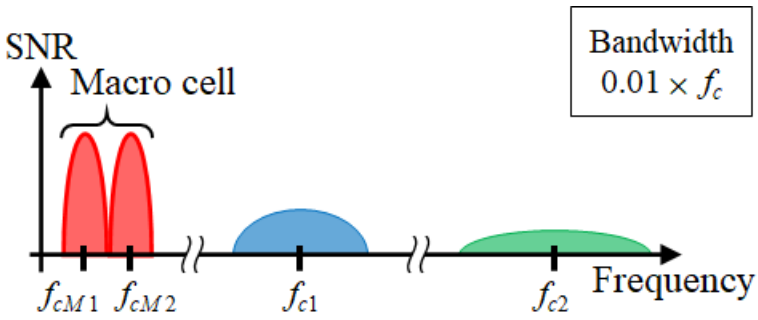

Figure 2.5: Relationship between frequency band and bandwidth.

1%, the frequency band that can be used for communication can be expected to increase when using the high frequency band.

In general, the higher the frequency, the greater the amount of information that can be transmitted. This is because the number of oscillations per second increases.

However, as the frequency used increases, the degree of attenuation in radio wave propagation increases. Figure 2.6 shows the propagation loss at 800 MHz $\sim$ 30 GHz over a transmission/reception distance of 100 m. The propagation loss LOS is as shown in the equation (2.1). Here, r is the propagation distance, λ is the wavelength, and a is the propagation loss coefficient.

$$LOS = (\frac{4\pi r}{\lambda})^a \tag{2.1}$$

The dotted line shown in Figure 2.6 shows the relative attenuation in the "line of Sight (LOS) environment" where there are no obstacles between the BS and UE and they can see each other. The propagation loss coefficient is the square law. However, the solid line shows the relative attenuation in the "nonline of Sight (NLOS) environment" where there are obstacles between the BS and UE, and the propagation loss coefficient at this time is the 2.6th power rule. From Figure 2.6, when trying to cover the same area as the 800 MHz band in the 2.4 GHz band, the propagation loss difference is 10.5 dB in the LOS environment, 16.2 dB in the NLOS environment, and the transmission power is also 10.5 dB. An increase of 16.2 dB is therefore needed. At 30 GHz in the millimeter wave band, the propagation loss difference is 32 dB in the LOS environment and 53 dB in the NLOS environment.

Next, Figure 2.7 shows the propagation loss for a distance of 1 $\sim$ 1000 m in free space for 800 MHz and 30 GHz and in an urban environment. The red line in Figure 2.7 shows the propagation loss in the ideal free space, and this propagation loss coefficient is 2. On the other hand, the blue line assumes an urban environment where structures such as buildings and houses exist between the BS and UE, and radio waves propagate while being diffracted and reflected. Meanwhile, the propagation loss coefficient

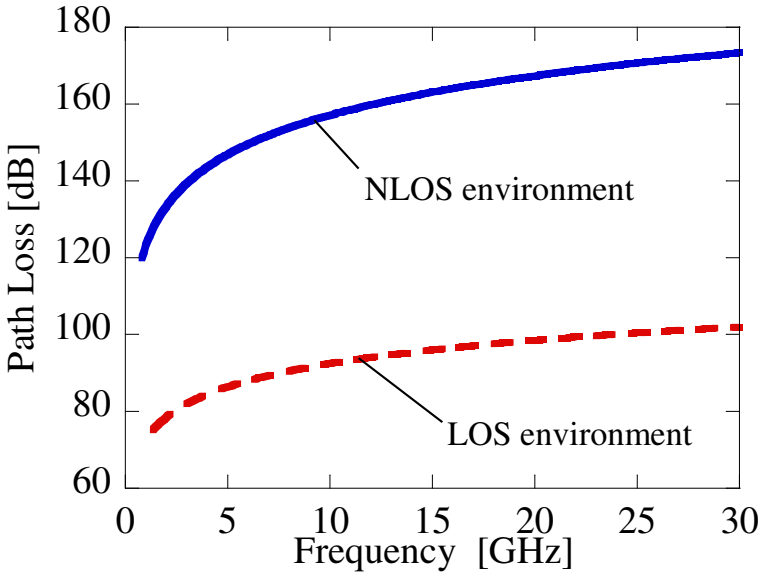

Figure 2.6: Propagation loss at 100 m for each frequency.

is 3.4. Regarding the propagation loss of free space and urban environment, 800 MHz is shown by a broken line, and 30 GHz is shown by a solid line. From Figure 2.7, when the transmission distance is doubled, the propagation loss increases by a factor of 4 in free space and by approximately 11 in an urban environment. Therefore, the transmitted power required for each frequency increases by a factor of 4 in free space and by a factor of approximately 11 in urban environments. However, if the transmission distance is halved, the required transmission power will decrease by 0.25 times in free space and by about 0.09 times in urban environments.

2.2.3 Achieving simultaneous communication using multiple terminals with a small number of calculations

Generally, in MIMO transmission, a known signal called a training signal is transmitted in advance to estimate the propagation channel information (CSI). After that, when applying the ZF, EM-BF, BD method, etc., the inverse matrix and eigenvalue decomposition are calculated for the estimated CSI. Because these calculations become complicated as the number of elements increases, there is a problem: the amount of signal processing increases. Figure 2.8 shows the variation of the amount of signal processing with respect to the number of elements. At this time, in addition to the amount of ZF signal processing that requires the calculation of the inverse matrix, the amount of signal processing of the MRC that does not require the calculation of the inverse matrix or eigenvalue decomposition for comparison is shown. When there is one desired user, the number of multiplications of ZF and

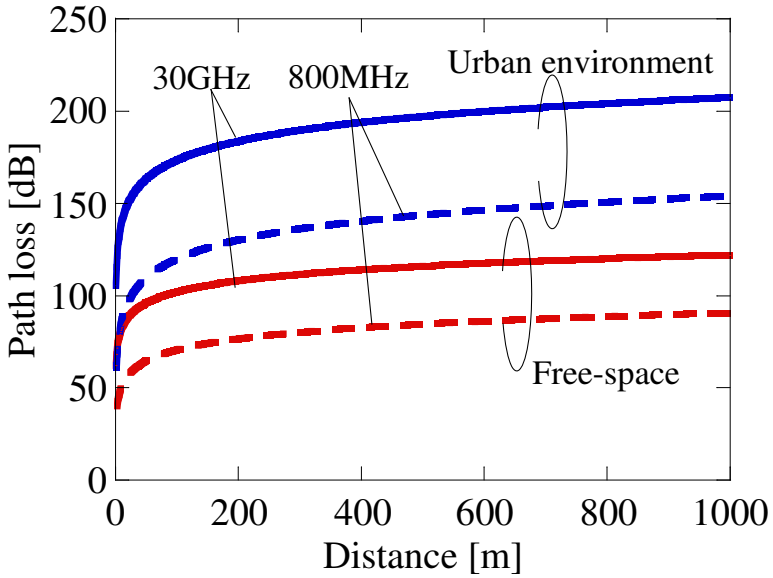

Figure 2.7: Comparison of propagation loss.

MRC is $O(N_{BS}^3)$ and $O(N_{BS})$, respectively, when the number of base station antennas N_{BS}. Reference [89] shows that the number of multiplications of ZF can be reduced to $O(N_{BS}^2)$ if N_{BS} is sufficiently larger than the number of users. However, here we assume the case where the general inverse matrix calculation is performed and the calculation load is the highest. The vertical axis in Figure 2.8 is the logarithmic axis, and it can be seen that the signal processing load increases significantly as the number of base station antennas increases when ZF is used.

Increased power consumption of base stations

All of the signal processing of MIMO transmission explained so far assumes a digital method, and when considered on the receiving side, all analog signals incident on each antenna end are converted into digital signals by each A/D converter. After that, signal processing is performed. Even if the power consumption per A/D converter is as low as 76 mW, in an environment where Massive MIMO is equipped with a 100-element antenna on the BS side, A/D conversion is performed. The power consumption of the device alone is 7.6 W, which is not realistic for mobile communication. As described above, as the number of elements increases, the number of D/A · A/D converters also increases, and the power consumption of the entire system increases.

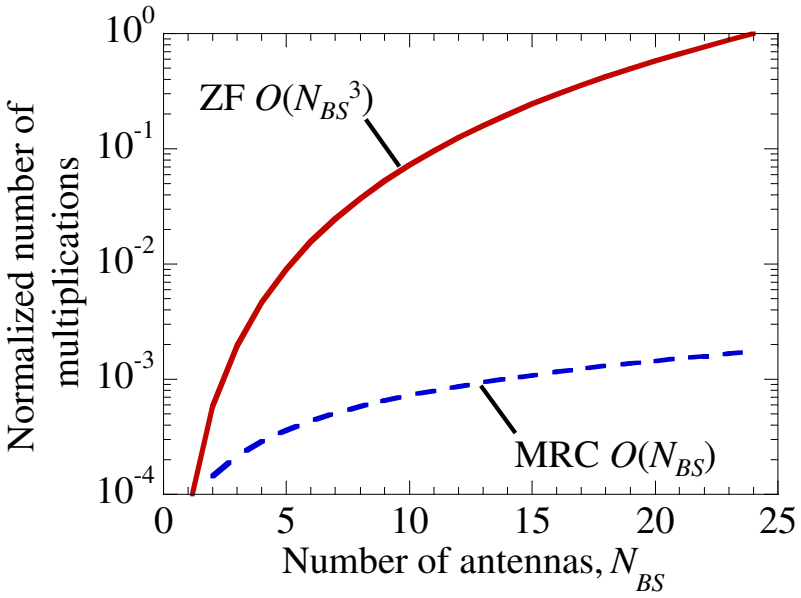

Figure 2.8: Relationship between the number of elements and the amount of signal processing.

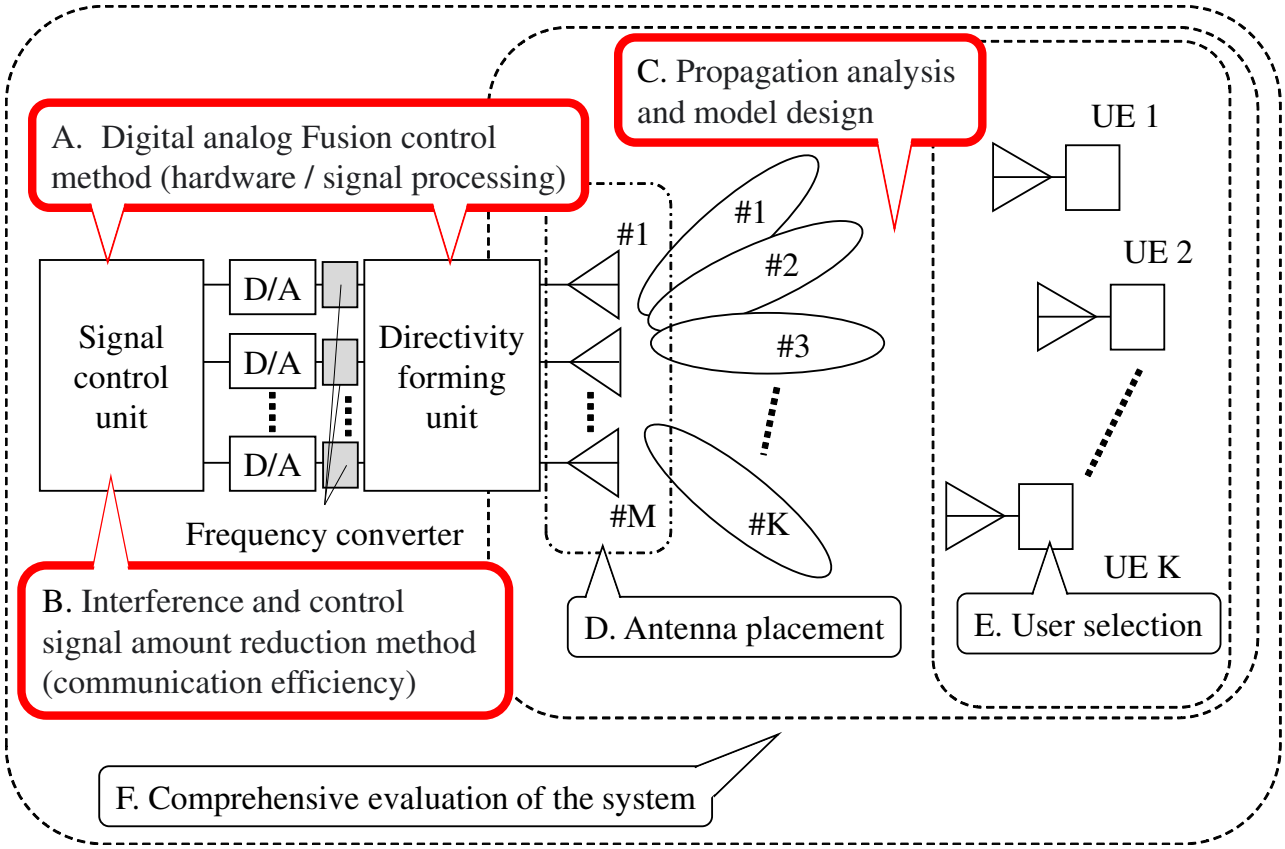

Figure 2.9: Massive MIMO tasks.

2.3 Challenges in Massive MIMO

There are various issues to be considered in order to realize a Massive MIMO system, such as realizing an effective antenna configuration, digital–analog fusion control, and an appropriate user selection method. There are many issues to be considered in order to realize Massive MIMO and fully demonstrate its performance. Figure 2.9 shows the problems in Massive MIMO from A to F.

In this paper, the author describes the results of studies on "A. Digital-analog fusion control method," "B. Interference elimination and control signal amount reduction method," and "C. Propagation analysis and model design."

2.3.1 A: Digital/analog fusion control method (hardware, signal processing)

To realize a Massive MIMO system, various methods such as digital control, analog control, digital–analog hybrid control, and analog multibeam can be considered as directivity formation methods. Each method has advantages and disadvantages related to the communication capacity, required number of calculations, cost, and size of the device, which are associated with the accuracy of directivity formation. In realizing the system, it is necessary to select a method that can sufficiently realize the required communication speed considering these advantages and disadvantages.

In this paper, the author shows a multibeam Massive MIMO system that forms multiple analog beam multibeams and digitally processes some of the received signals, and the study proposes and evaluates a method for receiving QAM signals without propagation channel information.

2.3.2 B: Interference control and control signal reduction method

In addition to the signal from the desired terminal, the received signal may interfere with other users. In the case of wideband single-carrier transmission, interference due to self-delay is also included. High-speed communication cannot be realized unless the communication efficiency is improved by reducing the number of control signals while eliminating these sources of interference. To realize Massive MIMO, it is necessary to propose and evaluate more accurate, high-speed, and realistic signal control methods.

In this paper, the author proposes and evaluates a method to reduce interference using deep learning.

2.3.3 C: Propagation analysis and model design

As mentioned above, in Massive MIMO, it is appropriate to use a frequency band (SHF band) that is relatively higher than the conventional frequency. The 28 GHz band is actually used in 5G [**?**] Because the SHF band has a larger propagation loss than the conventional UHF band and its propagation characteristics are different, it is not appropriate to employ the propagation model used in the evaluation of the system so far as is [80] [82]. It is necessary to analyze the propagation of the SHF band and design a new propagation model. There is already a propagation model targeting the SHF band proposed by the 3GPP (3rd Generation Partnership Project), but the configuration is very complicated; and its characteristics are close to Rayleigh fading. Thus, it is easier and more suitable for the actual propagation environment. The development of a close propagation model is essential.

In this paper, the author statistically analyzes the actual measurement results, and proposes and evaluates a propagation model for the high SHF band.

2.3.4 D: Examination of antenna arrangement

Because Massive MIMO has an extremely large number of antennas, ranging from several tens to hundreds, not only simple linear arrays but also various arrays such as circular arrays, cylindrical arrays, square arrays, and cubic arrays are candidates. Depending on the environment parameters, such as the installation location of the base station, the number of users, and the user position, it is necessary to set the optimum antenna arrangement.

2.3.5 E: Appropriate user selection

In the wireless mobile communication system assumed by Massive MIMO, the number of terminals is very large, ranging from a dozen to several tens, and their positions change from instantaneously. When the number of terminals is several tens, the influence of interference from each terminal is very large. In addition, it is desirable that the communication speed of each terminal be as uniform as possible. It is necessary to minimize interference between terminals and make appropriate user selections for communication as rapidly as possible.

2.3.6 F: Comprehensive system evaluation

As shown from A to E, there are many stages in the realization of Massive MIMO. The performance of Massive MIMO can be clarified by solving all the problems, integrating all of them, and evaluating the entire system. When evaluating the system, it is desirable to perform a comprehensive evaluation that includes not only the physical layer but also the MAC layer (medium access control).

Chapter 3

Basic performance of Massive MIMO in a real environment.

In this chapter, the basic performance of Massive MIMO is evaluated based on the measured propagation channels.

3.1 Introduction

Representative studies on massive MIMO systems have focused on theoretical studies of the channel capacity [36], computer simulations using the maximum ratio combining (MRC) and zero forcing (ZF) methods for linear control [91], and measurements of the actual propagation characteristics using a 128-element channel sounder [70]. The autho previously reported on the interference rejection performance of a cylindrical array using an actual outdoor propagation channel in the 2 GHz band [92]. In addition, there are reports of experiments in the 2 to 5 GHz bands regarding massive MIMO systems in actual environments [93]–[98] .

However, small cells in the high-frequency band will be the main target of massive MIMO [93][99] because the antenna size is very large when considering massive MIMO in the macro-frequency band. A linear or planar array in the horizontal and vertical planes can be used to evaluate small-cell environments in order to realize high beamforming resolution [93].

In this chapter, the author conduct measurements to determine the basic performance of massive MIMO systems when considering the high-frequency band in small-cell outdoor environments. Actual channel state information (CSI) was measured using a wideband sounder with a virtual linear array antenna in the 20 GHz band in an outdoor environment. The author show that ZF is essential as a transmission scheme in massive MIMO system. By contrast, the MRC method cannot reduce interference effectively in a real propagation environment, even for massive MIMO systems. In addition,

the author introduce analog-digital hybrid beamforming, where the desired signal is combined by the analog part to reduce interference in the digital part [100]–[102]. Our results show that analog-digital hybrid beamforming is effective at reducing the signal-processing burden and improving hardware implementation.

Furthermore, the author compared the Shannon capacity to the achievable bit rate (ABR) using ZF, when considering seven-user MIMO transmissions with 100 elements at the BS. When the number of degrees of freedom in the array antenna is sufficiently guaranteed, the ABR is almost the same as the Shannon capacity. Thus, multi-user transmission is realized by linear decoding methods such as ZF. This chapter shows that the channel capacity obtained by an actual small-cell environment is greatly decreased compared to that by an independent and identically-distributed (i.i.d.) channel, which is the representative propagation channel model in MIMO systems [16][49].

The remainder of this chapter is organized as follows. Section II describes the measurement environment and the configuration of a virtual linear array, and presents the delay and angular profiles. Section III shows the interference reduction performance from ZF, MRC, and analog-digital hybrid beamforming. Moreover, the section describes the evaluation of the channel capacity and ABR achieved using ZF. Finally, Section V concludes the works.

3.2 Measurement setup and delay and angular profiles

3.2.1 Measurement setup

Fig. 3.1 shows the measurement environment. The author conducted measurements considering a small-cell outdoor environment (viz., the Faculty of Engineering, Niigata University, Japan). Fig. 3.2 shows the relationship between the transmitter and receiver. Table 1 shows the measurement specifications. Seven users were assumed and the uplink channels were obtained from seven UEs ($N_U = 7$) to the BS. As can be seen in Fig. 3.2, the BS and UEs are located at the top of a building and car, respectively. The transmit distance from the UEs to the BS was from 30 to 100 m, because a small-cell environment was assumed using the 20 GHz band. The real CSI was measured by using a wideband channel sounder in the 20 GHz band. The CSI was separately measured for each UE. A massive array of 100 elements was assumed at 0.6 wavelength intervals for each user position.

To prevent the change in the propagation channel due to the different measurements among UEs, the author measured the CSI in a static propagation environment where there were no persons or obstacles such as cars between the transmitters and receivers. The author confirmed that the average SNR in this measurement is much greater than 10 dB, even in a non-line-of-sight (NLOS) environment.

Table 3.1: Measurement specifications

Radio frequency	19.85 GHz
Bandwidth	50 MHz
Transmission power	1 W
Transmission signal	OFDM-QPSK
Number of FFT points	1024
Number of subcarriers	449
Type of antenna (UE)	Sleeve antenna
Antenna height (UE)	2.5 m
Type of antenna (BS)	Sleeve antenna
Antenna height (BS)	$h_1 = 10.85$ or $h_2 = 11.55$ m
Number of antennas at BS (N_R)	100
Number of UEs (N_U)	7
Distance from BS to UE	30∼100 m

Hence, the measured propagation channel is assumed to be perfect CSI. In the evaluation, the author determined the noise power in order to set the target SNR. This equipment was modified by adding up and down converters with the channel sounder for a 2 GHz band [62]. Up converters, down converters, and oscillators with a frequency of 17.85 GHz were added to transmitters and receivers with a center frequency of 2 GHz to change the center frequency from 2 GHz to 19.85 GHz.

The configurations of the UEs and BS are shown in Fig. 3.3. The OFDM-QPSK signals were transmitted from the UEs to the BS. As shown in Fig. 3.3(b), a vertical linear array (100 elements) at the BS was realized by using a position controller with an interval of 0.6 wavelengths. Tx-A1, A4, and C4 are regarded as NLOS environments. In total, 100×7 MIMO channels were obtained with 449 subcarriers. In next section, the performance of massive MIMO is evaluated using the results from each subcarrier. Although the mutual coupling should be considered when considering the real environment, these effect is not included due to the use of virtual array for the simplification. The evaluation considering the mutual coupling effect should be studied as the future work.

Although an evaluation with a very wideband channel is essential when considering future wireless communications [93], the bandwidth was 50 MHz in this measurement environment, due to the limitations of our equipment. On the other hand, because the author assumed OFDM signals, the author confirmed that frequency selectivity was sufficient from the point of view of the propagation characteristic when considering the delay spread in this environment, even when the bandwidth was 50 MHz.

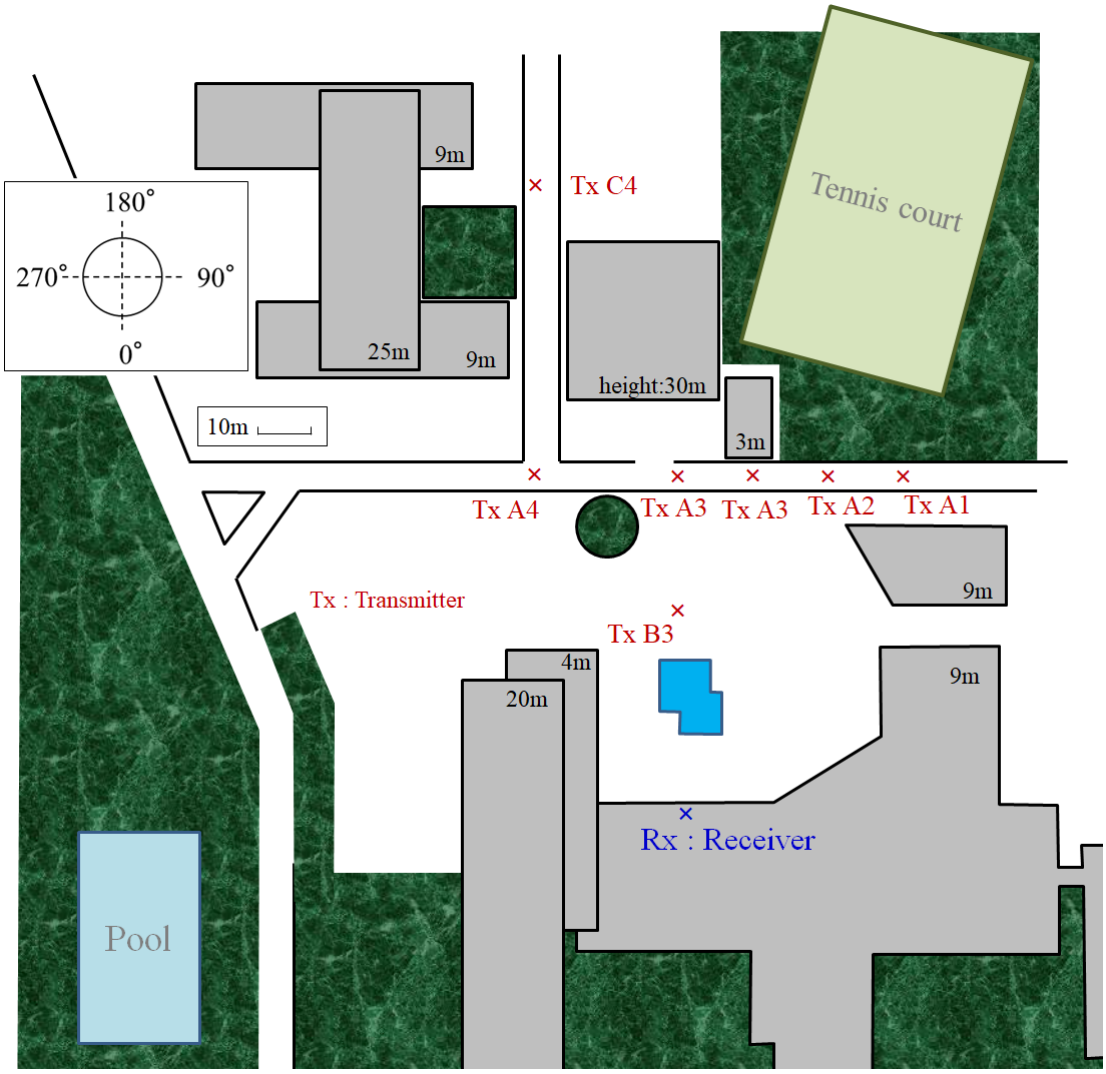

Figure 3.1: Measurement environment.

3.2.2 Delay and angular profiles

In order to analyze the propagation environment in Fig. 3.1, the delay and angle profiles were measured using a horn antenna instead of a sleeve antenna, as illustrated in Fig. 3.3. Fig. 3.4 shows the delay and angle profiles for all users and BSs in Fig. 3.1. The results were obtained using a beamformer method [103] with horn antennas (3-dB, with a beam width of 20°).

Each result was normalized such that the wave with maximum power among all measured UEs was at 0 dB: in this measurement, the directed wave from Tx-B3 to the BS was the maximum. As can be seen in Fig. 3.4, the power of the directed wave from the UE was the maximum at each measured point. Moreover, a few clusters using the reflected and diffracted waves were observed in addition to

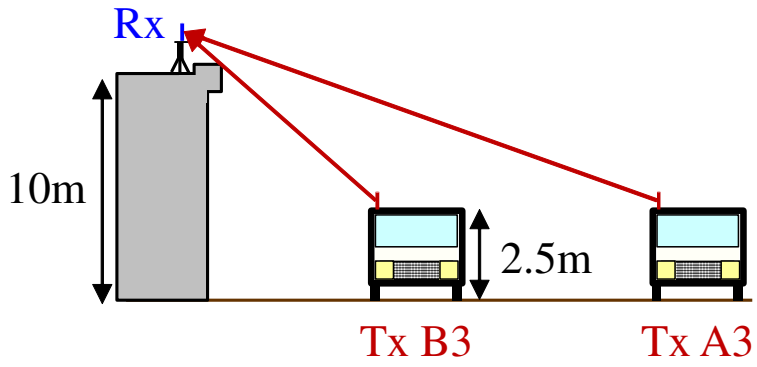

Figure 3.2: Relationship between the transmitter and receiver.

the cluster using the directed wave. Therefore, it was found that the actual propagation environment is completely different from the i.i.d. Rayleigh environment.

3.3 Performance evaluation of massive MIMO in the 20 GHz band using measured CSI

3.3.1 Analog-digital hybrid massive MIMO

Fig. 3.5 shows one example of analog-digital hybrid beamforming in the uplink channel [93] [100]–[102]. Generally speaking, the multiplication number by ZF is $O(N^3)$ when the number of BSs is N, because channel matrix inversion is required for ZF. In order to reduce the calculation complexity by ZF, when N is sufficiently larger than the number of users, it is shown that the number of multiplications by ZF can be reduced below $O(N^2)$ [34]. However, there is still a considerably large load when considering massive MIMO, even when the number of multiplications is $O(N^2)$. Moreover, the power consumption by the A/D and D/A converters is very large when the up and down converters are connected to all the massive array antennas with the high-frequency band.

To solve the above problems, analog-digital hybrid beamforming has been proposed [93]. As can be seen in Fig. 3.5, outputs of each sub-array are connected with the down converters, and the number of down converters can be reduced from the number of massive array antennas to the number of conventional antennas in MIMO systems [93].

Assuming that the number of divided sub-arrays is N_S and the number of antennas per sub-array is N_L, the total number of antennas is $N = N_S \times N_L$. As shown in the figure, the analog weight is prepared for the desired signal for each sub-array. For simplicity, in this chapter, the analog weight is

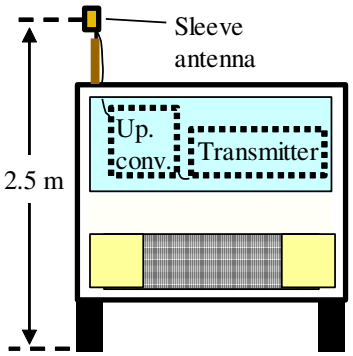

(a) UE (Tx)

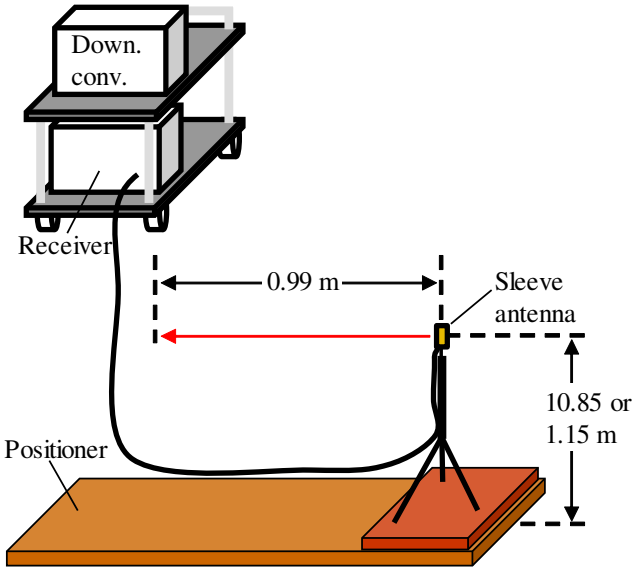

(b) BS (Rx)

Figure 3.3: Configuration at the BS.

assumed to be the weight from MRC. A linear decoding algorithm such as ZF or the minimum mean-square error (MMSE) is employed in the digital part after A/D conversion by using the output signals on the analog part. In this chapter, ZF is adopted. The number of multiplications can be reduced from $O(N^3)$ to $O(N_S^3)$ through analog-digital hybrid beamforming, as opposed to ZF with all of the antennas.

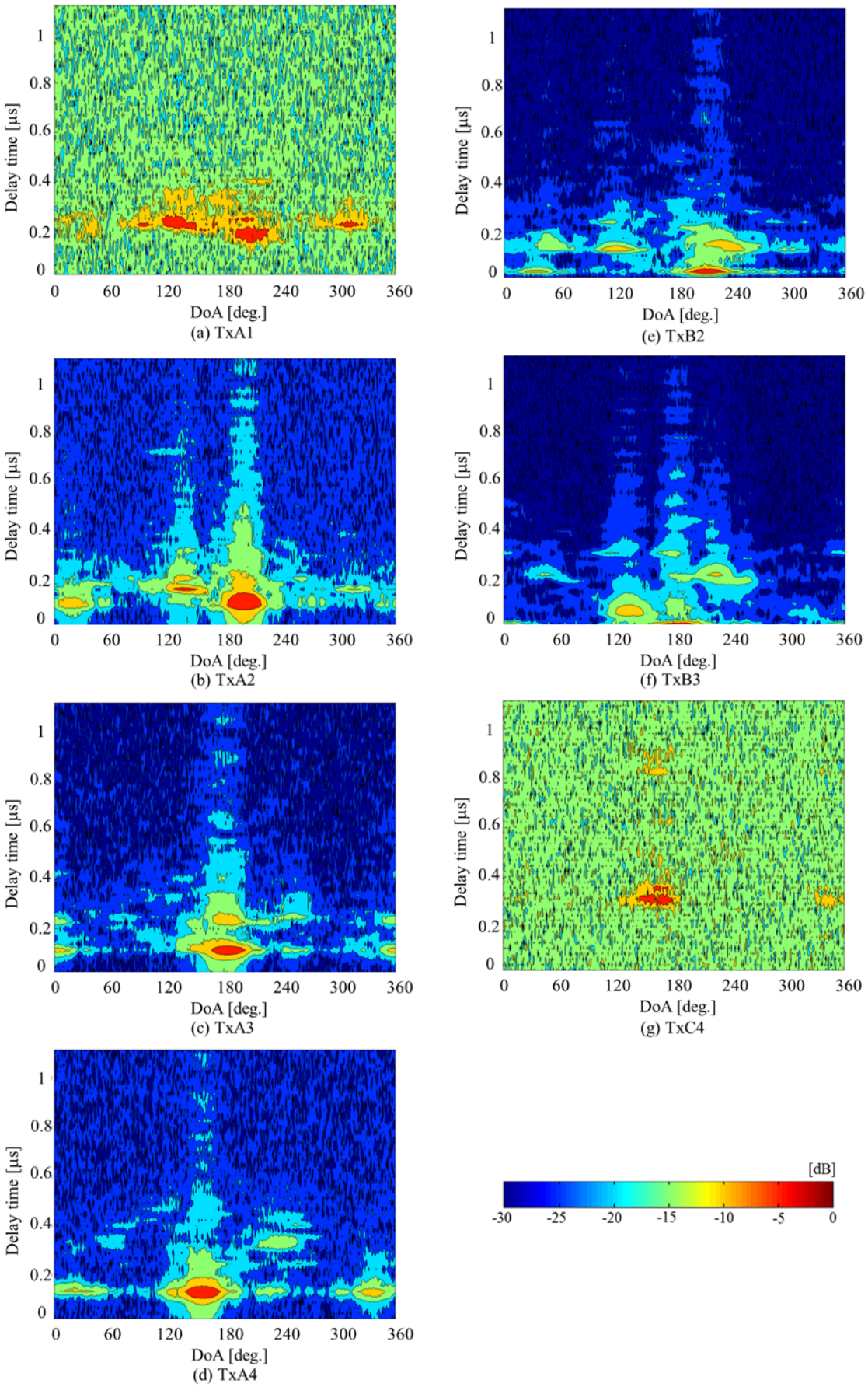

Figure 3.4: Angle of arrival and delay characteristics.

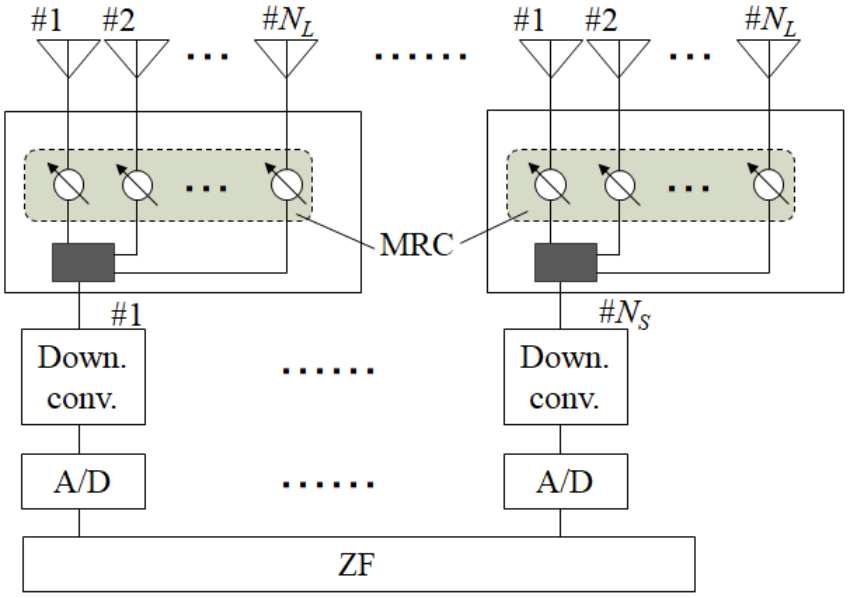

Figure 3.5: An example of analog-digital hybrid beamforming (Uplink).

3.3.2 Calculating the signal-to-interference-plus-noise power ratio (SINR)

The propagation channel for the desired terminal is $h_S \in \mathbb{C}^{N\times 1}$, the propagation channel for the j-th interference terminal is $h_{I(j)} \in \mathbb{C}^{N\times 1}$, and the number of interference terminals is k. Assuming that the l-th propagation channel divided into N_S sub-arrays is $h_S^l \in \mathbb{C}^{N_L\times 1}$ and $h_{I(j)}^l \in \mathbb{C}^{N_L\times 1}$, respectively, the total propagation channel $\boldsymbol{H} \in \mathbb{C}^{N_L\times 1}$ is expressed by the following equation:

$$\begin{aligned}\boldsymbol{H} &= \begin{bmatrix}\boldsymbol{h}_S & \boldsymbol{h}_{I(1)} & \cdots & \boldsymbol{h}_{I(k)}\end{bmatrix} \\ &= \begin{bmatrix}\boldsymbol{h}_S^{(1)} & \boldsymbol{h}_{I(1)}^{(1)} & \cdots & \boldsymbol{h}_{I(k)}^{(1)} \\ \vdots & \vdots & \ddots & \vdots \\ \boldsymbol{h}_S^{(N_S)} & \boldsymbol{h}_{I(1)}^{(N_S)} & \cdots & \boldsymbol{h}_{I(k)}^{(N_S)}\end{bmatrix}\end{aligned} \tag{3.1}$$

The weights $\boldsymbol{w}_{MRC} \in \mathbb{C}^{1\times N}$ and $\boldsymbol{w}_{ZF} \in \mathbb{C}^{1\times N}$ are expressed by the following equations:

$$\boldsymbol{w}_{MRC} = \boldsymbol{h}_S^H \tag{3.2}$$

$$\boldsymbol{w}_{ZF}^T = (\boldsymbol{H}^*\boldsymbol{H}^T)^{-1}\boldsymbol{h}_S^* \tag{3.3}$$

Here, ^{H} is a complex conjugate transpose, * is a complex conjugate, and ^{T} denotes the transposition. Assuming that the thermal noise vector is $n(t) \in \mathbb{C}^{N\times 1}$, the signal-to-interference-plus-noise power ratios (SINRs) for MRC and ZF are expressed by the following equations:

$$SINR_{MRC} = \frac{|\boldsymbol{w}_{MRC}\boldsymbol{h}_S|}{\sum_{j=1}^{k}|\boldsymbol{w}_{MRC}\boldsymbol{h}_{I(j)}| + |\boldsymbol{w}_{MRC}\boldsymbol{n}(t)|} \tag{3.4}$$

$$SINR_{ZF} = \frac{|\boldsymbol{w}_{\boldsymbol{ZF}}\boldsymbol{h}_S|}{\sum_{j=1}^{k}|\boldsymbol{w}_{\boldsymbol{ZF}}\boldsymbol{h}_{I(j)}| + |\boldsymbol{w}_{ZF}\boldsymbol{n}(t)|} \tag{3.5}$$

Moreover, assuming that the MRC weight at the l-th sub-array in the analog part with analog-digital hybrid beamforming is $\boldsymbol{w}_{MRC}^{(l)} \in \mathbb{C}^{1\times N_L}$, it is expressed by the following equation:

$$\begin{cases} \boldsymbol{w}_{MRC}^{(1)} = \boldsymbol{h}_S^{(l)H} \\ \quad\vdots \\ \boldsymbol{w}_{MRC}^{(N_S)} = \boldsymbol{h}_S^{(N_S)H} \end{cases} \tag{3.6}$$

Signals $\boldsymbol{H}_{H_y} \in \mathbb{C}^{N_S\times(k+1)}$, $\boldsymbol{h}_{H_y,S} \in \mathbb{C}^{N_S\times 1}$, and $\boldsymbol{h}_{H_y,I(j)} \in \mathbb{C}^{N_S\times 1}$ multiplied by analog weights are expressed by the following equations.

$$\begin{aligned} \boldsymbol{H}_{H_y} &= \begin{bmatrix} \boldsymbol{h}_{H_y,S} & \boldsymbol{h}_{H_y,I(1)} & \cdots & \boldsymbol{h}_{H_y,I(k)} \end{bmatrix} \\ &= \begin{bmatrix} \boldsymbol{h}_{H_y,S}^{(1)} & \boldsymbol{h}_{H_y,I(1)}^{(1)} & \cdots & \boldsymbol{h}_{H_y,I(k)}^{(1)} \\ \vdots & \vdots & \ddots & \vdots \\ \boldsymbol{h}_{H_y,S}^{(N_S)} & \boldsymbol{h}_{H_y,I(1)}^{(N_S)} & \cdots & \boldsymbol{h}_{H_y,I(k)}^{(N_S)} \end{bmatrix} \end{aligned} \tag{3.7}$$

$$\boldsymbol{h}_{H_y,S}^{(l)} = \boldsymbol{w}_{MRC}^{(l)}\boldsymbol{h}_S^{(l)} \tag{3.8}$$

$$\boldsymbol{h}_{H_y,I(j)}^{(l)} = \boldsymbol{w}_{MRC}^{(l)}\boldsymbol{h}_{I(j)}^{(l)} \tag{3.9}$$

The ZF weight $\boldsymbol{w}_{ZF,H_y} \in \mathbb{C}^{1\times N_S}$ of the digital part and the SINR for analog-digital hybrid beamforming are expressed by the following equations:

$$\boldsymbol{w}_{ZF,Hy}^{T} = (\boldsymbol{H}_{H_y}^{*}\boldsymbol{H}_{H_y}^{T})^{-1}\boldsymbol{h}_{Hy,S}^{*} \tag{3.10}$$

$$SINR_{Hybrid} = \frac{|\boldsymbol{w}_{\boldsymbol{ZF},\boldsymbol{H_y}}\boldsymbol{h}_{H_y,S}|}{\sum_{j=1}^{k}|\boldsymbol{w}_{\boldsymbol{ZF},\boldsymbol{H_y}}\boldsymbol{h}_{H_y,I(j)}| + |\boldsymbol{w}_{ZF,H_y}\boldsymbol{n}(t)|} \tag{3.11}$$

3.3.3 SIR and SINR comparison among MRC, ZF, and hybrid beamforming

The cumulative probability distribution of the signal-to-interference power ratio (SIR) for each UE is plotted in Fig. 3.6, with the desired user located at Tx-B3. Although Tx B3 is closest to the BS, as can be seen in the figure, the range of SIR is approximately from -4 to 6 dB. Therefore, because this environment is regarded as interference dominant, there is the possibility that the SINR is very small, even when the SNR is very high, when interference-cancellation techniques are not used.

The SINR versus location for each UE is plotted in Fig. 3.7 when the desired user is located at Tx-B3 and the other users are interference users. Here, 10% values of the CDF are shown in Fig. 3.7 when the average SNR at Tx-B3 is 30 dB. Note that the relative received power difference among users is reflected in this evaluation. The number of antennas at the BS is 100. The results for BS antennas at $h_1 = 10.85$ and $h_2 = 11.15$ m are plotted in this figure. With analog-digital hybrid beamforming, the number of sub-arrays is 4 and the number of antennas per sub-array is 25. Due to the measurement time, there were no results regarding A1 and C4 when $h_1 = 10.85$ m.

As shown in Fig. 3.7, an SINR greater than 20 dB was obtained using ZF. On the other hand, the SINR with MRC depended on the relationship between the two users. Although the SINR of the analog-digital hybrid beamforming is smaller than that of ZF, the difference is only approximately 1 dB. Hence, hybrid beamforming is effective with fewer receivers. When $h_2 = 11.15$ m, the SINR was greater than 15 dB for A1 and C4 by MRC, because the differences in the angle of arrival between B2 and A1 (C4) were relatively large. However, the SINR was approximately 10 dB for A2, A3, A4, and B2. Although a massive array can reduce interference effectively when considering an i.i.d. channel, it was found that interference could not be sufficiently reduced by MRC in a real propagation environment.

Fig. 3.8 shows the SINR versus the number of antennas at the BS when all seven user terminals were assumed. The desired user was located at B3 and the interference users were located at Tx-A1, A2, A3, A4, B2, and C4. The SINR was 30 dB at B3 and the CDFs are plotted at 10%, 50%, and 90%. The antenna height of the BS was $h_2 = 11.15$ m. With analog-digital hybrid beamforming, the number of sub-arrays was 4, 7, and 10. As shown in Fig. 3.8, the SINR using ZF was greater than 15 dB. When the number of antennas in the BS increased from 1 to 12, the SINR increased drastically. On the other hand, when there were more than 12 antennas, the improvement of the SINR gradually reduced. Moroever, in the case of $N_S = 4$, the SINR from analog-digital hybrid beamforming has insufficient degrees of freedom with respect to the number of UEs, and the SINR is close that with MRC. On the other hand, when $N_S = 7, 10$, where the degrees of freedom of the antenna were more than the number

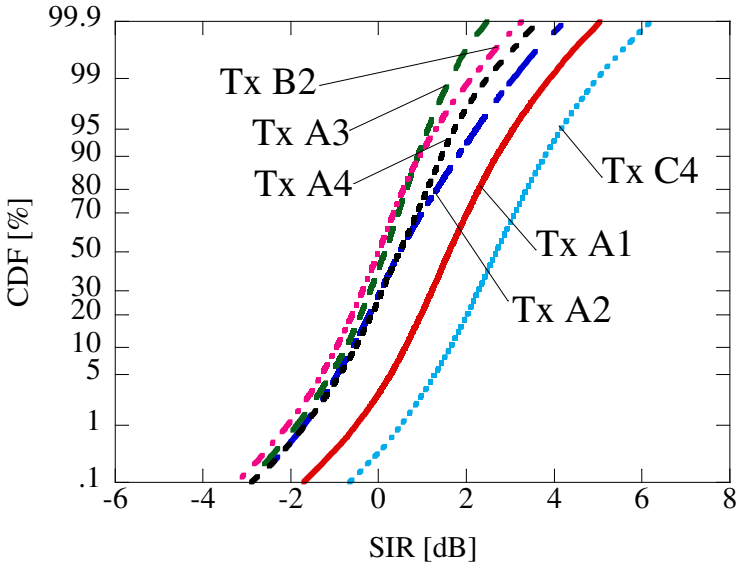

Figure 3.6: SIR of Tx B3 for each UE ($N_U = 2$, where the desired UE is located at Tx-B3).

of UEs, the reduction in SINR is relatively small compared to ZF.

Therefore, either ZF or analog digital hybrid beamforming is essential for interference reduction as a transmission scheme, where the number of sub-arrays is greater than that of the users in massive MIMO systems in real propagation environments. In addition, if SINR degradation can be tolerated, it is effective to use analog-digital hybrid beamforming in terms of reducing the signal-processing burden and improving hardware implementation. If this degradation cannot be tolerated, however, the exclusive use of ZF should be preferred.

3.3.4 Eigenvalue distribution

Fig. 3.9 shows the eigenvalue distribution with 7×7 and 100×7 MIMO channels. The average SNR was 30 dB. The eigenvalue distribution of an i.i.d. channel is also plotted in Fig. 3.9. As shown in Fig. 3.9, when the number of antennas at the BS increased from 7 to 100, the eigenvalues also increased. On the other hand, even when 100 antennas were used at the BS, the sixth and seventh eigenvalues were much smaller than the other eigenvalues. It is therefore clear that this environment features highly correlated propagation channels.

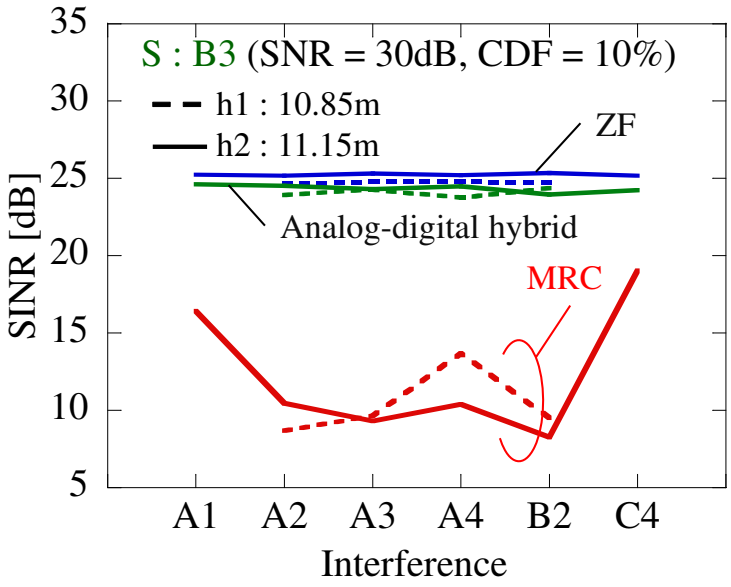

Figure 3.7: SINR comparison versus UE location ($N_U = 2$, where the desired UE is located at Tx-B3).

3.3.5 Channel capacity and achievable bit rate using ZF

the author next compared the Shannon capacity and ABR using ZF, considering an actual propagation channel at the 20 GHz band. The Shannon capacity in the uplink channel, C_S, is denoted as

$$C_S = \sum_{k}^{N_U} \log_2 \left(1 + \frac{P}{N_U \sigma^2} \lambda_k\right), \tag{3.12}$$

where λ_k is the k-th eigenvalue. The eigenvalues are obtained by singular value decomposition of the channel matrix $\boldsymbol{H}$. Here, P and σ^2 are the transmit power and the noise power, respectively. When considering the ABR using ZF, C_{ZF} is derived as follows:

$$C_{ZF} = \sum_{k}^{N_U} \log_2 \left(1 + \frac{SNR_{ZF,k}}{N_U}\right), \tag{3.13}$$

where $SNR_{ZF,k}$ is the k-th SNR obtained from interference cancellation by ZF for the k-th user. In the evaluation, the Shannon capacity (C_S) and ABR (C_{ZF}) are calculated from each subcarrier, and the averaged results are shown. Because the uplink channels were assumed, the transmit power among user terminals was the same. Moreover, the water-filling technique to optimize the received power was not applied to improve the results from Eqs. (3.12) and (3.13) [104].

The Shannon capacity and ABR using ZF for the $7 \times N_U$ and $100 \times N_U$ MIMO channels are plotted in Fig. 3.10, as N_U increased from two to seven. All possible users were selected when the number of users changed. As shown in Fig. 3.10, regardless of the number of users, the results show improved

eigenvalues, particularly for smaller eigenvalues. First, the author focused on the comparison between the Shannon capacity and ABR using ZF when considering the measured MIMO channels. Although the ABR using ZF was much smaller than the Shannon capacity, when $7 \times N_U$ MIMO was applied, the *maximum* achievable bit rate using ZF was obtained owing to massive MIMO transmissions using $100 \times N_U$ MIMO channels. Next, the author focused on the comparison between MIMO channels and i.i.d. channels. As shown in Fig. 3.10, the Shannon capacity for the MIMO channels was smaller than that for the i.i.d. channel, for both $7 \times N_U$ and $100 \times N_U$ MIMO channels, because of the relatively smaller eigenvalues with MIMO compared to those of the i.i.d. channel.

Fig. 3.11 shows the Shannon capacity and the ABR using ZF when 7×7 and 100×7 MIMO channels were assumed. The Shannon capacity and ABR obtained by the i.i.d. channels using ZF are plotted in this figure. As can be seen in Fig. 3.11, the Shannon capacity and ABR using ZF improved when a massive array was used. Although the ABR was much smaller than the Shannon capacity when 7×7 MIMO channels were used, the ABR was almost identical to the Shannon capacity: the maximum bit rate could be obtained even when linear decoding such as ZF was applied for the given propagation channel, owing to the massive number of antennas at the BS. On the other hand, owing to the highly correlated propagation channels, the Shannon capacity achieved by the MIMO channels was 10 to 15 bits/s/Hz smaller than that achieved by the i.i.d. channel.

The Shannon capacity and ABR obtained by ZF are plotted in Fig. 3.12 as the number of antennas at the BS increased. The Shannon capacity and ABR obtained by ZF for i.i.d. channels are plotted in this figure. As shown in Fig. 3.12, the Shannon capacity obtained by MIMO channels was approximately 10 bits/s/Hz smaller than that obtained by i.i.d. channels even when many antennas were used. This was because of the smaller eigenvalues for MIMO channels compared to i.i.d. channels, as shown in Fig. 3.9. On the other hand, when the number of antennas exceeded 50, the ABR obtained by ZF was almost the same as the Shannon capacity.

3.4 Conclusion

This chapter evaluated the basic performance of massive MIMO systems by considering the CSI in the 20 GHz band in outdoor environments. The results show that, unlike i.i.d. channels, MRC is unsuitable as a transmission scheme for massive MIMO systems, owing to highly correlated propagation channels. Therefore, either ZF or analog digital hybrid beamforming is essential for interference reduction as a transmission scheme, where the number of sub-arrays is greater than that of the users in massive MIMO systems in real propagation environments.

The Shannon capacity and ABR achieved by ZF were compared by considering seven-user MIMO transmissions with 100 elements at the BS. When the number of degrees of freedom in the array antenna was guaranteed, the ABR was almost the same as the Shannon capacity, and multi-user transmission was realized by linear decoding. Therefore, decoding methods such as ZF are effective in massive MIMO systems.

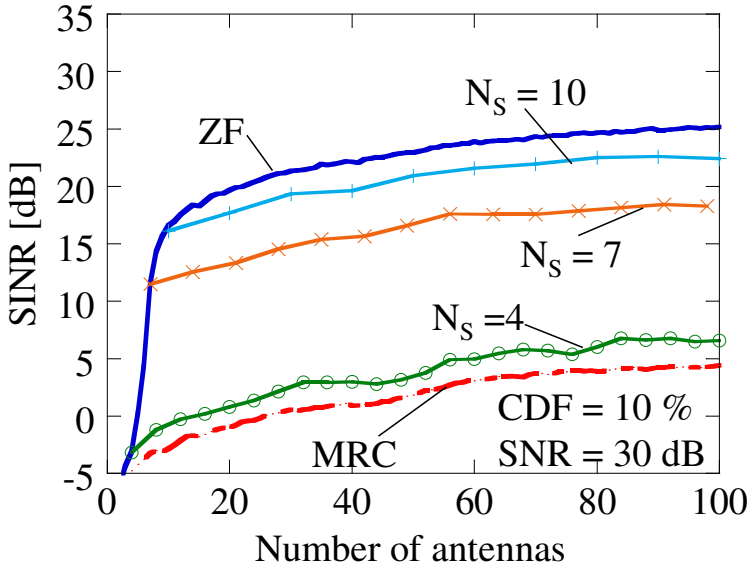

(a) CDF = 10 %

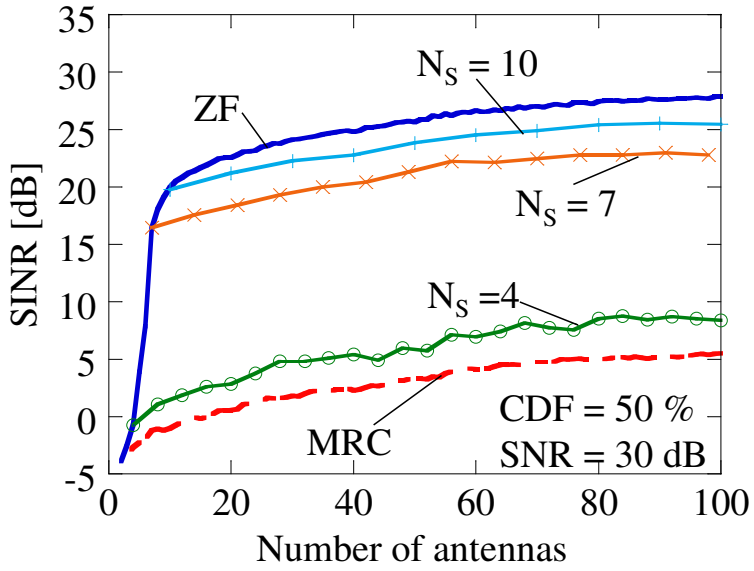

(b) CDF = 50 %

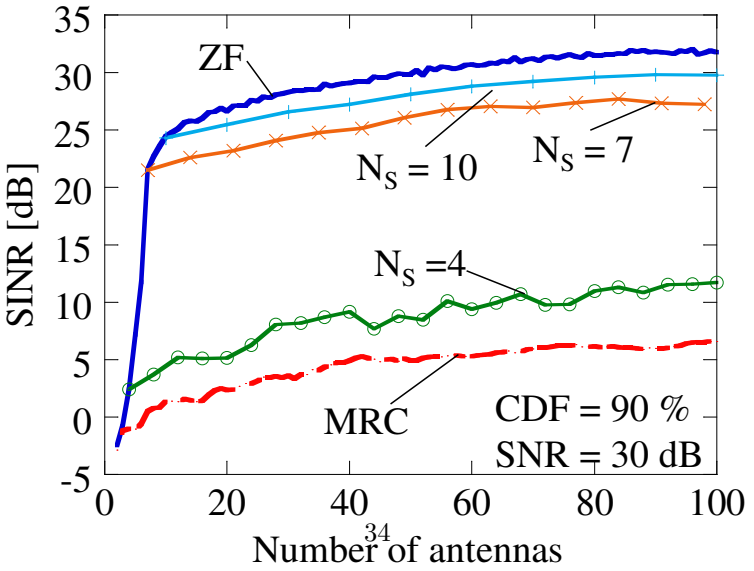

(c) CDF = 90 %

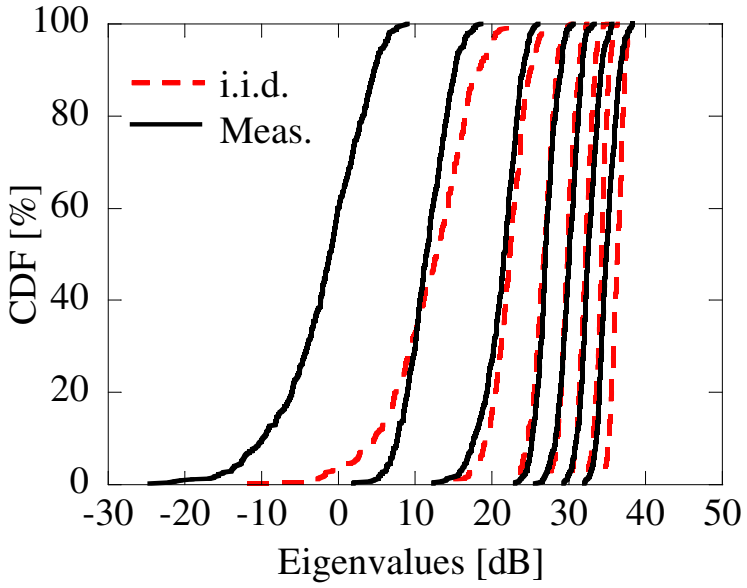

(a) 7x7 MIMO

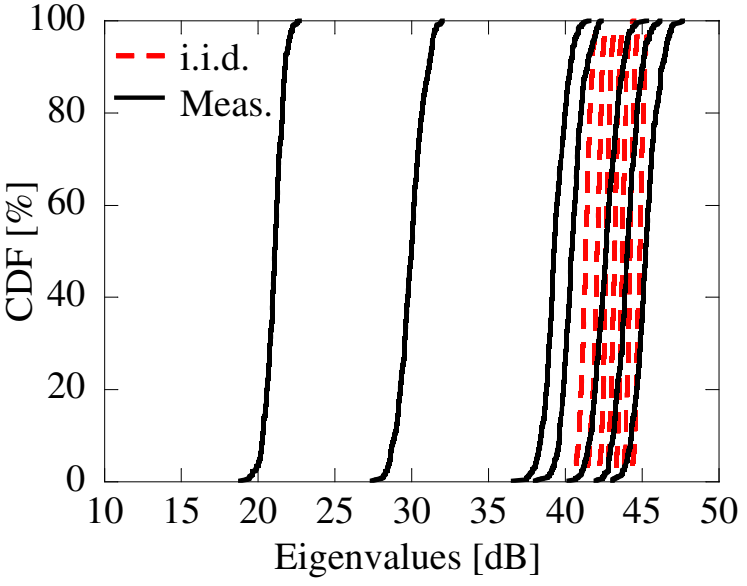

(b) 100x7 MIMO

Figure 3.9: Eigenvalue distributions (7x7 MIMO and 100x7 MIMO).

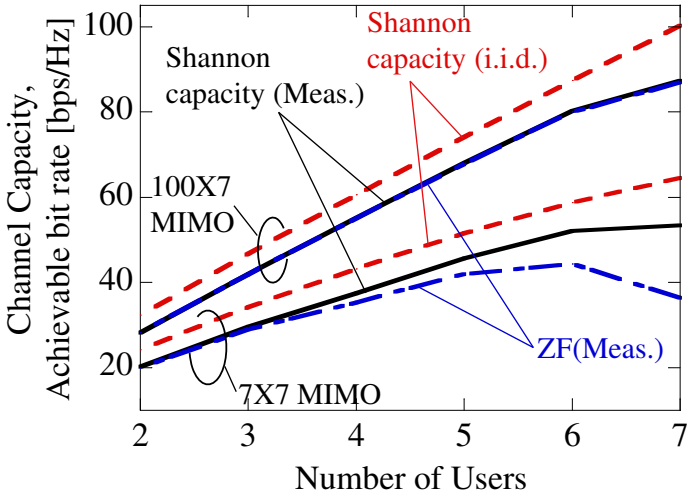

Figure 3.10: Channel capacity and ABR using ZF versus the number of users (SNR = 30 dB).

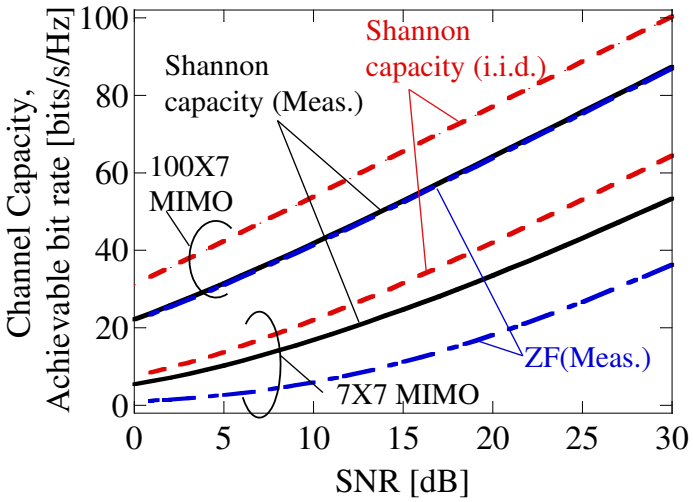

Figure 3.11: Channel capacity and ABR obtained by ZF versus SNR ($N_U = 7$).

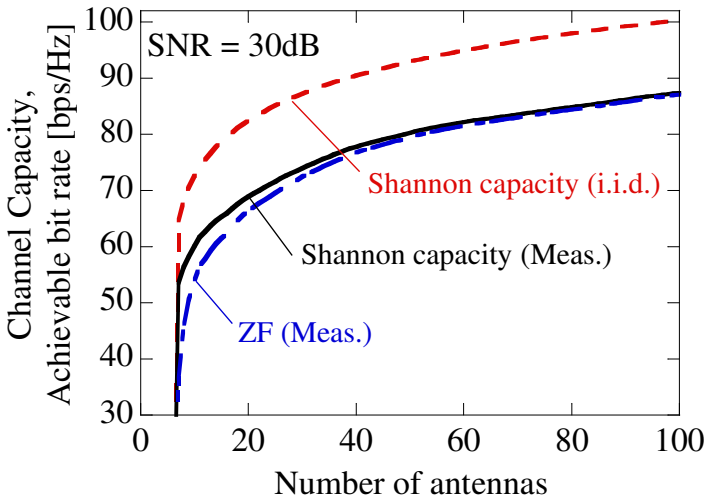

Figure 3.12: Channel capacity and ABR obtained by ZF versus the number of antennas at the BS ($N_U = 7$).

Chapter 4

Digital analog Fusion control method

This chapter describes the hardware configuration and signal processing method for digital-analog fusion control, which is one of the issues of Massive MIMO shown in chapter 2. First, the hardware configuration is shown, and the transmission / reception mechanism is briefly described. After that, a received signal demodulation method that does not require CSI is proposed and evaluated.

4.1 Introduction

Massive MIMO enables low-complexity signal processing, because the inter-user interference is easily mitigated by a high beamforming resolution [36].

Generally speaking, it is essential to estimate the channel state information (CSI) in MIMO/MU-MIMO systems [22]. However, when CSI feedback from user terminals (UTs) to the BS is employed, there occurs a very large overhead compared with the communication data, especially when there are a large number of antennas at the BS. The countermeasure of *implicit* beamforming (IBF) has been proposed [106]. IBF exploits channel reciprocity in time-division duplex (TDD) mode: the transmit frequency is the same as the receive frequency. IBF can be used in WLAN systems. Because massive MIMO will be used in small cell systems, the TDD mode should be used from the point of view of frequency utilization. However, calibration technique is essential for IBF and several methods have been proposed [107][108]. However, even if implicit beamforming is applied for the massive MIMO system, the CSI estimation itself is still large overhead when considering the short packet communications such as Wireless LAN systems [**?**].

The authors have proposed analog-digital hybrid massive MIMO configuration which eliminates CSI estimation itself by applying analog multi-beam and their selection and blind algorithm using

constant modulus algorithm (CMA) [109][110]. In conventional analog-digital hybrid massive MIMO configuration [93], although CSI estimation itself is not needed, beam scanning is required for user tracking and overhead to determine analog weight values arises. Unlike conventional analog-digital hybrid massive MIMO configuration, *analog* multi-beams are created for initial user tracking and several beams that received powers are high are selected. Thanks to selected narrow beams, interference signals can be mitigated and residual interference is cancelled by using CMA [**?**] which does not require any training signals in digital part. Because the proposed method does not need CSI estimation, very high transmission efficiency can be obtained and flexible communication with random user transmission by user terminal (UT) can be realized. Via computer simulation, the basic performance and effectiveness was evaluated by the proposed method. "In [110], the practical switch configuration has proposed using many-one switch instead of matrix switch. In the configuration, beam with maximum power from each switch is selected and the transmission performance by using many-one switch is not degraded compared to that by using matrix switch. Hence, the proposed configuration realizes realistic beam selection. Hence the author assume ideal beam selection with high power using matrix switch.

In the previous study, QPSK signals are uses as modulation scheme because CMA basically focus on modulation schemes with constant modulus such as GMSK and QPSK [111][112]. However, it is essential to use high order modulation schemes when considering very high throughput with massive MIMO systems. It is reported that QAM signals can be utilized with CMA by applying data smoothing that weights of CMA are averaged with multiple samples [113][114]. However, these evaluations are based on basic two wave propagation condition without Rayleigh fading [113] and deferential detection to decode QAM signal [114]. In the differential detection, the signals are decoded by using two adjacent signals at the receiver. In this chapter, amplitude and phase compensation method for high order modulation schemes such as QAM signals is proposed in order to realize a practical implement considering fading environment and coherent detection which are essential for mobile communication systems, when using analog multi-beam massive MIMO with CMA in the digital part. Moreover, the effectiveness of proposed method is verified by bit error rate (BER) with coherent detection when assuming Rayleigh fading with angular spread environment.

This chapter is organized as follows. In Sect. 2, the author begin with the principle of analog multi-beam massive MIMO with CMA in the digital part. The issue of CMA when using QAM signals with coherent detection in fading environment is shown in Sect. 2. The proposed amplitude and phase compensation method for QAM signals is denoted in Sect. 3. The BER performances are presented to verify the effectiveness of the proposed method in Sect.4.

4.2 Multi-beam massive MIMO configuration using CMA and its issue for high order modulation scheme

4.2.1 Multi-beam massive MIMO configuration using CMA

Fig. 4.1 shows the configuration by using *analog* multi-beam massive MIMO and CMA in the digital part. The configuration in Fig. 4.1 assumes uplink communications. The flowchart using proposed configuration in Fig. 4.1 is shown in Fig. 4.2. The detailed flow in Fig. 4.2 is shown hereafter. In the proposed method, M orthogonal multiple beams are prepared at analog part. Fig. 4.3 shows an example of multi-beam patterns. The received powers for all the users are measured at the output of multiple beams. Selected number of beams is identical to or more than number of users (K). The user tracking is realized by the beam selection without CSI estimation.

Key question is how to realize the hardware of multi-beamforming network in the analog part. It is well known that butler matrix realizes multi-beam pattern [115][**?**]. In addition, lens antenna was proposed to realize multi-beam forming network.

The MU-MIMO transmission without CSI estimation for each user is realized by the circuit in Fig.4.4. However, when direction of arrivals (DoAs) are close among users, same beam must be utilized for each user. Moreover, the signals by users except intended user are actually received at side lobe and the interference cannot be rejected by only multi-beam forming network. In order to realize the perfect interference rejection, digital beam forming (DBF) based blind adaptive array is introduced at the output of selected multi beams.

In this chapter, constant modulus algorithm (CMA) is used as the blind adaptive algorithm [**?**][**?**]. The CMA works only received signals and does not need CSI. In addition, CMA reduces the interference with environment where carrier and timing offset exist. Hence, hybrid configuration with multi beams in the analog part and blind algorithm in the digital part is suitable for efficient transmission in massive MIMO system.

The proposed configuration can be regarded as FFT based CMA adaptive array [79]. The configuration in [79] is digital beam forming (DBF) and multi-beam forming network is in the digital part. On the other hand, main feature of proposed configuration is that multi-beam is realized by analog part and the numbers of frequency convertors and analog to digital / digital to analog convertors can be reduced unlike DBF configuration. Moreover, transmission timings by UTs are not needed to be synchronized.

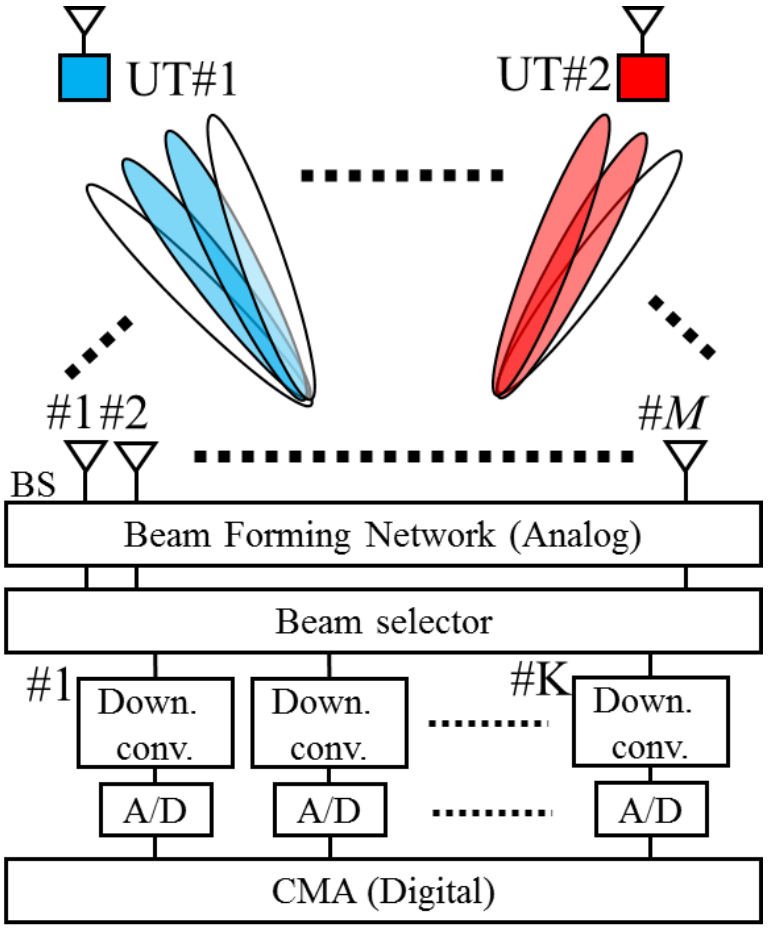

Figure 4.1: Configuration by using multi-beam massive MIMO and CMA

4.2.2 Principle of CMA and its issue for high order modulation

The principle of CMA is explained hereinafter. The CMA is categorized as blind adaptive array because this algorithm requires only information of received signals and the CMA works with constant amplitude modulation such as GMSK and QPSK. When using the CMA after multi-beam selection in massive MIMO configuration, miscapture problem, which the interference is captured and the desired signal is cancelled, is solved. The cost function Q of CMA is denoted as

$$Q = E\left[\left||y(t)|^p - \sigma^p\right|^q\right], \tag{4.1}$$

where y is output electricity of the array and $\sigma(>0)$ is a constant value and usually set to be power of desired signal. p and q are positive integer and these values are one or two.

Although the weight of CMA adaptive array is updated by using Eq.(4.1), it is not possible to express the optimum weight directly in closed form, because Eq.(4.1) is non-linear with respect to the

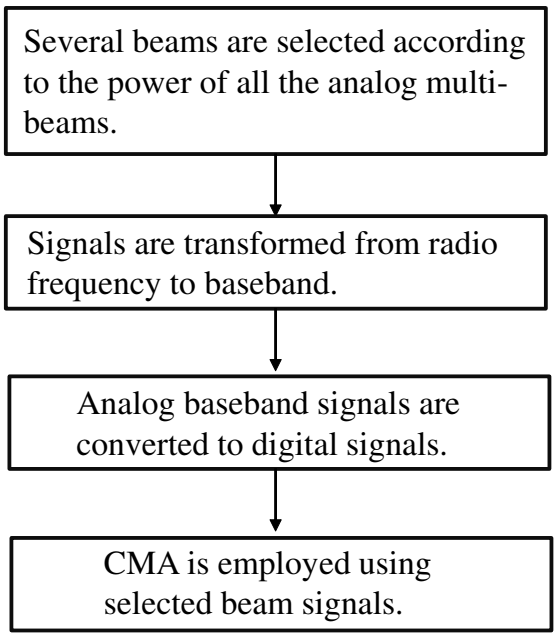

Figure 4.2: Flowchart using proposed configuration.

weight. Therefore the weight of CMA is controlled by an asymptotic technique such as the steepest descent method so that Eq.(4.1) is minimized. Fig. 4.4 shows the block diagram of CMA adaptive array.

If the weight and the cost function after m iterations are $\boldsymbol{W}(m)$ and $Q(m)$, then the weight updating equation by the steepest descent method is

$$\boldsymbol{W}(m+1) \quad = \quad \boldsymbol{W}(m) - \mu \nabla_W Q(m), \tag{4.2}$$

where m is the repetition number of times of the weight update.

Where μ is the step size. Also, $\nabla_W Q(m)$ is the slope vector of Q with respect to $\boldsymbol{W}$. In the steepest descent method, step size determines convergence characteristics of weight on the CMA adaptive array.

In order to improve the performance of CMA adaptive array, least square CMA (LS-CMA) is proposed [**?**]. The convergence of weight by LS-CMA is much faster than that by steepest descent method. The weight updating equation by LS-CMA is denoted as

$$\begin{aligned} \boldsymbol{W}_{L+1} &= \boldsymbol{W}_L - \Gamma(i) \sum_{i=1}^{N} \boldsymbol{X}(i) \left[y^*(i) - \delta^*(i) \right] \\ &= \Gamma(i) \left[\sum_{i=1}^{N} \boldsymbol{X}(i) \delta^*(i) \right]^{-1} \end{aligned} \tag{4.3}$$

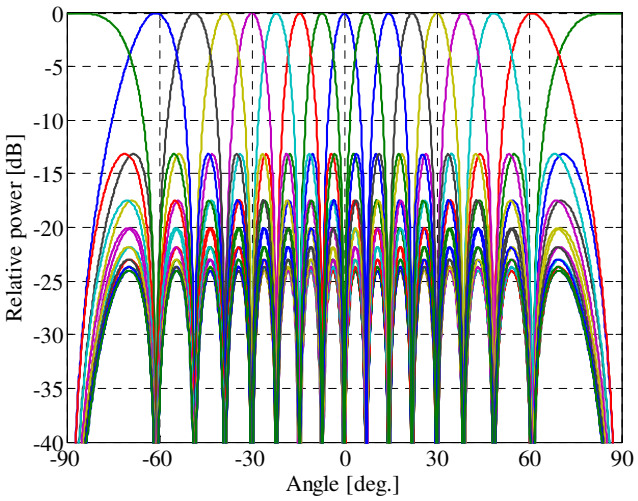

Figure 4.3: Multi-beam patterns (16-beam).

$$\Gamma(i) = \left[\sum_{i=1}^{N} \boldsymbol{X}(i)\boldsymbol{X}^H(i)\right]^{-1} \tag{4.4}$$

$$\delta^*(i) = \frac{\sigma}{|y(i)|}y(i) \tag{4.5}$$

$\boldsymbol{X}(i)$ and $y(i)$ are input vector and output signal at i-th sample ($i = 1, \cdots, N$), respectively. Fig. 4.5 shows an example of constellation when CMA is applied for QPSK and 16QAM signals. In this simulation, only two waves and AWGN channel are assumed: Rayleigh fading is not considered. The direction of arrivals (DoAs) on two waves are 0 and 60 degrees, respectively. Four element linear array is used and element spacing is 0.5 wavelengths. The signal to interference power ratio (SIR) and signal to noise power ratio (SNR) are set to be 3 and 20 dB, respectively.

As can be seen in Fig.4.5(a)(b), it is observed that CMA cancels the interference when using not only QPSK signal but also 16 QAM signals. On the other hand, because the carrier offset compensation is not employed when considering only CMA, the constellations have a tilt for both QPSK and 16QAM. Moreover, because differential detection was applied in the previous studies [113][114], the ability of CMA must be evaluated when considering fading environment and coherent detection which are essential for mobile communication systems

4.3 Amplitude and phase compensation method

As shown in Sect. 2, it is necessary to correct amplitude and phase errors after the convergence of weight by CMA because CMA dose not control the phase information. Fig.4.6 shows an example of

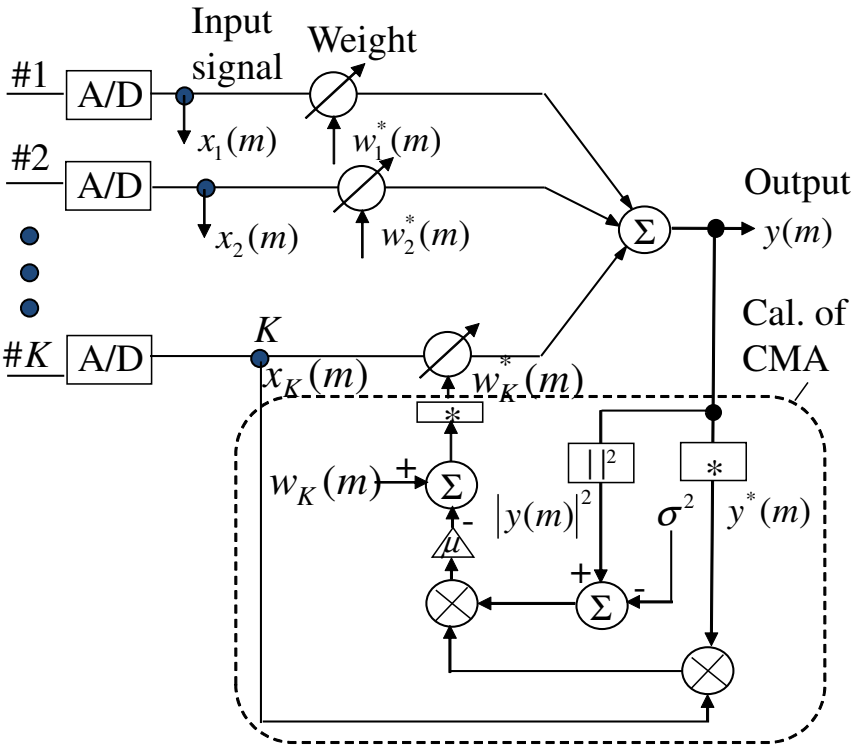

Figure 4.4: Block diagram of CMA adaptive array with steepest descent method (p=2, q=2).

constellation on 16QAM when applying the CMA in Rayleigh fading environment. Because the CMA does not control the phase, the signals are rotated like AWGN channel. Moreover, amplitude is also changed due to fading channel. Although differential detection, which does not need amplitude and phase offset compensation, can be applicable for QPSK, the coherent detection is essential for QAM.

In this chapter, the amplitude and phase compensation method is introduced as the processing after the CMA by using training signal which is applied for user identification (ID). Because user ID is basically essential for general wireless communication systems, this training signal is not overhead at all compared to the control signal for CSI estimation.

When P_k and P'_k are k-th transmit signal and receive signal after the CMA, respectively, compensated amplitude, A and phase, θ is denoted as

$$A = \frac{1}{n}\sum_{k=1}^{n}\frac{|P'_k|}{|P_k|} \tag{4.6}$$

$$\theta = \frac{1}{n}\sum_{k=1}^{n}(\tan^{-1}(P_k) - \tan^{-1}(P'_k)), \tag{4.7}$$

where L is number of training bits. The received signal can be compensated by using A and θ.

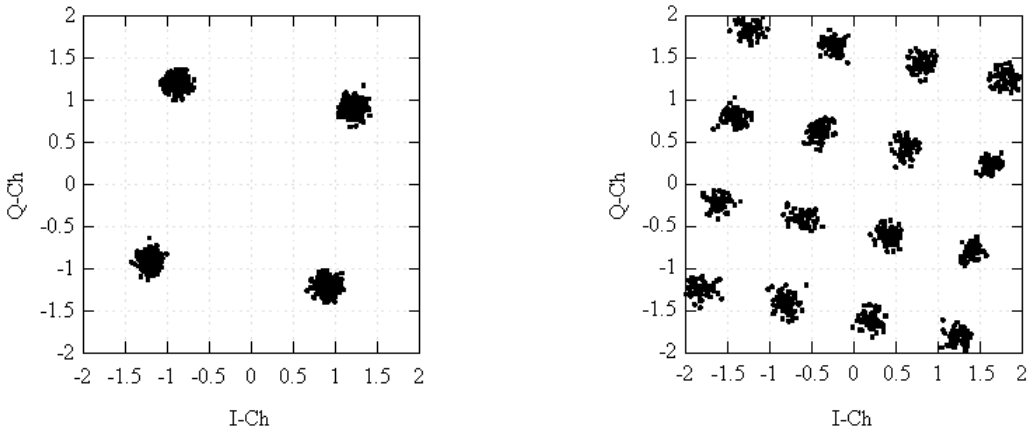

(a) QPSK (b) 16QAM

Figure 4.5: Constellations after CMA. (2-wave, AWGN channel, Input SNR=20dB, Iuput SIR=3dB)

When $\boldsymbol{Y}$ is the output signal after CMA, compensation signal, $\boldsymbol{Y'}$ is denoted as

$$\boldsymbol{Y'} = \frac{\boldsymbol{Y}}{A} \exp(j\theta). \tag{4.8}$$

The CMA itself dose not distinguish a desired signal and interference signal, because the user who transmits the desired signal is unclear. Hence, it is essential to identify the desired user. It is solved by giving a header of user ID. Because a certain frame basically gives user ID in advance, this ID can be decoded after the proposed method with CMA.

4.4 Effectiveness of proposed method

The effectiveness of proposed method is verified by using QAM signals when considering Rayleigh fading and angular spread. Table 1 shows basic simulation parameters. The trial for different propagation conditions are carried out and the bit rate is obtained. When the bit rate is R, R is denoted as $R = S(1 - BER)$ [bits/symbol] where S denotes number of bits per symbol [116][117]. If the BER is greater than 10^{-3}, the author assume that R is zero [116][117]. Table I shows the simulation conditions. The proposed method was assessed by computer simulation based on the above-mentioned principle.

Fig. 4.7 shows the definition of multipath model in the simulation. As can be seen in Fig. 4.7, scattering ring model around UTs and angular spread at the BS are assumed. Rayleigh fading channel is generated by using multipath signals for scattering ring model. The number of waves is 11 for each user and phase conditions are different between users: i.i.d. Rayleigh fading scenario is assumed.

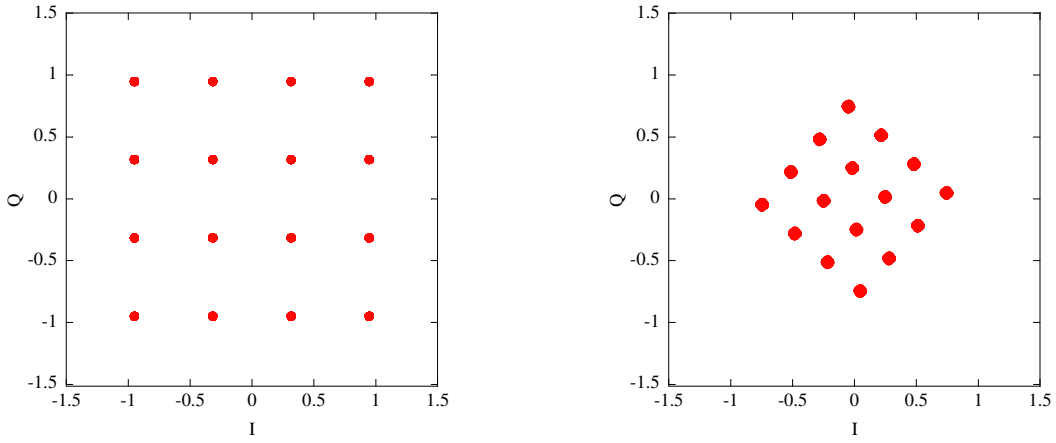

(a) Before CMA
(Transmit signal)

(b) After CMA
(Receive signal)

Figure 4.6: An example of constellation in Rayleigh fading channel (16QAM).

Table 4.1: Simulation conditions.

Number of receiving antennas and beams	64
Number of beams for each user	1
Number of UTs	2
Angular spread	10 degrees
Number waves	11
Data length	1,024
Data smoothing size for weight update CMA	16
Trial number	10,000
Training bits for compensation of amplitude and phase errors after the CMA	5

The liner array is used in this chapter. When the number of received anntenas is N_R and r_i and $\theta_i (i = 1, \cdots, L)$ are i-th amplitude and phase of received signal propagation channel, h_n which is $n (= 1, \cdots, N_R)$-th propagation channel is denoted as

$$h_n = \frac{1}{\sqrt{L}} \sum_{i=1}^{L} r_i \exp(j\theta_i) \exp(j \frac{2\pi}{\lambda_0} d(n-1) \sin \phi_i) \tag{4.9}$$

where L is number of waves for each UT and $\phi_i (i = 1, \cdots, L)$ is i-th angle of arrival (AoA). AoA means that direction at the received array and the definition of $\phi_i (i = 1, \cdots, L)$ is denoted in Fig. 4.7. Angular spread is $\phi_L - \phi_1$ in this chapter.

The effectiveness of proposed amplitude and phase compensation method for analog multi-beam

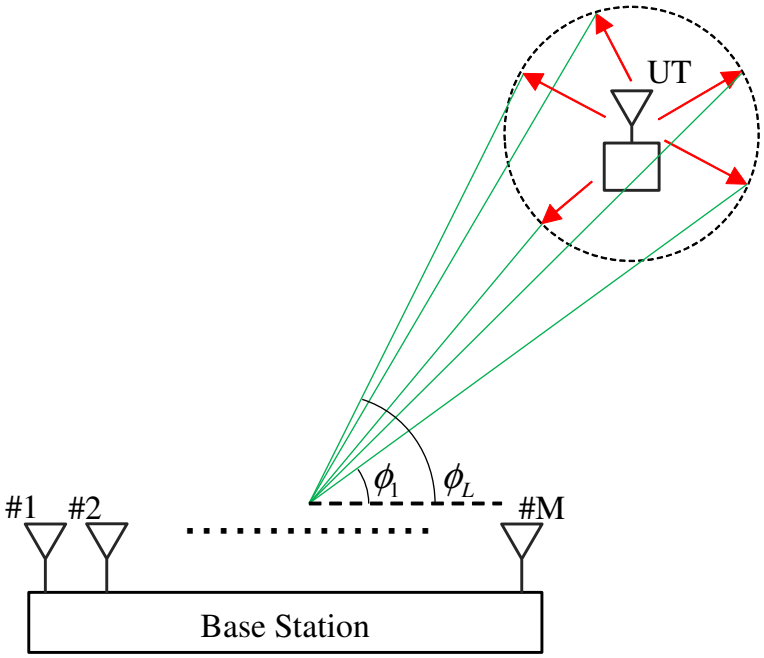

Figure 4.7: Concept of scattering ring model and the angular spread.

massive MIMO with CMA in the digital part is verified. Fig. 4.8 shows the BER versus the SNR. 256QAM is applied in this simulation. As shown in Fig. 4.8, BER is not improved at all even if the SNR is increased without amplitude and phase compensation. On the other hand, with the proposed compensation shown in Sect. 3, the BER can be improved to some extent when the SNR is increased. This result shows that the amplitude and phase compensation is essential after the CMA. However, the BER is not sufficiently improved even in SNR = 30 dB.

In order to exam how to reduce the BER in Fig. 4.8 when cumulative distribution function (CDF) is considered, the CDF versus BER is plotted in Fig.4.9. The SNRs are set to be 10, 20, and 30 dB in Fig.4.9. When the SNRs are 10, 20, 30 dB, the CDFs is 0, 28, and 85% where the BER is not less than 10^{-3}. Therefore, the BER cannot be improved even if the high SNR is obtained in average sense. Generally speaking, the modulation scheme should be selected according to a given propagation condition. Next, the author show the bit rate when applying adaptive modulation scheme which selects optimal modulation scheme. In the following results, the adaptive modulation means that the highest order modulation scheme is selected when the BER is less than 10^{-3}. The adaptive modulation is applied to the results in Figs. 4.11, 4.12 and 4.13.

In order to verify the effectiveness by the adaptive modulation scheme, Fig.4.10 shows the selection probability for each modulation scheme versus the SNR by multi-beam processing, CMA, and proposed

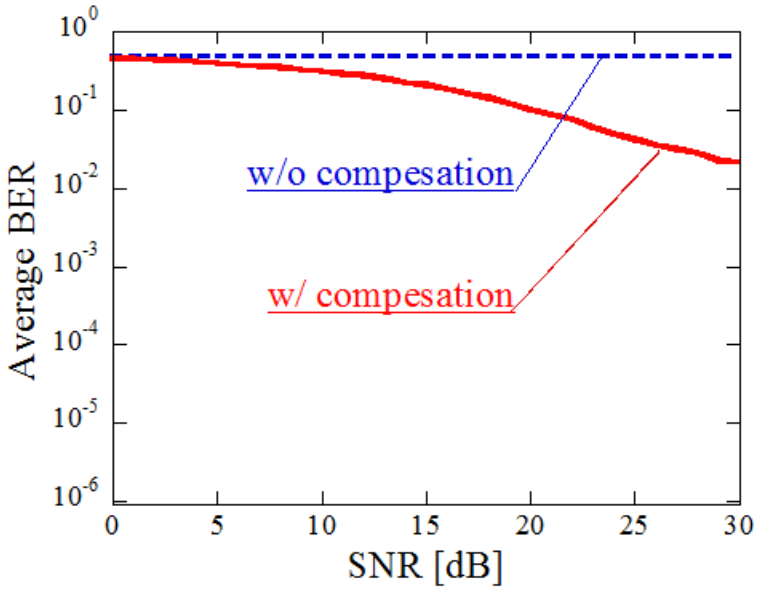

Figure 4.8: BER versus the SNR.

amplitude and phase compensation method. The difference of AoA between two users is 60 degree. As can be seen in Fig.4.10, the higher order QAM is selected, when the SNR is increased.

Fig. 4.11 shows bit rate versus the SNR. In Fig.4.11, the modulation scheme with maximum bit rate is selected to when BER is less than 10^{-3}. The difference of AoA between two users is set to be 0 to 60 degrees. As can be seen in Fig.4.11, the bit rate is improved when the AoA is wider and the performance is saturated when the AoA is greater than 30 degree. From these result, it is shown that QAM signals can be applicable for the multi-beam Massive MIMO system by using the proposed amplitude and phase compensation method.

Fig. 4.12 shows bit rate versus the AoA. Fig. 4.13 shows bit rate versus angular spread when SNR is 20dB. As can be seen in Fig.4.12, the bit rate is saturated at AoA = 30 deg. in each SNR. This is because the angular spread is 10 deg. As can be seen in Fig.4.13, the bit rate is decreased when the angular spread is wider. However, the influence due to wider angular spread is small when the AoA is greater equal to 30 deg. This results indicate that users which are spatially separated should be selected by using spatial correlation.

4.5 Conclusion

In this chapter, in order to achieve the further higher transmission rate, the amplitude and phase compensation scheme is proposed when using the CMA with amplitude and phase modulation scheme

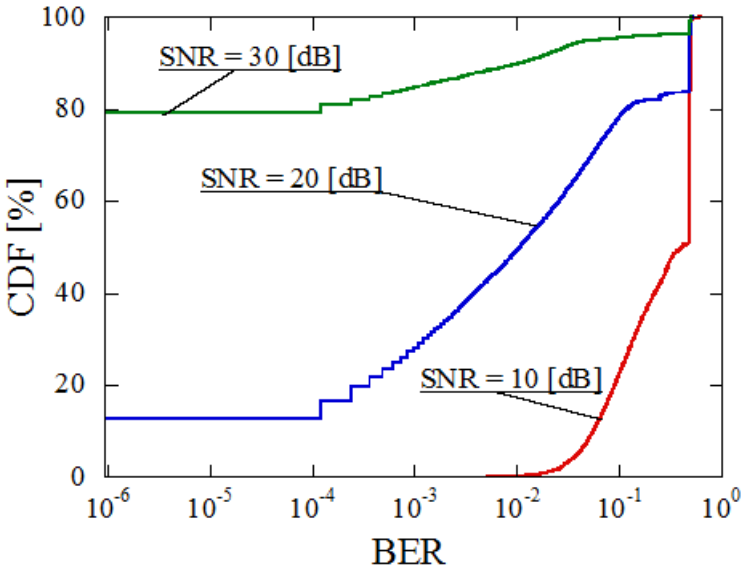

Figure 4.9: Cumulative distribution function versus BER.

such as QAM. The effectiveness of proposed method is verified by the computer simulation. It is shown that QAM signals can be applicable for the multi-beam Massive MIMO system with CMA by using the proposed amplitude and phase compensation method, even if the multi path environment with QAM signals is assumed.

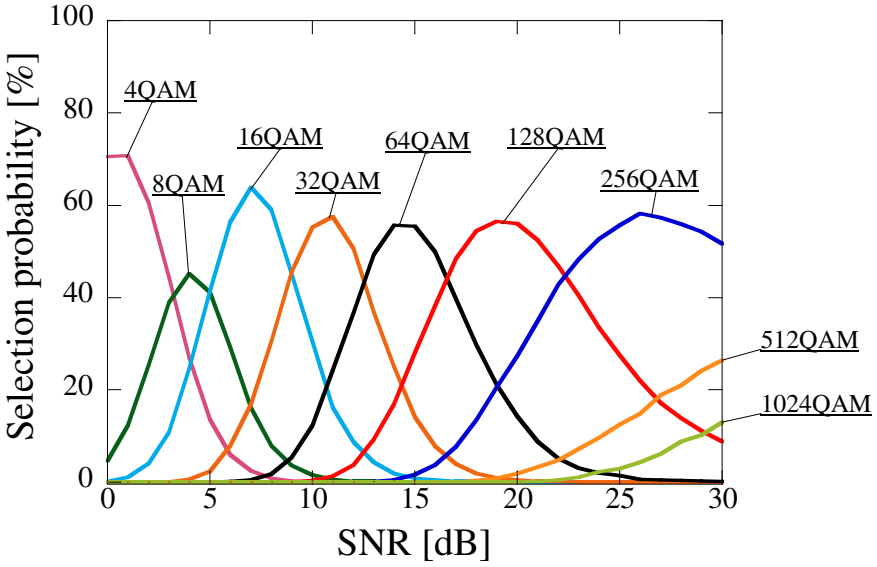

Figure 4.10: Selection probability versus the SNR.

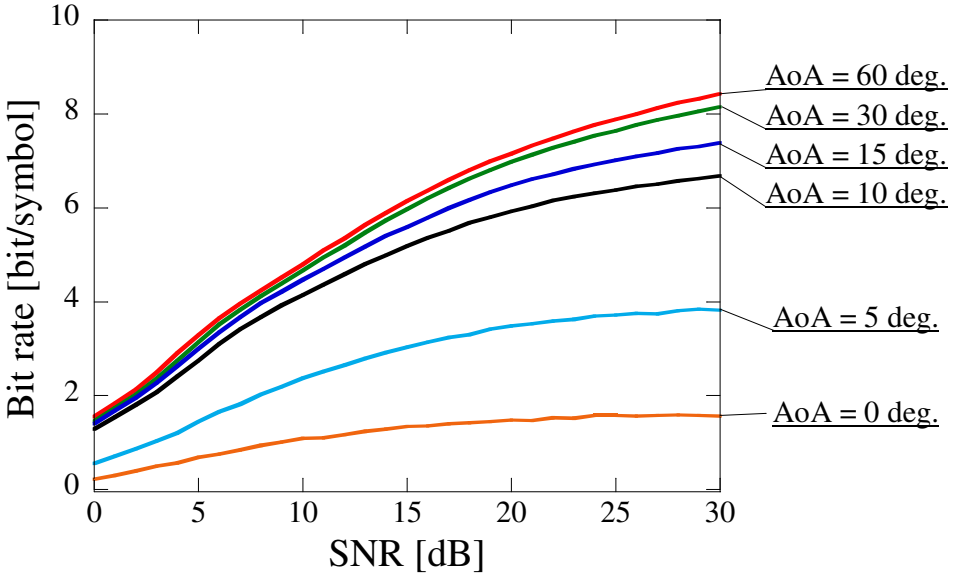

Figure 4.11: Bit rate versus the SNR.

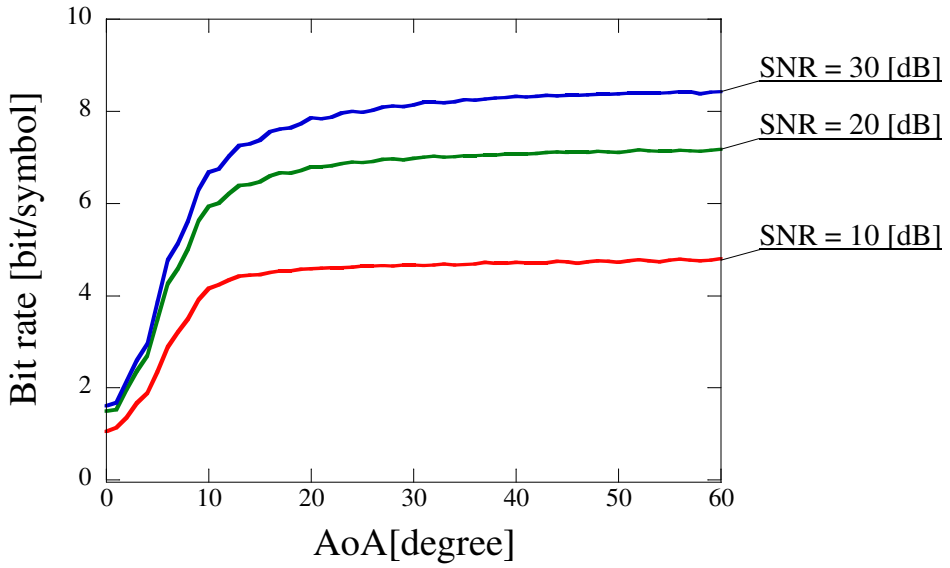

Figure 4.12: Bit rate versus AoA.

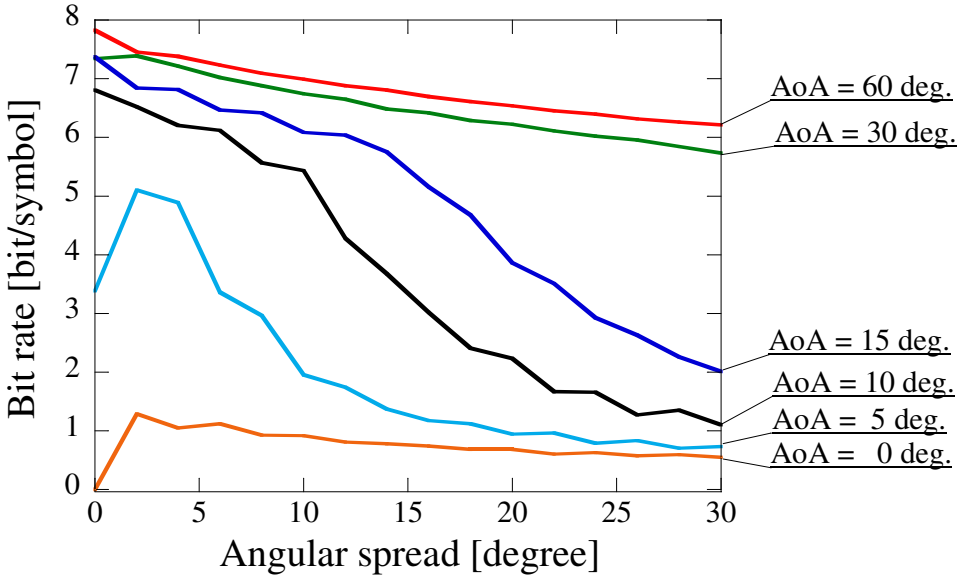

Figure 4.13: Bit rate versus angular spread.

Chapter 5

Interference Elimination and Control Signal Reduction Method

This chapter evaluates and describes modulation method estimation using deep learning as one of the methods for eliminating interference and reducing the number of control signals.

5.1 Introduction

In the study of MIMO and MU-MIMO, including Massive MIMO, the directivity control on the transmitting side and the decoding technology on the receiving side have been the primary focus in [**?**]. That is, many studies have been conducted on the physical layer (PHY). However, in MIMO / MU-MIMO, using the information of the propagation channel (Channel State Information: CSI) is a major premise, which expresses the propagation characteristics during transmission and reception, so the efficiency with which this information can be acquired should be considered. In other words, it is important to evaluate not only the PHY level but also the MAC layer [**?**]. In particular, when using transmission directivity control, which is essential for MU-MIMO, it is generally necessary to feedback CSI from the terminal to the base station, which significantly reduces communication efficiency. In addition, as an improvement method, a method that eliminates the need for CSI feedback (Implicit Beamforming: IBM) [**?**] has been proposed. However, even if IBF is used, if the data size is small, the application of Massive MIMO will reduce the overall communication efficiency [132].

Therefore, the authors proposed a method that eliminates the need for CSI estimation itself in the analog–digital hybrid Massive MIMO control method by forming a multibeam in the analog section [**?**]. In the conventional analog / digital hybrid Massive MIMO control method, it is premised that the phase shifter is used for analog control. [**?**]-[130]. However, in this case, to form a beam to a desired terminal in the analog unit, it is necessary to perform a beam scan while changing the phase shifter,

which causes a problem in that initial acquisition to the desired terminal takes time. In the proposed method, multibeam formation is performed in the analog section, and beam selection is performed to select only the beam with a high received power. Only the output signal is frequency converted to realize digital signal processing. In the digital section, the Constant Modulus Algorithm (CMA) [72], which realizes interference elimination only with the received signal, is applied. The proposed system allows terminals to send information at random. In addition, the effectiveness of the proposed system has been clarified by performing computer simulations [133] [134].

In the studies so far, the author has evaluated the operating characteristics of a system that uses multibeam Massive MIMO and CMA together when multi-value modulation is used. At that time, when applying CMA by multivalue modulation, it is necessary to correct the phase rotation and amplitude value after weight convergence, so the author proposed a correction method using a pilot signal **??**. However, this method assumes that the modulation method is known. In actual communication, communication starts with the modulation method being unknown, thus it is necessary to share the modulation method by transmission and reception in advance; but in that case, the communication increases the overhead requirements. Therefore, in this chapter, we estimate the modulation method of the received signal of multibeam Massive MIMO using a convolutional neural network (CNN) [127], which involves machine learning, and we verify its basic performance.

5.2 Convolutional neural network

A convolutional neural network (CNN) is a deep learning method employed for classification problems using images as inputs [127]. Figure 5.1 shows the configuration of a CNN, which is a neural network composed of three layers, namely, a convolutional layer, pooling layer, and fully connected layer, and it is modeled on the vision of living things [137]. The image is first input to the convolution layer. Then, the convolution layer and the pooling layer are repeated several times, and it is afterward connected to the fully connected layer and becomes an output. In the convolution layer, the input image is processed by multiple filters, and because of the filtering, the input image is converted into multiple images representing the features. Next, the size of the image is compressed in the pooling layer so that it does not impair the characteristics of the image, and it is connected to the fully connected layer.

5.3 Modulation method estimation using CNN

In this chapter, a model is created using CNN and the modulation method is estimated. For the image shown in Figure 5.2, determine whether the received signal is $4 \sim 64$ QAM. The table 6.1 shows

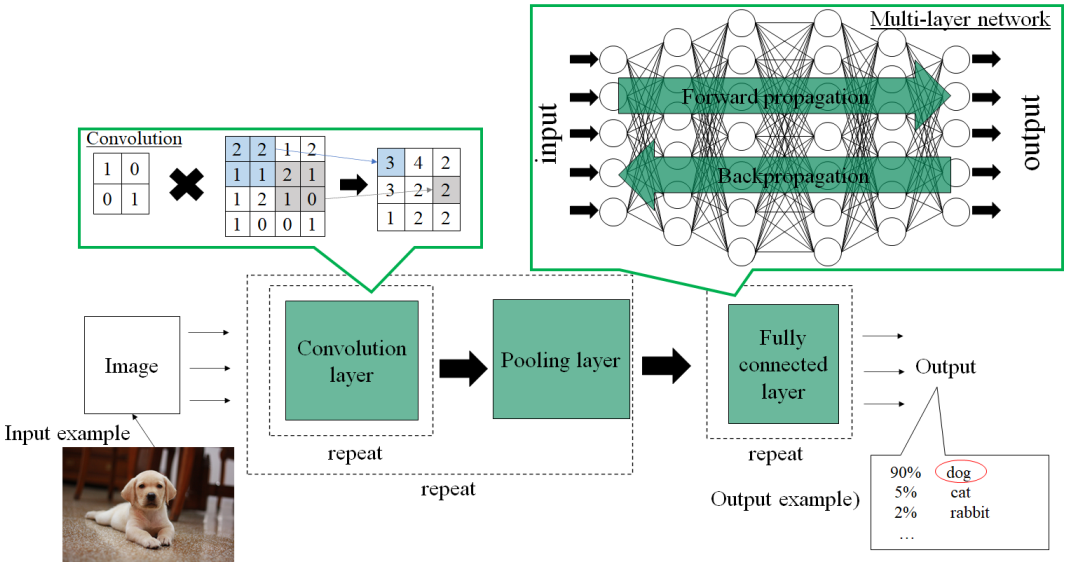

Figure 5.1: CNN configuration.

the specifications for the simulation. The SNR was changed from 0 to 30 dB. Assuming an uplink, the number of user terminals is two; one is the desired terminal and the other is the interference terminal. The angle difference between the users was 60 ㎭, the reception angle spread was 10 ㎭, and the propagation model assumed Rayleigh fading. For each modulation method, 1000 samples of received signals were prepared for each SNR, of which 700 samples were used as model training data, and 300 samples were used as test data. The batch size was five, loss function was cross entropy, and optimizer was stochastic gradient descent.

Table 5.1: Multi-beam Massive MIMO and CNN specifications.

SNR	0 ∼ 30 dB
Number of user terminals	2
User angle difference	60 deg.
Angle spread	10 deg.
Propagation model	Rayleigh fading
Modulation method	4QAM(QPSK),8QAM,16QAM,32QAM,64QAM
Number of data for training	700 Samples / modulation method
Number of test data	300 samples / modulation method
Batch size	5
Loss function	Cross entropy
Optimizer	Stochastic gradient descent

Figure 5.3 shows the identification result of the modulation method in which a CNN is applied to the received signal of multibeam Massive MIMO. The highest identification rate was 8QAM, and the identification rate was always 100% for all SNRs. With 32QAM, which had the next highest

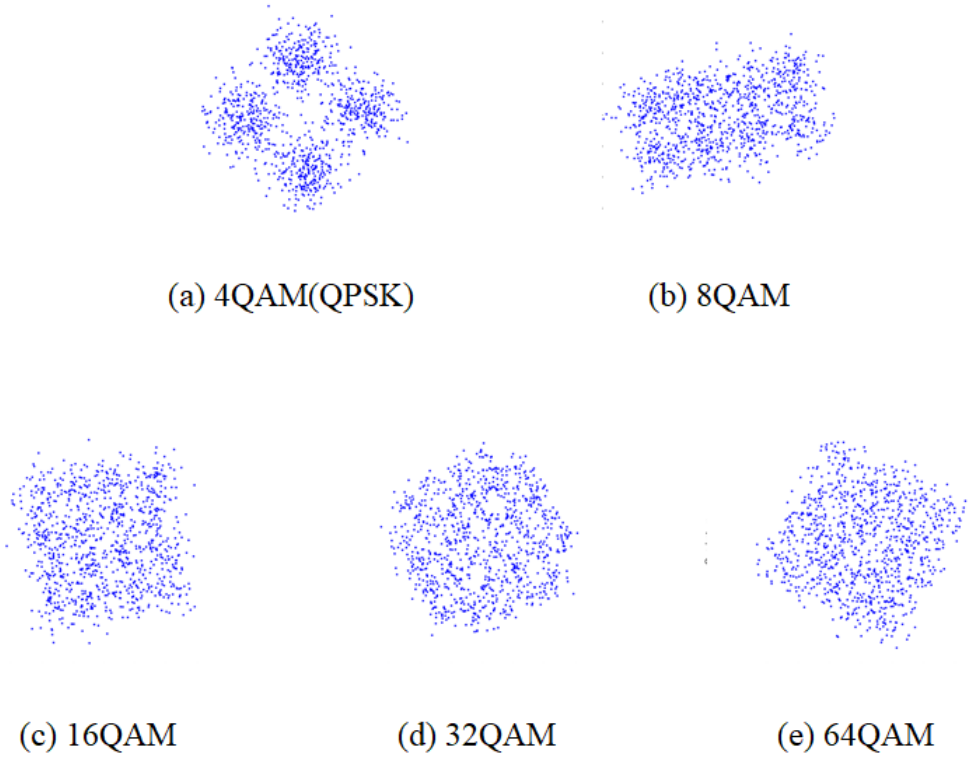

Figure 5.2: Example of actual input image.

discrimination rate, it was possible to correctly discriminate with an accuracy of 96.7% even when SNR = 0 dB. However, the lowest discrimination rate was 16QAM, with SNR <3 dB, and the discrimination rate was less than 50%. At SNR <10 dB in Figure 5.3, the discrimination rate of 32QAM, which has a larger number of values than 4QAM, is large. Here, the signal points of the generated transmission signal are shown in Figure 5.4. As can be seen from the figure, 16QAM has a square outer shape of the signal point. When the SNR decreases, the signal is dispersed, and 16QAM and 64QAM have a sloppy outline. Therefore, there are many cases where 16QAM is recognized as 64QAM, and at low SNR, the recognition rate of 16QAM is lower than that of 32QAM.

Here, Figure 5.5 shows the error rate characteristics of multibeam Massive MIMO in the case of Table 5.3. 4QAM is not shown in the table because SNR = 0 dB, and the error rate was 0. Here, if the error rate is less than 10^{-3}, it is evaluated as error correctable [117]. In Figure 5.5, 64QAM with a high error rate at a higher SNR exceeds the error rate of 10^{-3} at an SNR of about 12 dB or more. However, in the figure 5.3, the discrimination rate of 64QAM is 99.8From the above, the modulation method

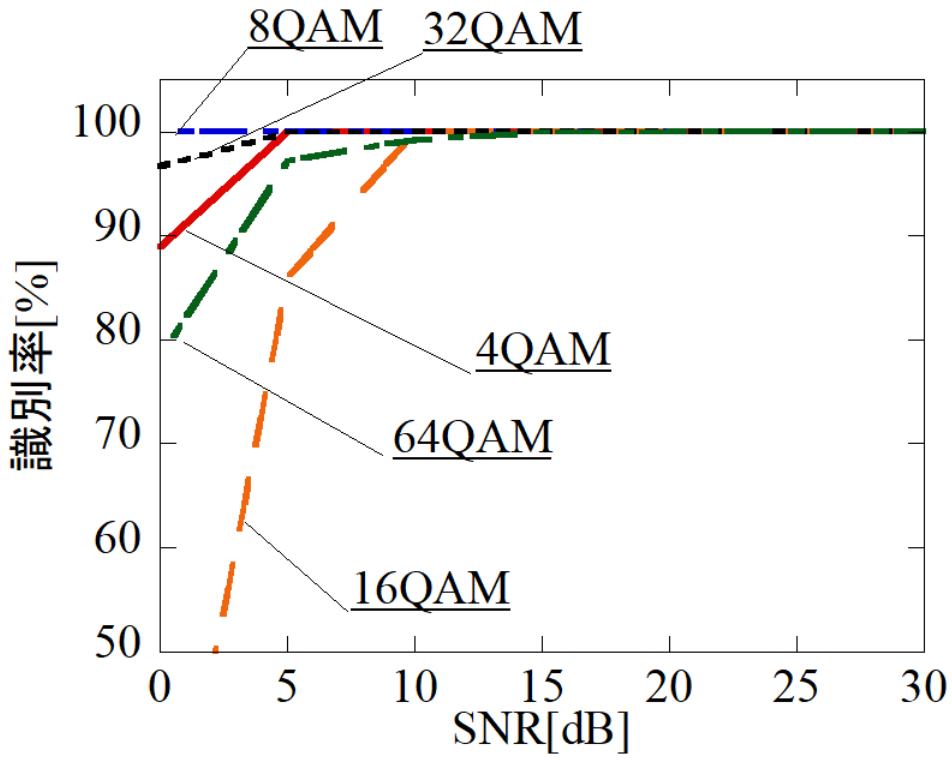

Figure 5.3: Modulation method estimation result using CNN.

estimation using CNN showed sufficient performance to be applied to multibeam Massive MIMO.

5.4 Conclusion

In this chapter, the author estimated the modulation method of the received signal of multibeam Massive MIMO using a CNN, which is a type of machine learning, and verified its basic performance. The phase of the received signal of multibeam Massive MIMO is rotated, and the amplitude is fluctuated owing to the influence of CMA, which is a blind algorithm that removes interference. A method for correcting this received signal has been proposed, but as it is premised that the modulation method used in this method is known, sharing of the modulation method during transmission and reception is an overhead in actual communication. Therefore, in this case, the modulation method of the received signal was estimated using a CNN with the aim of enabling correction and demodulation of the received signal without sharing the modulation method in advance for transmission and reception. It shows the discrimination method of the modulation method using CNN for the received SNR and the error rate characteristic of multibeam Massive MIMO, respectively, and shows that the performance of the

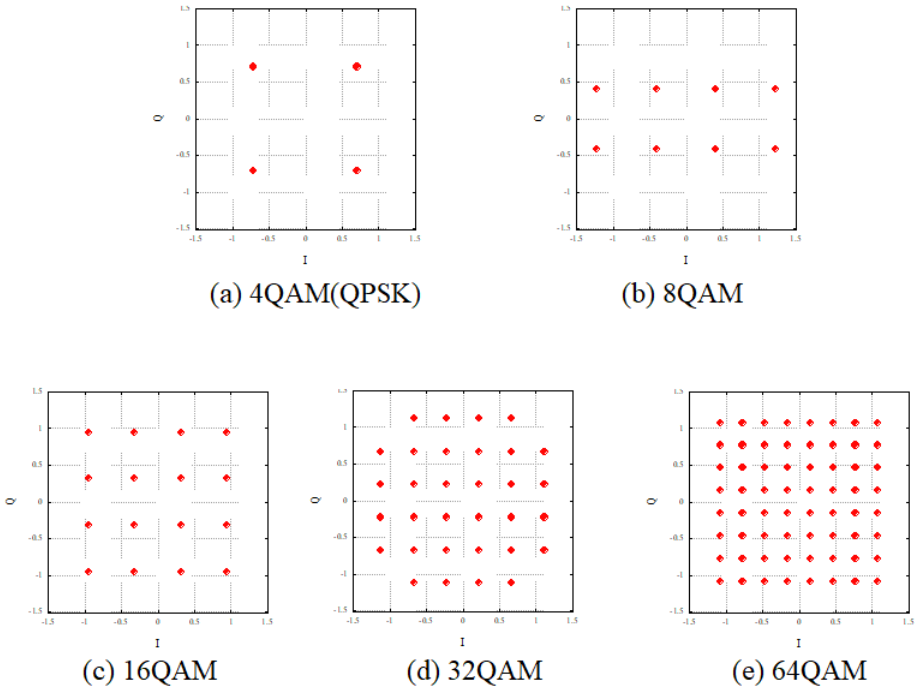

Figure 5.4: Original signal point.

modulation method estimation using CNN is suitable for its application to multibeam Massive MIMO.

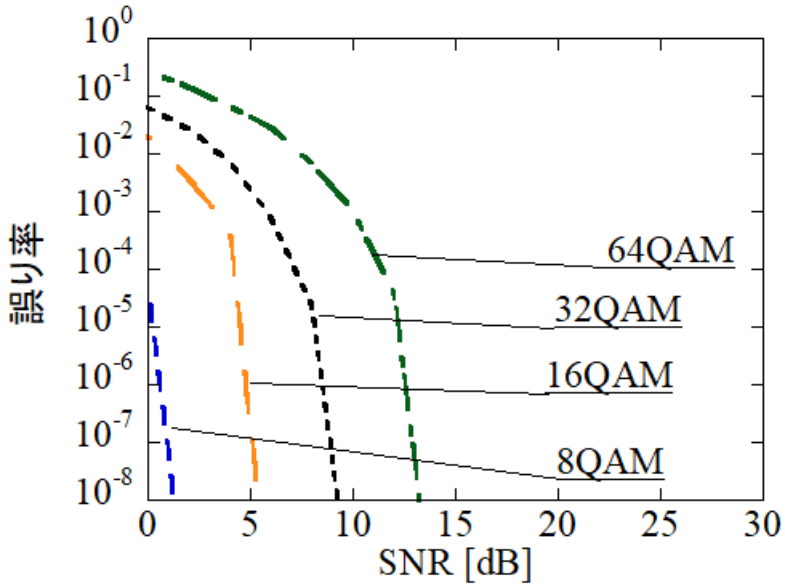

Figure 5.5: Error rate characteristics of multi-beam Massive MIMO.

Chapter 6

Propagation analysis and model design

In this chapter, I measure 28GHz used in 5G in a real environment, analyze the measurement results, and propose a new propagation model.

6.1 Introduction

In April 2020, 5th generation mobile communication systems (5G systems) were implemented to support the increasing amount of wireless communication. In particular, 5G systems represent an advanced mobile communication system following LET and 4G, which consists of a macro cell that enhances the coverage range and a small cell that enhance the communication rate in the local range. Low and high super high frequency (SHF) bands, such as those of 5 and 28 GHz, are adopted for macro and micro cells, respectively. Furthermore, the characteristics of the high SHF band used in 5G systems are different from those of the frequency bands (below the low SHF band) used in the existing mobile communications [**?**]. The model proposed by the Third Generation Partnership Project (3GPP) can be used to evaluate 5G systems. Specifically, this model supports the frequency band in the range of 0.5 to 100 GHz, which covers the frequency band used in 5G systems. However, the 3GPP propagation model is highly complex as it involves numerous parameters and is difficult to implement. Consequently, a novel propagation model that can enable convenient evaluation of 5G systems must be established. This study was aimed at developing such a propagation model, focusing on the number of radio wave path clusters. Fig. **??** shows the distribution of the number of clusters in a simulation of the uplink communication pertaining to an existing building of Niigata University in Japan for each transmission point. In the simulation, the path was estimated through ray tracing and clustered using the k-means ++ algorithm [**?**]. The part surrounded by the red frame represents the area of interest of the simulation. Ray tracing was

performed using the ray launching method, with a transmission height of 11.5 m, reception height of 2 m, transmission power of 1 W, center frequency ranging from 800 MHz to 28 GHz, and reflection diffraction frequency of three times. Clustering was performed using the k-means ++ algorithm, and clusters that were within 10 deg. or less were considered to be one cluster. The figure indicates that a higher frequency corresponds to fewer clusters. Specifically, 4–6 clusters occur in the frequency range of 800 MHz to 5 GHz, which is primarily adopted in conventional mobile communications; however, at 28 GHz, which is the frequency used in Japanese 5G systems, approximately three clusters occur at most positions. Furthermore, a physical phenomenon different from the i.i.d. Rayleigh fading, in which radio waves arrive from all directions, can be observed. In addition, several experiments demonstrated that radio waves arrive not from all directions in the SHF band, but from a limited direction, as observed in the aforementioned simulation [**?**]. This aspect indicates that if a conventional model such as i.i.d. Rayleigh fading is applied to 5G system evaluation, the system cannot be accurately evaluated. Therefore, in this study, radio wave propagation measurement was performed in a real environment based on the simulation results, and parameters such as the number of clusters, spread of cluster angles, and power difference between the clusters were determined. Furthermore, based on these parameters, the author proposed and evaluated a novel propagation model consisting of several clusters.

The remaining paper is organized as follows: Section 2 presents a literature review of the conventional radio wave propagation measurement techniques in a real environment.

Section 3 describes the measurement environment and specifications.

Section 4 presents the results of the statistical analysis of the measurement results for the cluster.

Section 5 describes the concept of the novel propagation model and its evaluation based on the analyzed cluster parameters.

6.2 Measurement environment and method

The measurement environment is shown in Fig. 6.4. The measurement was performed at the Ikarashi Campus of Niigata University in Japan. This environment represents the actual location of the environment model used in the simulation shown in Fig **??**. The transmission / reception position in which the measurement was performed is shown. Moreover, the scale and definition of the direction of arrival are shown in the upper left of the figure. Because the received power decreases significantly beyond the line of sight (LOS), all the transmission positions were set to be within the LOS. The measurement specifications are listed in Table 6.1. Assuming an uplink communication environment with a 5G system, the device was designed to ensure sufficient transmission / reception power, delay time,

Figure 6.1: Transmitting antenna located on a car equipped with a transmitting device

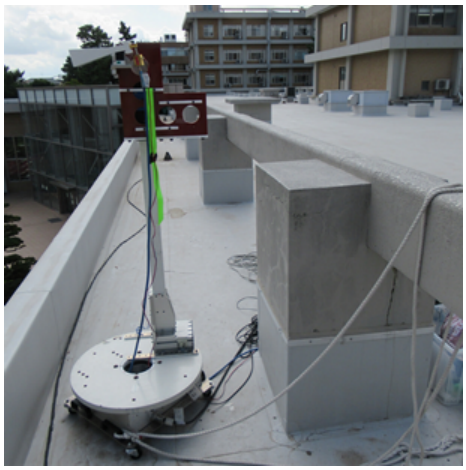

Figure 6.2: Rotation mechanism and receiving antenna installed on the roof

and arrival direction resolution to evaluate the proposed propagation model. The configurations of the transmitting and receiving antennas are shown in Figs. 6.1 and 6.2, respectively. The measurements were performed remotely to avoid any interference related to human movement. The receiving antenna was installed on a turntable and rotated 1 deg. in the horizontal direction for each measurement to perform 360 deg. measurements. In addition, the elevation angle of the receiving antenna was set such that when the center of the directional horizontal angle faced the transmitting antenna, the center of the directivity of the elevation angle faced the transmitting antenna.

6.3 Experimentally determined cluster parameters

6.3.1 Delay Time and Angle of Arrival characteristics

The measured received power of the radio waves against the arrival direction and delay time is shown in Fig. **??**.

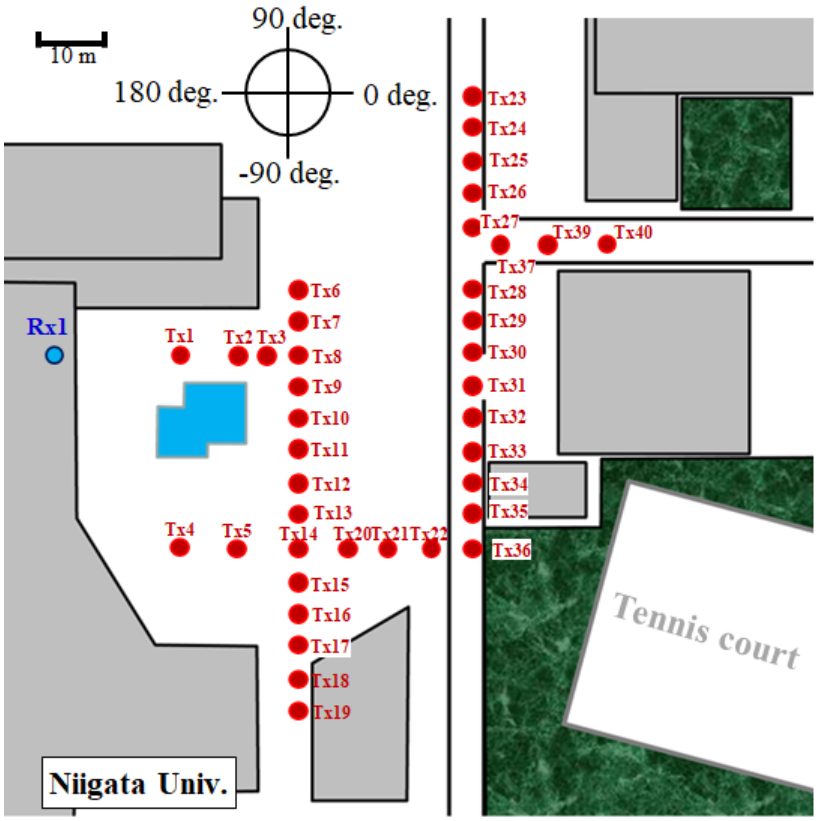

Figure 6.3: Measurement environment.

The delay power characteristics were derived by performing an inverse Fourier transformation on the propagation channel information per subcarrier of the orthogonal frequency-division multiplexing (OFDM) signal obtained in the measurement. The power was normalized such that the maximum received power was 0 dB at each measurement point. Observations were performed for a delay time of up to 60 *mu*s; however, the received power after 1.5 *mu*s corresponded to noise, and thus, only the results for the range 0 to 1.5 *mu*s are displayed. Moreover, among the numerous measurement points, the results for only six points are shown. The part corresponding to the cluster with a relatively high power was covered in this range. In both the cases, the number of incoming radio wave clusters ranged from 1 to 3. In Fig. **??** (a) Tx1, (c) Tx23, (e) Tx23, and (f) Tx40, only one cluster arriving from the LOS direction can be observed. In Fig. **??** (d) Tx30, there exist two clusters, including the cluster arriving directly from the direction. Furthermore, three clusters can be observed in Fig. **??** (b) Tx4 and (d) Tx30. The results shown in Fig. **??** indicate the presence of fewer clusters owing to problems such as reception sensitivity; however, it can be confirmed that the propagation environment is different from that of i.i.d. Rayleigh fading, in which radio waves arrived from all directions. Moreover, the

Table 6.1: Measurement specifications

Center frequency	27.8 GHz
Modulation method	OFDM
Transmission power	10 W
Bandwidth	199.92 MHz
Number of subcarriers	98000
Transmission antenna	sleeve antenna
Transmission gain	2 dBi
Transmitter height	3.0 m
Receiving antenna	horn antenna
Receive gain	2 dBi
Receiver height	12 m

characteristics of the measurement results are similar to those of the calculation results.

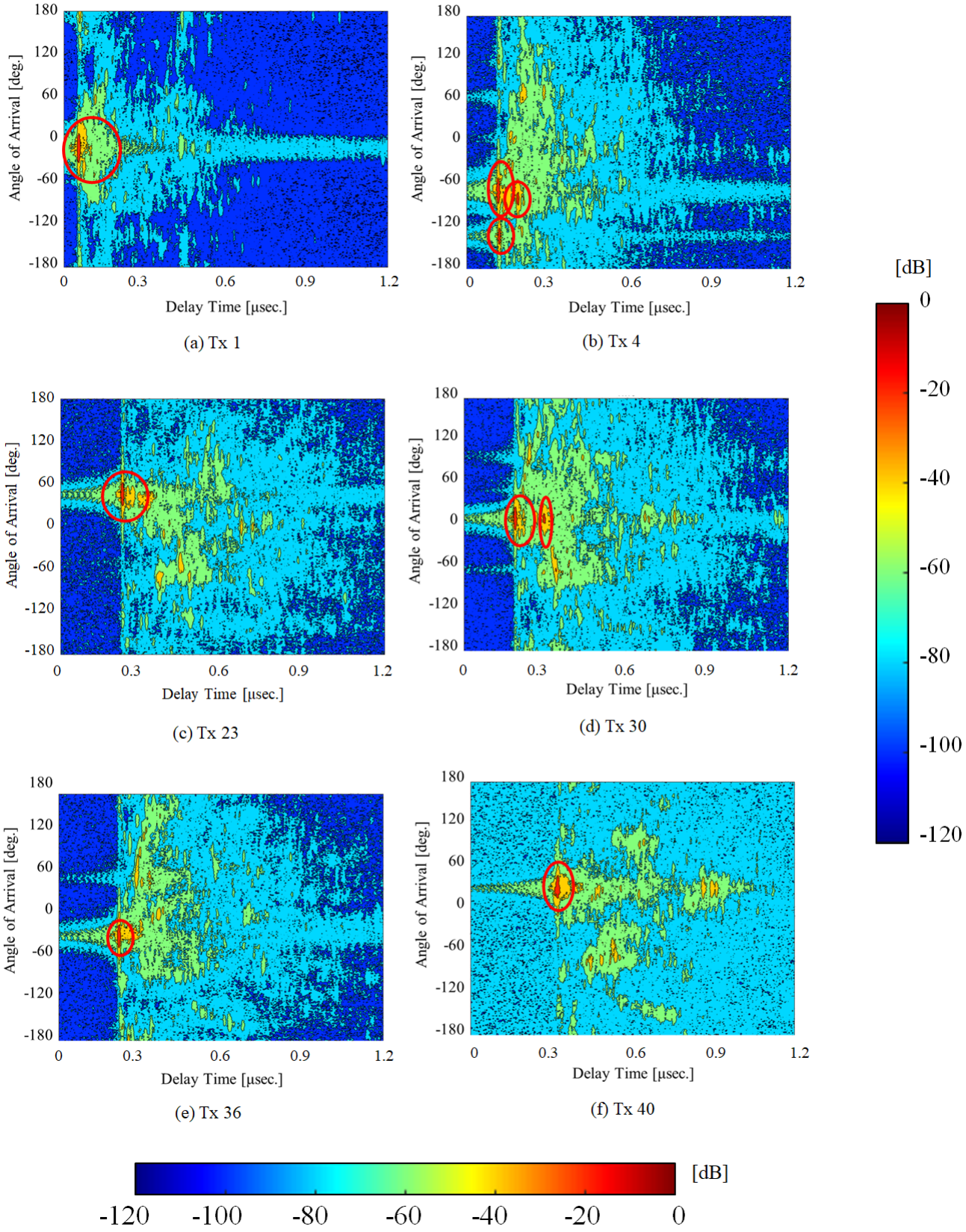

Figure 6.4: colermap

6.3.2 Definition of clusters

Before the development and evaluation of the proposed propagation model, certain parameters for the cluster were derived from the experiment results. Herein, the author describe the method to derive the clusters. First, the peak of the cluster was detected. Paths with less than a certain power were excluded from the normalized measurement data, as shown in Fig. 6.5 (a) (fig. 6.5(b)). The path with a low power was not considered as a cluster because it did not considerably influence the performance of the propagation model. The threshold value for the result of normalization with maximum power was set as -20 dB. The k-means++ algorithm was applied to the result [149]. Because clustering was performed with the specified number of clusters in the k-means++ algorithm, the execution result pertained to a group of small clusters, as shown in Fig. 6.5(c). Therefore, as shown in Fig. 6.5(d), the adjacent clusters are regarded as the same cluster. In this manner, the power peak of each obtained cluster could be determined. The reception power characteristics of the obtained power peak arrival direction and delay time are shown in Figs. 6.5 (e) and (f). In fig. 6.5 (e), the angular width at which the received power is above a certain level around the peak is defined as the angular spread of the cluster. Similarly, in Fig. 6.5(f), the delay width, which is the power above a certain level from the peak, is defined as the delay spread of the cluster.

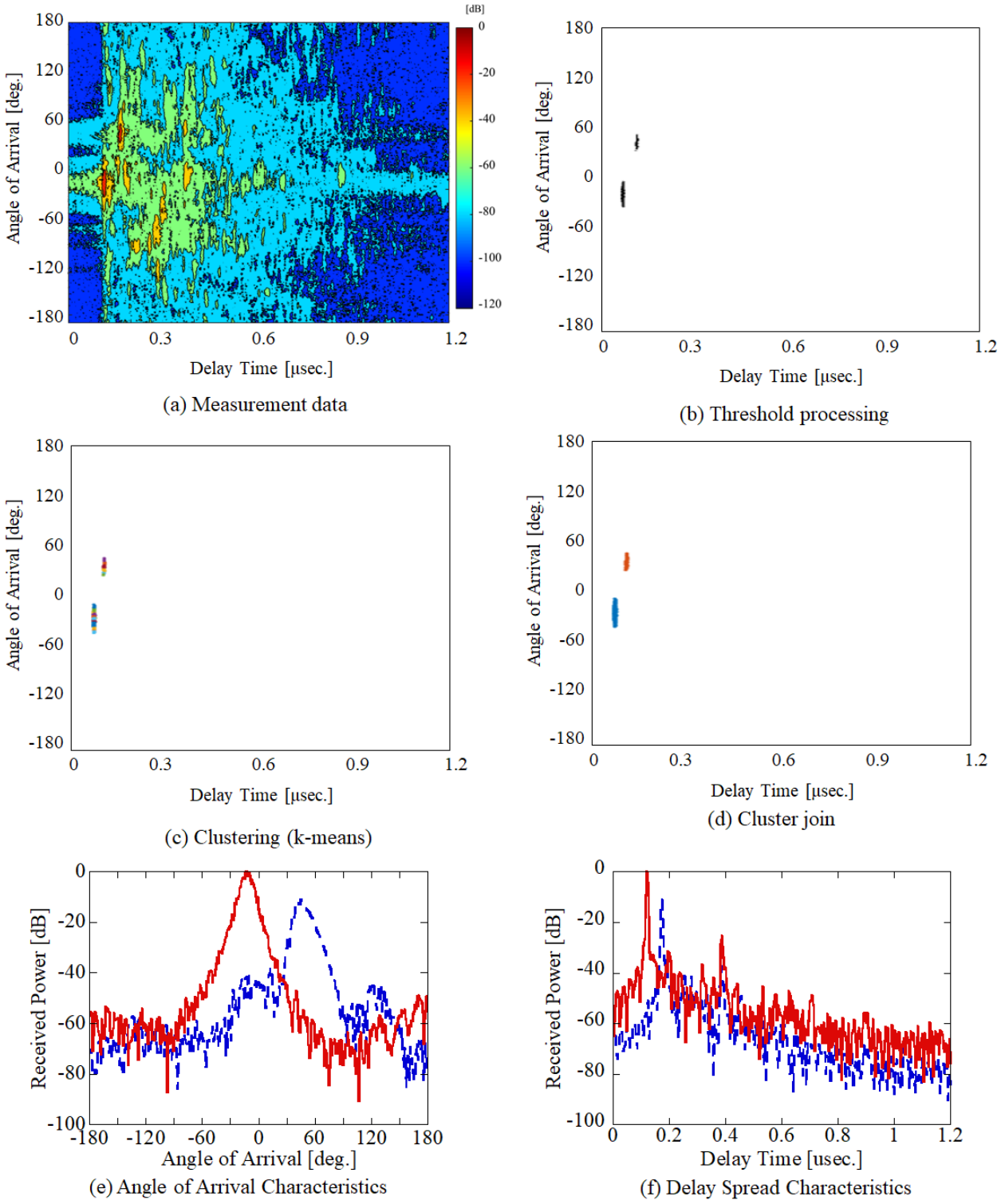

Figure 6.5: Cluster derivation method

$$P_t = \alpha \log_{10} t + \beta \tag{6.1}$$

6.3.3 Statistical value of each parameter

This section describes the statistical analysis of the parameters from the derived cluster. Table 6.2 presents the median and variance of each parameter. When the 1st, 2nd, ... nth clusters are considered in descending order of the peak power, each value is presented as $[x_1, x_2, ...x_n]$, where x_n denotes the value of the parameter of the nth cluster. The probability of existence of the 1st to 3rd clusters is [100 63.41 31.70]%, and the median variance is recorded only when each cluster exists. For example, the probability that the third cluster exists is 31.70%, and thus, there exist no median of "(E) Angle spread". Therefore, the results in the table indicate the median and standard deviation pertaining to only the measurement results of the case in which the third cluster exists with a probability of 31.70%. "(F) α of the nth cluster" in Table 6.2 is the value that minimizes the value of the power reduction equation in the delay direction of each cluster, as shown in equation(6.2), and the least squares error of the actual measurement. In equation (6.2), P_t is the received power at time t, and β is the peak power of the cluster.

$$P_t = \alpha \log_{10} t + \beta \tag{6.2}$$

6.4 Cluster model

6.4.1 Concept of the proposed model

Based on the parameters obtained from the actual measurement, a propagation model for the high SHF band for 5G systems was established. Fig 6.6 shows the framework of the proposed propagation model. First, the peak arrival direction, delay time, and power of the first cluster were determined. The arrival direction of the model was that of the assumed transmission terminal. The direction of arrival of the first cluster was that of the assumed transmitting terminal. The delay time was d/c [m], with c [m/s] being the speed of light, and d [m] being the communication distance. The power was attenuated through the propagation loss in space. Next, the author determined whether the second and third clusters existed with a probability of [100 63.41 31.70]%. For the existing clusters, (A) $\sim$ (F) values were determined for each cluster based on the median and standard deviation presented in Table 6.2. The power in the angular spread direction corresponded to a normal distribution, as

Table 6.2: Parameters obtained from the experimentally obtained clusters

	Median($\mu\sigma$)	Standard division
(A) Peak power of nth cluster relative to 1st cluster	[0, -11.59, -18.76] dB	[0, 3.71, 5.97]
(B) Delay time of nth cluster with relative to 1st cluster	[0, 0.085, 0.095] $\times 10^{-6}$ μs	[0, 0.060, 0.046] $\times 10^{-6}$
(C) Angle spread of the nth cluster	[69, 45, 42] deg.	[5.62, 9.59, 9.90]
(D) Standard deviation of power at peak arrival time of nth cluster	-	[12.51, 9.91, 6.77, 6.03]
(E) Delay spread of the nth cluster	[0.44, 0.42, 0.34] $\times 10^{-6}$ μs	[0.11, 0.11, 0.14] $\times 10^{-6}$ μs
(F) α of the nth cluster	[-32.48, -28.79, -26.09]	[10.04, 5.38, 6.03]

obtained based on the "(D) Standard deviation of power at the peak arrival time of the nth cluster". Furthermore, the power in the delay spreading direction was expected to conform to equation (6.2).

6.4.2 Simple evaluation method for 5G systems

This section describes a simple evaluation method for 5G systems considering single-input single-output (SISO) transmission. Previously, the author developed a method to calculate the transmission rate and throughput without performing the bit error rate (BER) calculation in the case of wireless LAN [140]. This method can also be extended to MIMO transmission, as described in the subsequent section. The transmission rate of the 5G system was derived using the MATLAB 5G Toolbox [**?**]. First, the relationship between the signal to noise ratio (SNR) and BER at 4.5 GHz (low SHF) and 28 GHz (high SHF), when using the actual 5G system signal, was obtained. Subsequently, the relationship between the SNR with BER = 10^{-7} or less, transmission rate, and coding rate was formulated. The results are shown in Figs. 6.7 and 6.8. Table 6.3 summarizes the relationship between the modulation method, coding rate, and SNR. N_{MOD} and $R_{\max}$ indicate the number of bits per symbol and coding rate, respectively. It can be noted that when the QPSK (2-bits / symbol) coding rate = 0.12, the SNR

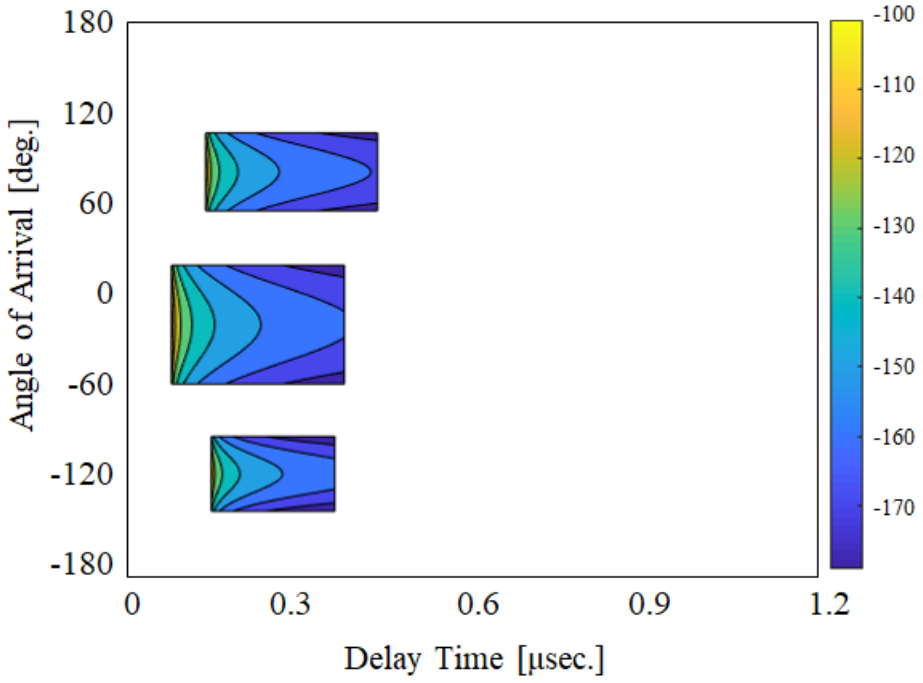

Figure 6.6: Framework of the proposed model

operates at -5 dB. Moreover, when 256QAM (8-bits / symbol) is adopted with coding rate = 0.93, the required SNR is 25 dB.

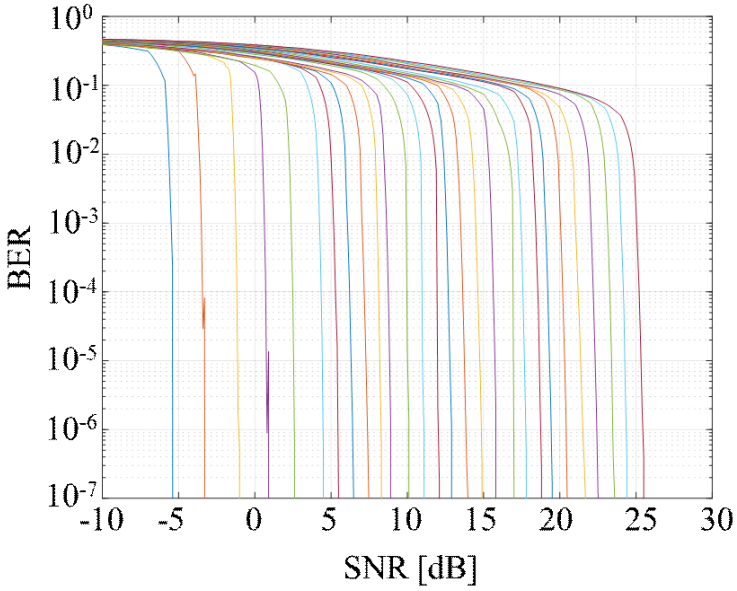

Figure 6.7: Relationship between SNR and BER (Sub-6-GHz, BW=100 MHz, $N_{\mathrm{RB}} = 135$

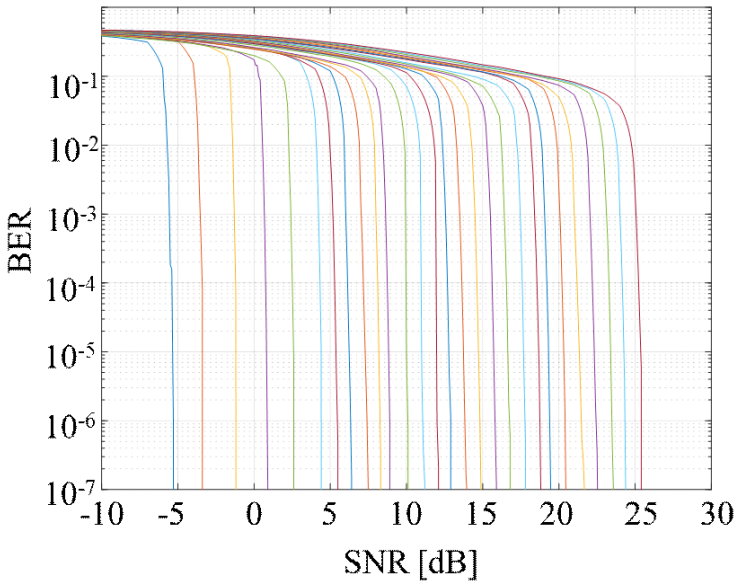

Figure 6.8: Relationship among SNR and BER (28 GHz, BW=100 MHz, $N_{\mathrm{RB}} = 264$)deg.

Table 6.3: Relationship among modulation method, code rate, and SNR

MCS Index	N_{MOD}	$R_{\max}$	SNR (Sub-6) [dB]	SNR (28GHz) [dB]
0	2	0.12	-5.5	-5.3
1	2	0.19	-3.5	-3.4
2	2	0.3	-1.1	-1.2
3	2	0.44	0.9	0.9
4	2	0.59	2.7	2.6
5	4	0.37	4.6	4.4
6	4	0.42	5.5	5.5
7	4	0.48	6.5	6.4
8	4	0.54	7.5	7.4
9	4	0.6	8.4	8.3
10	4	0.64	9	8.9
11	6	0.46	10.2	10.1
12	6	0.5	11.2	11.2
13	6	0.55	12.2	12.1
14	6	0.6	13	12.9
15	6	0.65	14	13.9
16	6	0.7	15	14.8
17	6	0.75	15.9	15.9
18	6	0.8	17.1	16.8
19	6	0.85	17.9	17.8
20	8	0.67	18.9	18.8
21	8	0.69	19.6	19.4
22	8	0.74	20.5	20.4
23	8	0.78	21.7	21.6
24	8	0.82	22.6	22.5
25	8	0.86	23.7	23.5
26	8	0.9	24.5	24.3
27	8	0.93	25.6	25.4

Using the listed values, the transmission rate can be calculated by calculating the SNR through ray tracing or measurement. In 3GPP standardization, the data rate C is calculated using the following formula: [142].

$$\begin{aligned} C &= N_{\mathrm{MIMO}} \times N_{\mathrm{MOD}} \times R_{\max} \times N_{\mathrm{RB}} \times 12/T_{\mathrm{symbol}} \\ &\quad \times (1 - R_{\mathrm{OH}}) \times R_{\mathrm{DL/UL}}. \end{aligned} \tag{6.3}$$

Table 6.4 presents the explanation of each parameter in equation (6.3) and the adopted value. The values of N_{MOD} and $R_{\max}$ change depending on the modulation signal used in the 5G system and the SNR obtained at a certain code rate.

6.4.3 Evaluation result

Fig. 6.9 illustrates the comparative evaluation of the actual measurement and proposed model considering the 5G system. The actual measurement and proposed model were virtually set to have the following configurations: 1 transmission, 1 reception, 4 transmissions, 4 receptions, and 1 transmission,

Table 6.4: Parameter values used in expression (6.3)

Parameters	Description	4.5 GHz	28 GHz
N_{MIMO}	Number of MIMO streams	1	1
N_{MOD}	Bits per modulated symbol	$2 \sim 8$	$2 \sim 8$
$R_{\max}$	Code rate	1/4 *sim* 5/6	$1/4 \sim 5/6$
N_{RB}	Number of resource blocks per CC	135	264
T_{symbol}	Time length per 1 OFDM symbol [μ sec]	17.8	8.93
R_{OH}	Overhead rate per wireless frame	0.14	0.2
$R_{\mathrm{DL/UL}}$	TDD DL / UL allocation rate	4/5	4/5

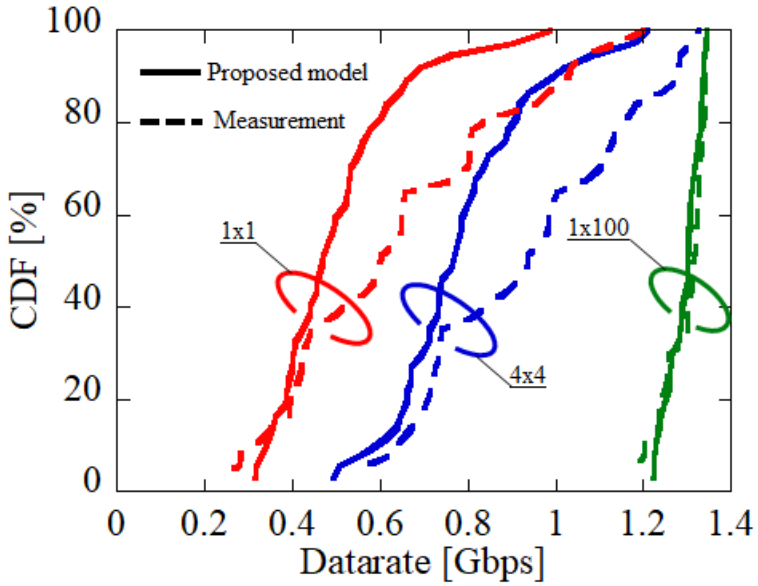

Figure 6.9: Actual measurement considering 5G system and simple evaluation of the proposed model

100 receptions. The uplink was evaluated. Specifications and parameters are based on the tables 6.1 and 6.2. In addition, the terminal position in the proposed model was set to match the measured measurement point. Comparing the proposed model with the measured data rate at CDF 50%, the difference between the 1 transmission 1 reception and 4 transmission 4 reception cases was within -0.15 Gbps. In addition, the data rates were nearly identical for the 100 receptions per transmission.

6.5 Conclusion

Through a simulation based on the ray tracing method and prior experiments, it was confirmed that the propagation characteristics of the high SHF band used in 5G systems are different from the conventional propagation models such as i.i.d. Rayleigh fading. In addition, the model proposed by 3GPP involves numerous parameters and is difficult to implement, necessitating the development of a propagation model to easily evaluate a 5G system. Therefore, the author conducted propagation measurements focusing on the arrival direction and delay time and proposed and evaluated a novel propagation model focusing on clusters of radio waves. A cluster was extracted from the measurement results, and the mean and variance of the parameters of that cluster were derived. The obtained parameters were applied to a new proposed model, and a simple evaluation of the 5G system was performed. The results indicated that the propagation characteristics of the proposed model were similar to those of the actual measurement. However, in this study, only a certain environment was considered. In future work, measurements and evaluations must be performed at various locations to further enhance the approach.

Chapter 7

Conclusion

In this paper, the following two are presentedgiven as guidelines tofor further speeding up MIMO transmission.

- Use of high frequency band
- Increase in the number of transmitting and receiving elements

In this paper, the author described the studies conducted on Massive MIMO,. which is a system based on this. Massive MIMO has the following characteristics, which are explained in this paper.and in this paper, the author pays particular attention to them and explain them.

- Very large number of antenna elements
- Frequency is higher than conventional system
- Simultaneous Ccommunication is possible at the same time with multiple terminals with a small numberamount of calculations
- Increased power consumption of base stations

In addition, there are many issues to be addressed to realize Massive MIMO , and these are as follows.

- Digital / analog fusion control method (hardware / signal processing)
- Interference elimination and control signal amount reduction method (communication efficiency)
- Propagation analysis and model design
- Examination of antenna arrangement

- Appropriate user selection
- Comprehensive evaluation of the system

Among these issues, in this paper, “”digital-analog fusion control method (hardware / signal processing),”, “”interference elimination and control signal amount reduction method (communication efficiency),”, and “”propagation model and model design” were examined.

First, in order to clarify the basic characteristics of Massive MIMO, the author evaluated Massive MIMO based on the measured propagation channels. In the experiment, 19.55 GHz was used, and the measurement as Massive MIMO was virtually performed by moving the base station antenna horizontally 100 times. Based on the measurement results, the SINR of Massive MIMO assuming full digital (ZF), full analog (MRC), and analog / digital hybrid was shown, and the effectiveness of Massive MIMO usingby analog / digital hybrid was shown. In addition, the propagation characteristics of the SHF band are different from the conventional propagation characteristics, and the incoming signalswaves arrive in several clusters;, further,and the values of the 6th and 7th eigenvalues at the time of seven7 transmissions are extreme in Massive MIMO. It was clarified that it decreased.became smaller.

Next, regarding the “”digital-analog fusion control method,” which is the first issue of Massive MIMO, the outline of the multi-beam Massive MIMO system that forms an analog multi-beam is shown as the Massive MIMO system of the analog-digital hybrid. The author also proposed a signal processing method that does not require CSISCI estimation in this system, and demonstrated its effectiveness.

After that, with respect toregarding the second method of Massive MIMO, the “”interference elimination and control signal amount reduction method,” the author proposed a signal identification method using a CNN, which is a commonly used deep learningtypical method, of deep learning, and demonstrated its effectiveness. It was. CNN is a method that is primarilymainly used for image identification, and this is applied by consideringregarding the received signal as an image. When the SNR was extremely low, it was not possible to completely determine the interference of the modulation method received signal with a large number of values. However, in the first place, when SNR is low in multi-beam Massive MIMO, a modulation method with a large number of values is not used, so thus it was clarified that it has sufficient processing capabilitiesjudgment ability when applied to this system.

Then, with respect toregarding the third issue of Massive MIMO, “”propagation analysis and model design,” the author measured 28 GHz using radio waves, clarified the propagation characteristics, and designed the propagation model. For the measurement results, the peaks of the clusters were detected

using the k-means method, and parameters such as the peak power of the clusters, delay time, and angular spread were derived based on the peaks. Based on these parameters, the author proposed a new propagation model and simply evaluated it in 5G to show its effectiveness.

Acknowledgement

This work was supported by JSPS KAKENHI, Grant Number JP19J1194.

I would like to express my gratitude to Associate Professor Kentaro Nishimori, Department of Electrical and Information Engineering, Graduate School of Natural Science and Technology, Niigata University, for his polite and enthusiastic guidance as an instructor in advancing this research.

I would like to express my sincere gratitude to Professor Hiroki Yamada of Niigata University, Professor Shigenobu Sasaki of Niigata University, Professor Tatsuya Yamazaki of Niigata University, Professor Shogo Muramatsu of Niigata University, Professor Tetsuro Imai of Tokyo Denki University, Professor Takeshi Hiraguri of Nippon Institute of Technology.

I would like to express my deepest gratitude to all the Nishimori Lab graduates who made their daily research life meaningful and gave us a lot of advice, and to all the Nishimori Lab graduates who have continued to share their vitality even after graduation.

This paper is the result of the great guidance and cooperation of many people, including the above. I would like to express my sincere gratitude.

Bibliography

[1] 3GPP LTE, *http* : *//www.*3*gpp.org/article/lte*

[2] IEEE 802.11, *http* : *//www.ieee*802.*org*/11/

[3] IEEE 802.16, *http* : *//www.ieee*802.*org*/16/

[4] 総務省, “情報通信白書令和 2 年版,” *http* : *//www.soumu.go.jp/johotsusintokei/whitepaper/*

[5] 庄木, 田邉, “無線通信はどこまで高速化できるか？,” 電子情報通信学会 通信ソサエティマガジン 2009 冬, No.11.

[6] IEEE 802.11a, *http* : *//www.ieee*802.*org*/11*a*/

[7] IEEE 802.11b, *http* : *//www.ieee*802.*org*/11*b*/

[8] IEEE 802.11g, *http* : *//www.ieee*802.*org*/11*g*/

[9] IEEE 802.11n, *http* : *//www.ieee*802.*org*/11*n*/

[10] IEEE 802.11ac, *http* : *//www.ieee*802.*org*/11*ac*/

[11] IEEE 802.11ax, *http* : *//www.ieee*802.*org*/11*ax*/

[12] 守倉, 久保田, “改訂版 802.11 高速無線 LAN 教科書,” インプレス R&D，2005.

[13] 西森, 平栗, “MIMO 伝送の基礎と無線 LAN 環境における通信効率,” 電子情報通信学会 コミュニケーションクオリティ基礎講座ワークショップ, 2015.10.

[14] 服部, 藤岡, “ワイヤレス・ブロードバンド HSPA+/LTE/SAE 教科書,” インプレス R&D，2009.

[15] A. Ghosh, R. Ratasuk, B. Mondal, N. Mangalvedhe, T. Thomas, “LTE-advanced: next-generation wireless broadband technology,” IEEE Wireless Communications, vol.17, Issue 3, pp.10–22, June 2010.

[16] G. J. Foschini and M. J. Gans, “On limits of wireless communications in a fading environment when using multiple antennas,” Wireless Pers. Commun., vol. 6, no. 3, pp. 311–335, 1998.

[17] 総務省, “電波政策ビジョン懇談会 最終報告書,” $http : //www.soumu.go.jp/menu_news/s - news/01kiban09_02000151.html$

[18] 高橋, “電波政策の最新動向について ～電波政策ビジョン懇談会をふまえて～,” ITU ジャーナル, Vol. 45, No. 4, pp. 36–40, 2015.4.

[19] 第 5 世代モバイル推進フォーラム, “Network Technology Concept for 5G,” $http : //5gmf.jp/cp - bin/wordpress/wp - content/uploads/2015/02/5GMF_NetArch_Whitepaper_v17.pdf$

[20] 岸山, ベンジャブール, 永田, 奥村, 中村, “ドコモの 5G に向けた取組み –2020 年での 5G サービス実現に向けて–,” NTT DOCOMO テクニカル・ジャーナル, Vol.23, No. 4, pp.6–17, Jan. 2016.

[21] 竹田, “改訂版 ワイヤレス・ブロードバンド時代の 電波/周波数教科書,” インプレス R&D，2008.

[22] Q. H. Spencer, C. B. Peel, A. L. Swindlehurst, and M. Haardt, “An introduction to the multi-user MIMO downlink,” IEEE Communication Magazine, Vol. 42, No. 10, pp. 60–67, Oct. 2004.

[23] 西森健太郎, “マルチユーザ MIMO の基礎,” コロナ社, 2014.

[24] NTT DOCOMO ’DOCOMO 5G White Paper 5G Radio Access: Requirements, Concept and Technologies’

[25] NFC Forum, $http : //nfc - forum.org/$

[26] TransferJet コンソーシアム, $http : //www.transferjet.org/ja/index.html$

[27] TransferJet コンソーシアム, “タッチでつながる世界,” TransferJet ホワイトペーパー, Revision 1.2, Sep. 2015.

[28] J.Jiang and M. A. Ingram, “Spherical-wave model for short-range MIMO,” IEEE Trans. Commun. Vol.53, No.9, pp.1534–1541, Sept. 2005.

[29] N. Honma, K. Nishimori, T. Seki and M. Mizoguchi, “Short Rragen MIMO communciations,” Proc. of EuCAP2009, pp.1763–1767, Berlin, Germany, March 2009.

[30] I. Sarris and A. R. Nix, “Design and performance assessment of high capacity MIMO architectures in the presence of a line-of-sight component,” IEEE Trans. Veh. Technol., vol. 56, no. 4, pp. 2194–2202, Jul. 2007.

[31] F. Bohagen, P. Orten, and G. E. Oien, “Design of optimal high-rank line-of-signt MIMO channels,” IEEE Transactions on Wireless Communications, vol. 6, no. 4, pp. 1420–1425, April 2007.

[32] F. Bohagen, P. Orten, and G. E. Oien, “Optimal Design of Uniform Rectangular Antenna Arrays for Strong Line-of-Sight MIMO Channels,” EURASIP Journal on Wireless Communications and Networking, Volume 2007, Article ID 45084, 10 pages, doi:10.1155/2007/45084.

[33] K. Nishimori, N. Honma, T. Seki, and K. Hiraga, “On the Transmission Method for Short-Range MIMO Communication,” IEEE Trans. Veh. Technol., vol. 60, no. 3, pp. 1247–1251, March 2011.

[34] E. G. Larsson, “Very large MIMO systems,” ICASSP 2012 Tutorial.

[35] F. Rusek, D. Persson, B. K. Lau, E. G. Larsson, T. L. Marzetta, O. Edfors, and F. Tufvesson, “Scaling Up MIMO – Opportunities and challenges with very large MIMO–,” IEEE Signal Processing Magazine, pp.40–60, Jan. 2013.

[36] J. Hoydis, S. ten Brink, and M. Debbah, “Massive MIMO in the UL/DL of Cellular Networks: How Many Antennas Do We Need ?,” IEEE Journal of Selected Areas on Communications, Vol. 31, No. 2, pp.160–171, Feb. 2013.

[37] 安部田, “LTE/LTE-Advanced の目指すもの,” 電子情報通信学会誌, Vol.96, No. 3, pp.144–149, 2013.

[38] 安部田, 河原, 二方, “さらなる LTE の進化，スマートライフをサポートする LTE-Advanced の開発,” NTT DOCOMO テクニカル・ジャーナル, Vol.23, No. 2, pp.6–10, Jul. 2015.

[39] H. Hirayama, G. Matui, N. Kikuma and K. Sakakibara, “Channel Capacity Improvement in Short-Range MIMO Using Side and Back Reflectors,” IEICE Trans. Commun., Vol.E94-B, No.5, pp.1280-1283, May 2011.

[40] K. Hiraga, T. Seki, K. Nishimori and K. Uehara, “Effectiveness of Short-Range MIMO using Dual-Polarized Antenna,” IEICE Trans. Commun., Vol. E95-B, No.1, pp87-96, Jan. 2012.

[41] D. Zhang, T. Hori and M. Fujimoto, “Effect of HPBW on channel capacity in near-field MIMO system,” IEICE Communications Express, Vol.1, No.5, pp.177–183, Oct. 2012.

[42] D. Zhang, T. Hori and M. Fujimoto, “Channel Capacity Improvement in Near-Field MIMO System Using Metal Wires,” IEICE Trans. Commun., Vol.E96-B, No.5, pp.1141-1148, May 2013.

[43] C. Park and T. S. Rappaport, “Short-Range Wireless Communications for Next-Generation Networks: UWB, 60 GHz Millimeter-Wave WPAN, And ZigBee,” IEEE Wireless Communications, Vol.14, No.4, pp.70-78, Aug. 2007.

[44] Wireless HD, *http* : *//www.wirelesshd.org/*

[45] IEEE 802.11ad, *http* : *//www.ieee*802.*org/*11*ad/*

[46] J. B. Andersen, “Array gain and capacity for known random channels with multiple element arrays at both ends,” IEEE J. Sel. Areas Commun., vol. 18, No. 11, pp. 2172–2178, Nov. 2000.

[47] K. Miyashita, T. Nishimura, T. Ohgane, Y. Ogawa, Y. Takatori, and K. Cho, “High Data-rate Transmission with Eigenbeam-space Division Multiplexing (E-SDM) in a MIMO Channel,” Proc. IEEE VTC 2002-Fall, vol. 3, pp. 1302–1306, Sept. 2002.

[48] R. W. Lucky, “Automatic equalization for digital communication,” Bell Syst. Tech., pp. 547–588, April 1965.

[49] A. Paulaj, R. Nabar, and D. Gore, “Introduction to Space-Time Wireless Communications,” Cambridge Univ. Press, 2003.

[50] G. H. Goiub, and C. F. Van Loan, “Matrix Computations,” The Johns Hopkins University Press, 1983.

[51] T. Maruyama, T. Hori, “Vector Evaluated GA-ICT for Novel Optimum Design Method of Arbitrarily Arranged Wire Grid Model Antenna and Application of GA-ICT to Sector-antenna Downsizing Problem,” IEEE Trans. Vol.E84-B, No.11, pp,3014-3022, Nov. 2001.

[52] NEC2, *http* : *//www.nec*2.*org/*.

[53] “アンテナ工学ハンドブック (第 2 版),” オーム社，12 章，2008.

[54] 稲垣, “電気 · 電子学生のための電磁波工学,” 丸善株式会社，1980.

[55] 平野, “素子間相互結合を表わすインピーダンス行列の計算方法,” *http* : *//www* − *antenna.ee.titech.ac.jp/ hira/hobby/edu/em/mom/equiv*$_c$*ircuit/impedance*$_m$*atrix.pdf*，2009.

[56] 大野，西, “大学課程電気回路 (1)(第 3 版),” オーム社，1999.

[57] 平野, “続遺伝的アルゴリズムと遺伝的プログラミング使いこなせる GA,GP,” パーソナルメディア，2006.

[58] K. Nishimori, R. Kudo, N. Honma, Y. Takatori, M. Mizoguchi, “16x16 MIMO testbed for MU-MIMO downlink transmission,” IEICE Trans. Commun., vol.E93-B, no.2, pp.345-352, Feb. 2010.

[59] 丹野, 森本, 阿部, 岸山, 中村, “LTE-Advanced におけるヘテロジニアスネットワーク,” 信学技報 RCS2009-317, 2010.3.

[60] Y. Ohwatari, N. Miki, T. Asai, T. Abe, H. Taoka, “Performance of Advanced Receiver Employing Interference Rejection Combining to Suppress Inter-Cell Interference in LTE-Advanced Downlink,” in Proc. of VTC Fall, Sept. 2011.

[61] K. Nishimori, K. Kusumi, M. Horio, K. Kitao and T. Imai, “Interference Rejection Characteristics by Adaptive Array at User Equipment Using Measured K-factor in Heterogeneous Networks,” IEICE Trans. Commun., Vol.E96-B, no.6, pp.1256-1264, June. 2013.

[62] K. Kitao, K. Saito, Y. Okano, T. Imai, and J. Hagiwara, “Basic Study on spatio-temporal dynamic channel properties based on channel sounder measurements,” in Proc. of APMC 2009, pp.1064–1067, Dec. 2009.

[63] 北尾, 今井, 齋藤, 奥村, “見通し内マイクロセル環境における 3D ビームフォーミングの性能評価のための基地局側垂直方向チャネル特性の実験的検討,” 信学技報 AP2013-42, June 2013.

[64] 荒田, 今井, 北尾, “MIMO チャネルサウンダの開発,” 光電技報 vol.24，pp.21–27，2008.

[65] 菊間信良, “アレーアンテナによる適応信号処理,” 科学技術出版, 1998.

[66] Q. H. Spencer, A. L. Swindlehurst, and M. Haardt, “Zero forcing methods for downlink spatial multiplexing in multiuser MIMO channels,” IEEE Trans. Sig. Processing, vol. 52, no. 2, pp.461–471, Feb. 2004.

[67] 岡崎, 井浦, 福井, 武, 岡村, “次世代無線アクセスに向けた高周波数帯活用の一検討,” 信学技報 RCS2014-81, 2014.6.

[68] 小原, 須山, シン, 奥村, “高周波数帯 Massive MIMO 伝送における選択ビーム数を増やした固定ビームフォーミングと固有モードプリコーディングの結合処理,” 信学技報 RCS2014-83, 2014.6.

[69] 須山, 小原, シン, 奥村, “アナログビームフォーミングとデジタルプリコーディングの結合処理を用いる高周波数帯 Massive MIMO におけるチャネル推定の影響,” 信学技報 RCS2014-166, 2014.10.

[70] Erik G. Larsson, Ove Edfors, Fredrik Tufvesson, Thomas L. Marzetta, “Massive MIMO for Next Generation Wireless Systems,” IEEE Communications Magazine, Vol. 52, No. 2, pp. 186–195, Feb. 2014.

[71] T. Nakamura, S. Nagata, A. Benjebbour, Y. Kishiyama, Tang Hai, Shen Xiaodong, Yang Ning, Li Nan, “Trends in small cell enhancements in LTE advanced,” IEEE Communications Magazine, Vol.51, No.2, pp.98–105, Feb. 2013.

[72] J. R. Treichler and B.G.Agee, “A New Approach to Multipath Correction of Constant Modulus Signals”, IEEE Trans. Acoust., Speech & Signal Processing, bol.ASSP-31, pp.459-472, Apr. 1983.

[73] J. Butler and R Lowe, “Beamforming Matrix simplifies design of electronically scanned antennas,” Electoron. Des., 9,8, pp.170-173, Apr. 1961.

[74] S. Yamamoto, J. Hirokawa, and M. Ando, “Single-Layer Hollow-Waveguide 8-Way Butler Matrix with Modified Phase Shifters,” Proc. of ISAP2015, Sept. 2015.

[75] 菊間信良, “アレーアンテナおける適応信号処理,” 科学技術出版, 1998.

[76] B. G. Agee, “The Least-Square CMA: A New Technique for Rapid Correction of Constant Modulus Signals,” Proc.IEEE ICASSP, pp.953-956, 1986.

[77] 藤本, 菊間, 稲垣, ”マルカート法を用いた CMA アダプティブアレーの多重波抑制特性,” 信学論 (B-II), no.3, pp.130-138, Feb. 1994.

[78] 千葉, 中条, 藤瀬, “ビームスペース CMA アダプティブアレーアンテナ,” 信学論 (B-II), vol.J77-B-II, no.3, pp.130-138, Feb. 1994.

[79] T. Tanaka, R. Miura, I. Chiba, Y. Karasawa, “ An ASIC Implementation Scheme to Realize a BeamSpace CMA Adaptive Antenna,” IEICE Trans., vol.E78-B, no.11, pp.1467-1473, Nov. 1995.

[80] R.Taniguchi, K. Nishimori, Ryochi Kataoka, Kohei Kameyama, Koshiro Kitao, Ngochao Tran, and Tetsuro Imai, “Evaluatio of massive MIMO considering real propagation characteristics in the 20 GHz band,” IEEE TRANSACTIONS ON ANTENNAS AND PROPAGATION Volume: 65, Issue: 12, pp.6703-6711, 2017.12.

[81] R.Taniguchi, K. Nishimori, Hideo Makino ,“Multi-beam massive MIMO using constant modulus algorithm for QAM signals employing amplitude and phase offset compensation,” IEICE TRANSACTIONS on Communications Vol.E100-B, No. 2, pp.262-268, 2017.1.

[82] R. Taniguchi, K. Nishimori, "Comparison of SNR and channel capacity with micro and milli-meter wave bands based on outdoor propagation measurement," IEICE Communications Express vol.9, No.6, pp.154-158, 2020.

[83] 3GPP TS36.912 V9.1.0, "Feasibility study for further advancement for E-UTRA (LTE-Advanced)," 2010.

[84] 3GPP, RWS-120045, "Summary of 3GPP TSG-RAN workshop on Release 12 and onward," June 2012.

[85] Docomo 5G White Paper,
https : *//www.nttdocomo.co.jp/english/corporate/technology/*
whitepaper$_5$*g/index.html*

[86] A. Khandekar, N. Bhushan, J. Tingfang, and V. Vanghi, "LTE advanced: Heterogeneous networks," European Wireless, pp. 978–982, Apr. 2010.

[87] D. Gesbert, M. Kountouris, R. W. Heath Jr., C.-B. Chae, and T. Salzer,"Shifting the MIMO paradigm," IEEE Signal Processing Magazine, Vol. 24, No. 5, pp. 36-46, Sept. 2007.

[88] T. Hiraguri and K. Nishimori, "Survey of transmission methods and efficiency using MIMO technologies for wireless LAN systems," IEICE Trans. Commun., Vol. E98-B, No.7, pp. 1250–1267, July 2015.

[89] F. Rusek, D. Persson, B. K. Lau, E. G. Larsson, T. L. Marzetta, O. Edfors, and F. Tufvesson,"Scaling up MIMO: Opportunities and challenges with very large MIMO," IEEE Signal Processing Magazine, pp. 40–60, Jan. 2013.

[90] L. Lu, "An Overview of Massive MIMO: Benefits and Challenges," IEEE Journal of Selected Topics in Signal Processing, Vol. 8, No. 5, pp. 742–758, Oct. 2014.

[91] H. Yang and T. L. Marzetta, "Performance of conjugate and zero-forcing beamforming in large-scale antenna systems," IEEE Journal on Selected Areas in Communications, Vol. 31, No. 2, pp. 172–179, Feb. 2013.

[92] R. Kataoka, K. Nishimori, N. Tran, T. Imai, and H. Makino, "Interference reduction characteristics by circular array based massive MIMO in a real microcell environment," IEICE Trans. Commun., Vol. E98-B, No. 8, pp. 1447–1455, Aug. 2015.

[93] H. Papadopoulos et al., "Massive MIMO Technologies and Challenges towards 5G," IEICE Trans. Commun., Vol. E99-B, No. 3, pp. 602–621, March 2015.

[94] A. Younis, et al., "Performance of Spatial Modulation using Measured Real-World Channels," 2013 IEEE 78th Vehicular Technology Conference, Sept. 2013.

[95] J. Hoydis et al., "Channel Measurements for Large Antenna Arrays," 2012 International Symposium on Wireless Communication Systems, Aug. 2012.

[96] X. Gao et al., "Massive MIMO channels – measurements and models," 2013 Asilomar Conference on Signals, Systems and Computers. Nov. 2013.

[97] X. Gao et al., "Massive MIMO performance evaluation based on measured propagation data," IEEE Transactions on Wireless Communications, Vol. 14, No. 7, pp. 3899–3911 July 2015.

[98] A. O. Martinez et al., "Towards Very Large Aperture Massive MIMO: a measurement based study," 2014 Globecom Workshops, Dec. 2014.

[99] Theodore S. Rappaport et al., "Millimeter Wave Mobile Communications for 5G Cellular: It Will Work!," IEEE Access, Vol. 1, pp335-349, May. 2013.

[100] X. Hou et al., " A novel hybrid beamforming transmission scheme for common channels and signals," 2015 21st Asisa-Pacific Conference on Communications, Oct. 2015.

[101] J. Geng et al., "Multiuser hybrid analog/digital beamforming for relatively large-scale antenna arrays," 2013 IEEE Globecom Workshops, Dec. 2013.

[102] Jian A. Zhang et al., "Massive hybrid antenna array for millimeter-wave cellular communications," IEEE Wireless Communications, Vol.22, Issue 1, Feb. 2015.

[103] T. J. Shan, M. Wax, and T. Kailath, "On spatial smoothing for direction-of-arrival estimation of coherent signals," IEEE Transactions on Acoustic Speech and Signal Processing, Vol. ASSP–33, no. 4, Aug. 1985.

[104] L. Ping, P. Wang, "Multi-User Gain and Maximum Eigenmode Beamforming for MIMO Systems with Rate Constraints," 2007 IEEE Information Theory Workshop on Information Theory for Wireless Networks, July. 2017.

[105] D. Gesbert, M. Kountouris, R. W. Heath Jr., C.-B. Chae, and T. Salzer, "Shifting the MIMO Paradigm," IEEE Signal Processing Magagine, vol.24, no.5, pp.36-46, Sept. 2007.

[106] T. Murakami, H. Fukuzono, Y. Takatori and M. Mizoguchi, “Multiuser MIMO with implicit channel feedback in massive antenna systems”, IEICE Communications Express, Vol.2, No.8 pp.336–342, Aug. 2013.

[107] K. Nishimori, K. Cho, Y. Takatori, and T. Hori, “Automatic Calibration Method using Transmitting Signals of an Adaptive Array for TDD Systems”, IEEE Trans. Veh. Tech., vol.50, no.6, Nov. 2001.

[108] K. Nishimori, K. Cho, Y. Takatori, and T. Hori, “A Novel Configuration for Realizing Automatic Calibration of Adaptive Array Using Dispersed SPDT Switches for TDD systems,” IEICE Trans. Commun., vol. E84-B, no.9, pp.2516-2522, Sept., 2001.

[109] K. Nishimori, T. Hiraguri, and T. Seki, and H. Yamada, ”Multi-beam Massive MIMO Using Analog Beamforming and DBF Based Blind Algorithm, ”Proc. of International Symposium on Antennas and Propagation (ISAP) 2015, pp.485-487, Nov. 2015.

[110] K. Kameyama, K. Nishimori, T. Hiraguri, H. Yamada and H. Makino, ”Analog Multi-beam Massive MIMO Transmission Eliminating CSI Estimation, ”IEICE Transaction Vol.J99-B, No.9, pp.743-752, Sep. 2016 (in Japanese Edition).

[111] T. Ohgane, ”Characteristics of CMA adaptive array for selective fading compensation in digital land mobile radio communications”, Electronics and Communications in Japan, Part 1: Communications, Vol. 75, No. 9, pp.43-53, Sept. 1991.

[112] M. Fujimoto, N. Kikuma, and N. Inagaki, ”Performance of CMA adaptive array optimized by the marquardt method for suppressing multipath waves”, Electronics and Communications in Japan, Part 1: Communications, Vol. 75, No. 9, pp.89–100, Nov. 1992.

[113] K. Nishimori, N. Kikuma and N. Inagaki, ”Performance analysis of CMA adaptive array for QAM signals”, Electronics and Communications in Japan, Part 1: Communications, Vol. 80, No. 11, pp.13-21, Nov. 1997.

[114] N. Kikuma, K. Takai, K. Nishimori, F. Saito and N. Inagaki, ”Consideration on performance of the CMA adaptive array antenna for 16QAM signals”, Proc. of Personal, Indoor and Mobile Radio Communications (PIMRC) 1995, Vol. 2, pp.677–681, Sept. 1995.

[115] J. Butler and R. Lowe, ”Beam-forming matrix simplifies design of electronically scanned antennas, ” Electron. Des., 9, 8, pp.170–173, April 1961.

[116] S. T. Chung and A. J. Goldsmith, "Degrees of freedom in adaptive modulation: a unified view," IEEE Trans. Commun., vol. 49, no. 9, pp. 1561-1571, Sep. 2001.

[117] K. Nishimori, H. Yomo, P. Popovski, "Distributed Interference Cancellation for Cognitive Radios Distributed Interference Cancellation for Cognitive Radios Using Periodic Signals of the Primary System," IEEE Transaction Wireless Communication, Vol.10, no,9, pp.2791-2981, Sept, 2011.

[118] Cisco Systems Inc., "Cisco Visual Networking Index: Global Mobile Data Traffic Forecast Update, 2016-2021 White Paper," Mar.2017

[119] I.E. Telatar, "Capacity of multiantenna Gaussian channels," Euro. Trans. Telecommun., vol.1, no.6, Nov./Dec. 1999.

[120] IEEE P802.11ac./D5.0, Part 11: Wireless LAN Medium Access Control (MAC and Physical Layer (PHY) specifications.

[121] H. Papadopoulos, C. Wang, O. Bursalioglu, X. Hou, and Y. Kishiyama, "Massive MIMO technologies and challenges towards 5G," IEICE Trans. Commun., vol. E99-B, no. 3, pp. 602?621, Mar. 2015.

[122] E. G. Larsson, "Very Large MIMO systems," ICASSP 2012 Tutorial.

[123] 西森, 堅岡，トラン，今井， "屋外環境における Massive MIMO の伝送レート評価," 信学技報 AP2016-120, Nov. 2016.

[124] E.G. Larsson et al., "Massive MIMO for next generation wireless systems,"IEEE Communications Magazine, Vol.52, Issue:2, pp.186- 195, Feb. 2014.

[125] R. Taniguchi, K. Nishimori, R. Kataoka, K. Kameyama, K. Kitao, N. Tran, T. Imai,"Evaluation of Massive MIMO Considering Real Propagation Characteristics in the 20–GHz Band," IEEE Transaction on Antennas and Propagation, Vol.65, No.12, pp.6703-6711, 2017.

[126] 谷口，西森, 亀山，牧野，'多値変調を用いたマルチビーム Massive MIMO 伝送の性能評価," 信学技報 AP2016-12, Apr. 2016.

[127] Alex Krizhevsky, Ilya Sutskever, Geoffrey E. Hinton, "ImageNet Classification with Deep Convolutional Neural Networks," Advances in Neural Information Processing Systems 25, 2012.

[128] IEEE P802.11ac./D5.0, Part 11: Wireless LAN Medium Access Control (MAC and Physical Layer (PHY) specifications.

[129] 井浦，中川，内田，平，岡崎，須山，小原，奥村，岡村, ”高周波数帯屋外伝搬測定結果を用いたアナログビームフォーミング MIMO システムの性能評価, ” 信学技報 AP2015-116, RCS2015-201, 2015.11.

[130] 須山，奥山，小原，奥村, ”5G 実現に向けた高周波数帯 Massive MIMO 技術, ” 信学技報 AP2015-137, RCS2015-222, 2015.11.

[131] 宮澤, 堅岡, 西森, トラン, 今井, “円形セルにおけるアナログディジタルハイブリッド型 Massive MIMO の性能評価, “信学技報 AP2014-176, Jan. 2015.

[132] 西森, 山田, 平栗, “キャリブレーション誤差を考慮した Massive MIMO 伝送の伝送効率評価,” 信学技報 AP2014-11, Nov. 2014.

[133] 亀山, 西森, 平栗, 山田, 牧野, “CSI 推定を不要とするブラインドアダプティブアレーを併用したマルチビーム Massive MIMO 伝送,” 信学技報 AP2015-59, July. 2015.

[134] 亀山, 西森, 平栗, 山田, 牧野, “マルチビーム Massive_MIMO のビーム選択に関する検討,” 信学技報 AP2015-121, Nov. 2015.

[135] 西森, 菊間, 稲垣, “QAM 信号に対する CMA アダプティブアレーの動作解析,” 信学論 (B-II) Vol. j79-B-II No.12, Dec. 1996.

[136] K. Nishimori, H. Yomo, P. Popovski, “Distributed Interference Cancellatition for Cognitive Radios Using Periodic Signals of the Primary System,” IEEE Transactions on Wireless Communications, Vol.10, No.9, Sep. 2011.

[137] P. Salamon, L.K. Hansen, “Neural Network Ensembles,” IEEE Transactions on Pattern Analysis

[138] G. O. Young, “Synthetic structure of industrial plastics,” in *Plastics,* 2nd ed., vol. 3, J. Peters, Ed. New York, NY, USA: McGraw-Hill, 1964,

[139] ”Cisco Annual Internet Report(2018–2023) White Paper, ” https://www.cisco.com/c/en/us/solutions/collateral/executive-perspectives/annual-internet-report/white-paper-c11-741490.html

[140] Takefumi Hiraguri and Kentaro Nishimori, ”Survey of Transmission Methods and Efficiency Using MIMO Technologies for Wireless LAN Systems,” in IEICE Transactions on Communications vol. E98-B, no. 7, pp. 1250–1267, Jul. 2015.

[141] https://jp.mathworks.com/products/5g.html

[142] 3GPP TS 38.306 4.1.2, 3rd Generation Partnership Project, Technical Specification Group Radio Access Network, NR, Physical layer procedures for data (Release 16), Dec. 2019.

[143] Yeijian Lv, Xuefeng Yin, Chao Zhang, and Haowen Wang, "Measurement-Based Characterization of 39 GHz Millimeter-Wave Dual-Polarized Channel Under Foliage Loss Impact," IEEE Access, vol. 7, pp. 151558–151568, Oct. 2019.

[144] Xiongwen Zhao, Shu Li, Qi Wang, Mengjun Wang, Shaohui Sun, and Wei Hong, "Channel Measurements, Modeling, Simulation and Validation at 32 GHz in Outdoor Microcells for 5G Radio Systems," IEEE Access, vol. 5, pp. 1062–1072, Jan. 2017.

[145] Ignacio Rodriguez, Huan C. Nguyen, Troels B. Sorensen, Jan Elling, Jens Age Holm, Preben Mogensen, and Benny Vejlgaard,"Analysis of 38 GHz mmWave Propagation Characteristics of Urban Scenarios," Proceedings of European Wireless 2015; 21st European Wireless Conference, Budapest, Hungary, Jul. 2015.

[146] Theodore S. Rappaport, Felix Gutierrez, Eshar Ben-Dor, James N. Murdock, Yijun Qiao, and Jonathan I. Tamir, "Broadband Millimeter-Wave Propagation Measurements and Models Using Adaptive-Beam Antennas for Outdoor Urban Cellular Communications," IEEE Transactions on Antennas and Propagation, vol. 61, no. 4, pp. 1850–1859, Apr. 2013.

[147] Eshar Ben-Dor, Theodore S. Rappaport, Yijun Qiao, and Samuel J. Lauffenburger, "Millimeter-Wave 60 GHz Outdoor and Vehicle AOA Propagation Measurements Using a Broadband Channel Sounder," 2011 IEEE Global Telecommunications Conference - GLOBECOM 2011, Houston, TX, USA, Jan. 2012.

[148] Celalettin Umit Bas, Rui Wang, Seun Sangodoyin, Dimitris Psychoudakis, Thomas Henige, Robert Monroe, Jeongho Park, Charlie Jianzhong Zhang, and Andreas F. Molisch, "Real-Time Millimeter-Wave MIMO Channel Sounder for Dynamic Directional Measurements," IEEE Transactions on Vehicular Technology, vol. 68, no. 9, pp. 8775–8789, Sep. 2019.

[149] David Arthur and Sergei Vassilvitskii, "k-means++: The Advantages of Careful Seeding", Technical Report. Stanford. Jun. 2006.